



Norwegian University of  
Science and Technology

# Catalysis for control of methane slip in marine machinery

Using platinum-based catalysts

**Hanna Marie Storrvik**

Chemical Engineering and Biotechnology

Submission date: June 2016

Supervisor: Hilde Johnsen Venvik, IKP

Co-supervisor: Rune Lødeng, SINTEF

Norwegian University of Science and Technology  
Department of Chemical Engineering



# Preface

This master's thesis was written as the final part of the study program Chemical Engineering at the Norwegian University of Science and Technology (NTNU). The thesis is written for the Catalysis group at the Department of Chemical Engineering.

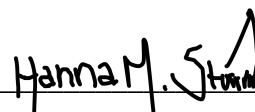
I would first and foremost like to thank my supervisor, Professor Hilde Venvik, for excellent guidance and support throughout the year. I would also like to thank my co-supervisor, Senior Scientist Rune Lødeng, for all academic guidance and productive discussions. A whole lot of gratitude goes to Research Scientist Jia Yang for practical guidance and advice, especially concerning the reaction rig. Last, but not least, I want to thank my friends and fellow students, who have made my years at NTNU so fabulous and memorable.

## Declaration of Compliance

*I declare that this is an independent work according to the exam regulations of the Norwegian University of Science and Technology (NTNU).*

Trondheim, Norway

June 10, 2016

A handwritten signature in black ink, reading "Hanna M. Storrvik", written over a horizontal line.

Hanna Marie Storrvik



# Abstract

Greenhouse gas abatement in the shipping industry has become increasingly relevant in the recent years, due to stricter laws and regulations. The use of ships running on liquid natural gas is thus growing rapidly in the shipping industry, being established as an attractive and environmentally friendly alternative to conventional ships running on bunker fuel. Ship engines operating in lean conditions have proven to be successful in maintaining high efficiency while reducing the  $\text{NO}_x$  emissions due to sufficiently low temperatures. This is, however, on the expense of  $\text{CH}_4$  slip. More research is consequently needed in order to develop catalysts with enhanced low temperature activity, suitable for complete combustion of methane in exhaust gas after-treatment systems on LNG ships.

In this project, alumina-supported platinum catalysts, with metal loading of 2 wt.% and 0.2 wt.%, have been synthesized by incipient wetness impregnation, using chloroplatinic acid as a precursor of Pt. The catalysts have been characterized with some of the main characterization techniques, including  $\text{N}_2$  physisorption, volumetric chemisorption, XRD and XRF. The catalysts have furthermore been investigated for complete oxidation of methane under stoichiometric and oxygen-rich conditions with  $\text{CH}_4$  to  $\text{O}_2$  ratios of 1:2 and 1:5, respectively. Different reactant concentrations have been tested within the given stoichiometry, to investigate the feed conditions that enhance low temperature activity for the synthesized catalysts.

Semi-crystalline  $\gamma$ -alumina was found to be the only compound detected in XRD analyzes, where absence of a detected platinum phase was suspected to be due to finely dispersed platinum particles with small crystallite sizes. This was substantiated by chemisorption experiments, revealing high dispersion and small particle sizes for both catalysts. Chlorine containing catalysts possessed a somewhat larger surface area than a non-chlorine containing catalyst, which is proposed to have a correlation, due to possible re-dispersion of platinum when exposed to  $\text{O}_2$  at high temperatures.

The 2 wt.% catalyst exhibited better performance than the 0.2 wt.% catalyst, and a temperature of about 70-90 °C more was necessary to obtain the same level of conversion with the lowest metal loading. Stoichiometric reactant concentrations were found to enhance low temperature activity of the catalysts, in comparison to oxygen-rich conditions. Higher concentrations of  $\text{PtO}_2$  are discussed to be the cause of the inferior activity displayed in excess  $\text{O}_2$ , as platinum is more likely to be oxidized to a greater extent in such conditions. The catalytic activity was furthermore found to increase with increasing methane concentration, whereas the temperature necessary to obtain complete conversion, decreased with decreasing methane concentration. The lowest temperature needed to obtain complete conversion, was observed in excess  $\text{O}_2$  with feed containing 1000 ppm  $\text{CH}_4$ , which resembles application relevant conditions the most among the tested.



# Sammendrag

Klimagassutslipp fra skipsindustrien har opplevd en økende aktualitet de siste årene, da nye lover og forskrifter stiller stadig strengere krav til utslipp. I marinsektoren er derfor bruken av skip drevet på flytende naturgass i sterk vekst, og er i ferd med å bli veletablert som et attraktivt og mer miljøvennlig alternativ til konvensjonelle skip drevet på bunkersolje. Skipsmotorer som opererer i oksygenrike forhold har vist stor suksess i å oppnå høy virkningsgrad samtidig som  $\text{NO}_x$ -utslippene holdes lave, grunnet tilstrekkelig lave temperaturer. Dette er imidlertid på bekostning av  $\text{CH}_4$  utslipp. Mer forskning er derfor nødvendig for å utvikle katalysatorer med god lav-temperaturaktivitet, egnet for fullstendig forbrenning av metan i avgassrensningssystemer på LNG-drevne skip.

I dette prosjektet har katalysatorer med 2 vekt% og 0.2 vekt% platina, båret på aluminiumoksid, blitt syntetisert via metoden «incipient wetness impregnation», ved bruk av heksakloroplatina som forløper for Pt. Katalysatorene har blitt karakterisert med teknikker som  $\text{N}_2$  fysisorpsjon, volumetrisk kjemisorpsjon, XRD og XRF. Katalysatorene er videre testet for fullstendig oksidasjon av metan under støkiometriske og oksygenrike betingelser, med  $\text{CH}_4$  til  $\text{O}_2$  forhold på henholdsvis 1:2 og 1:5. Ulike reaktantkonsentrasjoner er testet innen den gitte støkiometrien, for å undersøke hvilke fødebetingelser som gir best lav-temperaturaktivitet for de syntetiserte katalysatorene.

Semi-krystallinsk  $\gamma$ -alumina var det eneste stoffet som ble detektert i XRD analysene, og det ble mistenkt at fraværet av en detektert platina fase var grunnet finfordelte platinapartikler av liten størrelse. Dette ble stadfestet av kjemisorpsjonseksperimenter, som avslørte høy spredning av platina på overflaten og små partikkelstørrelser for begge katalysatorene. Katalysatorprøver som i henhold til XRF analyser inneholdt klor, besatt et noe større overflateareal enn ikke-klorinnholdene prøver, og en mulig sammenheng, grunnet potensiell re-dispergering av platina, er diskutert.

Katalysatoren med 2% Pt viste bedre aktivitet enn den med 0.2% Pt, og en temperatur på omtrent 70-90 °C mer var nødvendig for å oppnå samme grad av omsetning med lavest metallmengde. Støkiometriske reaktantbetingelser ga opphav til høyere katalysatoraktivitet, sammenliknet med oksygenrike betingelser. Det er diskutert om den dårligere aktiviteten fremvist i overskudd av  $\text{O}_2$  skyldes høyere  $\text{PtO}_2$  konsentrasjoner, da platina har større sannsynlighet for å i høyere grad bli oksidert under slike betingelser. Aktiviteten ble videre funnet å øke med økende metankonsentrasjon, mens temperaturen nødvendig for å oppnå fullstendig omsetning, minket med avtagende metankonsentrasjon. Den laveste temperaturen som måtte til for å oppnå fullstendig omsetning av metan, ble observert i overskudd av  $\text{O}_2$  med 1000 ppm  $\text{CH}_4$  i føden. Denne betingelsen ligner applikasjonsrelevante forhold mest blant de testede fødesammensetningene.





# Table of contents

<b>Preface</b> .....	<b>i</b>
<b>Abstract</b> .....	<b>iii</b>
<b>Sammendrag</b> .....	<b>v</b>
<b>Abbreviations</b> .....	<b>xi</b>
<b>List of Symbols</b> .....	<b>xiii</b>
<b>List of Figures</b> .....	<b>xv</b>
<b>List of Tables</b> .....	<b>xvii</b>
<b>1 Introduction</b> .....	<b>1</b>
1.1 Motivation .....	1
1.2 Objective .....	2
1.3 Previous work.....	2
<b>2 Theory</b> .....	<b>3</b>
2.1 Natural gas as fuel.....	3
2.2 Catalysts for methane combustion .....	5
2.2.1 Platinum and Palladium .....	5
2.2.2 Deactivation .....	6
2.3 Preparation of supported catalysts .....	8
2.3.1 Incipient wetness impregnation .....	9
2.3.2 Drying .....	9
2.3.3 Calcination .....	10
2.3.4 Electrostatic adsorption.....	10
2.4 Catalyst characterization .....	12
2.4.1 Nitrogen Physisorption .....	12
2.4.2 Volumetric Chemisorption.....	15
2.4.3 X-ray Diffraction .....	17
2.4.4 X-ray Fluorescence .....	18
2.5 Gas Chromatography .....	20
2.5.1 Principle .....	20

2.5.2	Detectors .....	21
<b>3</b>	<b>Experimental .....</b>	<b>23</b>
3.1	Risk Assessment.....	23
3.2	Catalyst Preparation .....	24
3.3	Catalyst Characterization .....	26
3.3.1	Nitrogen Physisorption .....	26
3.3.2	Volumetric Chemisorption.....	26
3.3.3	X-ray Diffraction .....	27
3.3.4	X-ray Fluorescence .....	27
3.4	Catalyst Testing.....	28
3.4.1	Experimental set-up .....	28
3.4.2	Reactor .....	30
3.4.3	Methane oxidation .....	31
3.4.4	Processing of analysis data .....	33
3.4.5	Calculation of activation energy .....	35
<b>4</b>	<b>Results .....</b>	<b>37</b>
4.1	Catalyst Characterization .....	37
4.1.1	Nitrogen Physisorption .....	37
4.1.2	Volumetric Chemisorption.....	38
4.1.3	X-ray Diffraction .....	42
4.1.4	X-ray Fluorescence .....	42
4.2	Catalytic Activity .....	44
4.2.1	Reference experiments.....	46
4.2.2	Temperature profiles.....	47
4.2.3	Effect of loading .....	49
4.2.4	Effect of stoichiometry .....	50
4.2.5	Effect of concentration.....	52
<b>5</b>	<b>Discussion.....</b>	<b>55</b>
5.1	Catalyst Characterization .....	55
5.1.1	Nitrogen Physisorption .....	55

5.1.2	Volumetric Chemisorption.....	56
5.1.3	X-ray Diffraction .....	58
5.1.4	X-ray Fluorescence .....	58
5.2	Catalytic Activity .....	61
5.2.1	Deactivation and “hot spots” .....	61
5.2.2	Effect of loading .....	62
5.2.3	Effect of stoichiometry .....	62
5.2.4	Effect of concentration.....	64
<b>6</b>	<b>Conclusion .....</b>	<b>67</b>
<b>7</b>	<b>Suggestions for further work .....</b>	<b>69</b>
	<b>References.....</b>	<b>71</b>
<b>A</b>	<b>Risk Assessment .....</b>	<b>I</b>
<b>B</b>	<b>Synthesis of catalysts.....</b>	<b>V</b>
B.1	Calculation of salt amount .....	V
B.2	Preparation of support .....	VI
B.3	Synthesis procedure .....	VI
<b>C</b>	<b>Volumetric Chemisorption.....</b>	<b>VII</b>
C.1	Procedure description.....	VII
C.2	Sample masses .....	VII
<b>D</b>	<b>Mass flow controllers.....</b>	<b>IX</b>
D.1	Calibration curves .....	IX
D.2	Calculations.....	X
<b>E</b>	<b>Carbon balances.....</b>	<b>XIII</b>
<b>F</b>	<b>Kinetics Calculations .....</b>	<b>XVII</b>
<b>G</b>	<b>Matlab script .....</b>	<b>XIX</b>
<b>H</b>	<b>Arrhenius plots.....</b>	<b>XXI</b>



# Abbreviations

0.2 wt.% Pt/Al <sub>2</sub> O <sub>3</sub>	0.2 weight percent platinum on $\gamma$ -alumina support, prepared from platinum chloride precursor
2 wt.% Pt/Al <sub>2</sub> O <sub>3</sub>	2 weight percent platinum on $\gamma$ -alumina support, prepared from platinum chloride precursor
$\mu$ GC	Micro gas chromatograph
BET	Brunauer, Emmet and Teller
BJH	Barrett, Joyner and Halenda
deNO <sub>x</sub>	NO <sub>x</sub> reduction
ECD	Electron capture detector
FID	Flam ionization detector
GC	Gas chromatograph
GHSV	Gas hourly space velocity
HSE	Health, safety and environment
LNG	Liquified natural gas
MFC	Mass flow controller
NGV	Natural gas vehicle
NTNU	Norwegian University of Science and Technology
ppm	Parts per million
SCR	Selective catalytic reduction
TCD	Thermal conductivity detector
TOF	Turnover frequency
WDXRF	Wavelength Dispersive X-ray Fluorescence
XRD	X-ray Diffraction
XRF	X-ray Fluorescence



# List of Symbols

$\alpha$	A constant $\frac{\chi-1}{V_0 \cdot \chi}$	$mm^{-3}$
$\beta$	Line broadening of peak	$rad$
$\eta$	A constant $\frac{1}{V_0 \cdot \chi}$	$mm^{-3}$
$\sigma$	Surface tension	$N \cdot m^{-1}$
$\rho$	Density	$g \cdot cm^{-3}$
$\lambda$	Wavelength	$nm$
$\tau$	Residence time	$s^{-1}$
$\varphi$	Contact angle	$^\circ$
$\theta$	Angle of diffraction peak	$^\circ$
$A$	Pre-exponential factor	-
$A_0$	Area occupied by one molecule	$nm^2 \cdot molecule^{-1}$
$A_i$	Area of peak of component $i$	$nm^2$
$A_t$	Total surface area	$nm^2$
$C_i$	Concentration of component $i$	$mol \cdot dm^{-3}$
$D$	Metal dispersion	%
$d$	Lattice spacing	$nm$
$E$	Error	%
$E_A$	Activation energy	$kJ \cdot mol^{-1}$
$F$	Stoichiometric factor	-
$F_i$	Molar flow rate of component $i$	$mol \cdot s^{-1}$
$F_{tot}$	Total molar flow rate	$mol \cdot s^{-1}$
$h$	Height of catalytic bed	$cm$
$\Delta H_f^\circ$	Heat of formation	$kJ/mol$
$k$	Rate constant	$s^{-1}$
$k_i$	Response factor of component $i$	$nm^{-2}$
$k'$	Scherrer's constant	-
$k_B$	Boltzmann's constant	$J \cdot K^{-1}$
$M_w$	Molecular weight	$g \cdot mol^{-1}$
$m_{cat}$	Mass of catalyst	$g$
$n$	Diffraction order	-
$n_s$	Number of metal atoms on surface	-
$n_t$	Total number of metal atoms	-
$P$	Pressure	$bar$
$P_0$	Equilibrium pressure of condensed gas	$bar$
$q_i$	Volumetric flow rate of component $i$	$Nml \cdot min^{-1}$
$q_{tot}$	Total volumetric flow rate	$Nml \cdot min^{-1}$
$R$	Gas constant	$J \cdot K^{-1} \cdot mol^{-1}$
$r$	Radius	$nm$
$r_A$	Reaction rate	$mol \cdot dm^{-3} \cdot s^{-1}$
$r_{CH_4}$	Experimental value of reaction rate	$mol \cdot g_{cat}^{-1} \cdot h^{-1}$

$S_{BET}$	Specific surface area	$m^2 \cdot g^{-1}$
T	Temperature	K
TOF	Turnover frequency	$s^{-1}$
V	Volume	$cm^3$
$V_0$	Volume of monolayer adsorbed gas	$mm^3$
$V_{bed}$	Volume of catalytic bed	$cm^3$
$V_m$	Molar volume	$cm^3 \cdot mol^{-1}$
$v_a$	Total volume of adsorbed gas	$mm^3$
$v_{ads}$	Uptake of chemisorbed molecules	$mm^3$
W	Weight	g
$\chi$	BET constant	-
$X_i$	Conversion of component $i$	-
$x_m$	Weight fraction of metal	-
$y_i$	Mole fraction of component $i$	-



# List of Figures

2.1. SCHEMATIC OVERVIEW OF INCIPIENT WETNESS IMPREGNATION AND DRYING. ....	8
2.2. PORE AND PARTICLE PROFILES AS FUNCTION OF DRYING RATE .....	10
2.3. HYSTERESIS EFFECT RESULTING FROM CAPILLARY CONDENSATION AND EVAPORATION OF N <sub>2</sub> IN THE PORES.....	14
2.4. THE IDEAL LANGMUIR ISOTHERM WITH QUANTITY OF GAS ADSORBED AS A FUNCTION OF PRESSURE .....	16
2.5. DISSOCIATIVE ADSORPTION OF HYDROGEN ON PLATINUM.. .....	16
2.6. SINGLE-SITED CHEMISORPTION OF CO ON PLATINUM.....	17
2.7. PRINCIPLE OF XRF ON AN ATOMIC LEVEL.....	19
2.8. BLOCK DIAGRAM OF A TYPICAL CHROMATOGRAPHIC SYSTEM.....	20
2.9. ILLUSTRATION OF A TYPICAL GAS CHROMATOGRAM.....	21
3.1. RISK MATRIX USED IN THE RISK ASSESSMENT .....	23
3.2. FLOW SHEET OF THE REACTION RIG, SET UP FOR METHANE OXIDATION EXPERIMENTS.....	29
3.3. SHAPE AND DIMENSIONS OF THE QUARTZ FIXED BED REACTOR, USED IN THE METHANE OXIDATION EXPERIMENTS.....	30
3.4. EXAMPLE OF ARRHENIUS PLOT, WHERE THE SLOPE YIELDS THE ACTIVATION ENERGY DIVIDED BY THE GAS CONSTANT.....	36
4.1. ADSORPTION ISOTHERMS FROM H <sub>2</sub> AND CO CHEMISORPTION OF 2 WT.% Pt/Al <sub>2</sub> O <sub>3</sub> CATALYST. ....	39
4.2. ADSORPTION ISOTHERMS FROM THREE DIFFERENT H <sub>2</sub> CHEMISORPTION EXPERIMENTS OF THE 0.2 WT.% Pt/Al <sub>2</sub> O <sub>3</sub> CATALYST.....	40
4.3. XRD PATTERNS OF THE DIFFERENT BATCHES OF CATALYSTS AND THE ALUMINA SUPPORT ..	42
4.4. METHANE CONVERSION AS A FUNCTION OF TEMPERATURE DURING HEATING AND COOLING OF THE REACTOR.....	45
4.5. MEASURED BED TEMPERATURE AS A FUNCTION OF POSITION WITHIN THE CATALYST BED, OBTAINED DURING EACH RUN OF THE SEQUENTIAL METHANE OXIDATION EXPERIMENTS, PERFORMED OVER THE 2 WT.% Pt/Al <sub>2</sub> O <sub>3</sub> CATALYST.....	47
4.6. MEASURED BED TEMPERATURE AS A FUNCTION OF POSITION WITHIN THE CATALYST BED OBTAINED DURING EACH OF THE SEQUENTIAL METHANE OXIDATION EXPERIMENTS, PERFORMED OVER THE 0.2 WT.% Pt/Al <sub>2</sub> O <sub>3</sub> CATALYST.....	48
4.7. COMPARISON OF TEMPERATURE VERSUS CH <sub>4</sub> CONVERSION CURVES OF THE 2 WT.% Pt/Al <sub>2</sub> O <sub>3</sub> CATALYST AND THE 0.2 WT.% Pt/Al <sub>2</sub> O <sub>3</sub> AT MATCHING CONDITIONS IN FOUR DIFFERENT EXPERIMENTS PERFORMED OVER EACH CATALYST. ....	49
4.8. INLET TEMPERATURE VERSUS CONVERSION COMPARED FOR OXYGEN RICH AND STOICHIOMETRIC CONDITIONS IN METHANE OXIDATION EXPERIMENTS OVER THE 2 WT.% Pt/Al <sub>2</sub> O <sub>3</sub> CATALYST. ....	51
4.9. INLET TEMPERATURE OF THE CATALYTIC BED, VERSUS CONVERSION COMPARED FOR DIFFERENT REACTANT CONCENTRATIONS IN METHANE OXIDATION EXPERIMENTS OVER THE 2 WT.% Pt/Al <sub>2</sub> O <sub>3</sub> CATALYST.....	53
4.10. TURNOVER FREQUENCY AS A FUNCTION OF METHANE CONCENTRATION, UNDER STOICHIOMETRIC CONDITIONS (1:2) AND OXYGEN RICH CONDITIONS (1:5).....	54

<b>D.1. CALIBRATION CURVES FOR THE MASS FLOW CONTROLLERS OF NITROGEN, METHANE, SYNTHETIC AIR AND HYDROGEN .....</b>	<b>IX</b>
<b>E.1. ERROR IN CARBON BALANCE IN THE OXIDATION EXPERIMENTS PERFORMED OVER THE 2 WT.% CATALYST.....</b>	<b>XIV</b>
<b>E.2. ERROR IN CARBON BALANCE IN THE OXIDATION EXPERIMENTS PERFORMED OVER THE 0.2 WT.% CATALYST.....</b>	<b>XVI</b>
<b>H.1. ARRHENIUS PLOTS USED TO CALCULATE ACTIVATION ENERGY IN THE OXIDATION REACTIONS PERFORMED OVER THE 2 WT.% CATALYST.. .....</b>	<b>XXI</b>
<b>H.2. ARRHENIUS PLOTS USED TO CALCULATE ACTIVATION ENERGY IN THE OXIDATION REACTIONS PERFORMED OVER THE 0.2 WT.% CATALYST .....</b>	<b>XVII</b>

# List of Tables

<b>3.1.</b> WEIGHTED AMOUNT OF SALT AND DEIONIZED WATER IN THE PRECURSOR SOLUTIONS USED FOR INCIPIENT WETNESS IMPREGNATION OF 10 G OF ALUMINA. ....	25
<b>3.2.</b> COMPOSITION OF THE DIFFERENT SAMPLES OF DILUTED CATALYST USED IN THE EXPERIMENTS, THE BED HEIGHT AND AN OVERVIEW OF THE RUNS THE DIFFERENT SAMPLES WERE USED IN. ....	31
<b>3.3.</b> AIR TO FUEL RATIO AND REACTANT CONCENTRATIONS IN THE DIFFERENT METHANE OXIDATION EXPERIMENTS PERFORMED. THE ORDER IN WHICH THE EXPERIMENTS WERE PERFORMED IN IS ALSO REPORTED, EXPRESSED AS RUNS. DUE TO THE LOW METHANE CONCENTRATION IN RUN 7 AND 8, THE CH <sub>4</sub> GAS TANK WAS SWITCHED OUT BY A 5% CH <sub>4</sub> IN N <sub>2</sub> GAS TANK WHEN THESE EXPERIMENTS WERE PERFORMED, IN ORDER TO HAVE THE FLOW CONFORM WITH THE MFC. ....	32
<b>4.1.</b> BET SURFACE AREA, PORE VOLUME AND PORE DIAMETER OF THE 2 WT.% Pt/AL <sub>2</sub> O <sub>3</sub> CATALYST, TWO DIFFERENT 0.2 WT.% Pt/AL <sub>2</sub> O <sub>3</sub> CATALYSTS AND OF THE ALUMINA SUPPORT. THE SURFACE AREAS AND THE PORE VOLUMES AND PORE SIZES ARE DETERMINED FROM THE BET- METHOD AND THE BJH-METHOD, RESPECTIVELY.....	37
<b>4.2.</b> DISPERSION AND CRYSTALLITE SIZE OBTAINED FROM CHEMISORPTION EXPERIMENTS PERFORMED ON THE 2 WT.% Pt/AL <sub>2</sub> O <sub>3</sub> CATALYST AND 0.2 WT.% Pt/AL <sub>2</sub> O <sub>3</sub> CATALYSTS....	38
<b>4.3.</b> COMPARISON BETWEEN CRYSTALLITE SIZE OBTAINED FROM CHEMISORPTION MEASUREMENTS, DENOTED BY ASAP, AND CALCULATED CRYSTALLITE SIZE FROM EQUATION ADAPTED FOR Pt PARTICLES. THE VALUES ARE BASED ON THE DIFFERENCE RESULTS FROM THE CHEMISORPTION EXPERIMENTS. ....	41
<b>4.4.</b> SAMPLE COMPOSITION OF THE DIFFERENT CATALYSTS AND THE SUPPORT, OBTAINED FROM XRF ANALYSIS. THE REPETITION OF THE ANALYSIS CONCERNING THE CATALYST FROM THE SPECIALIZATION PROJECT, WAS PERFORMED IN THIS PROJECT AFTER THE INSTRUMENT HAD BEEN RECALIBRATED. ....	43
<b>4.5.</b> CALCULATED PLATINUM CONTENT IN EACH OF THE CATALYST SAMPLES, BASED ON THE RESULTS FROM THE XRF ANALYSIS. THE DEVIATION FROM THE NOMINAL LOADING OF PLATINUM IS ALSO REPORTED FOR EACH SAMPLE. ....	43
<b>4.6.</b> NUMERIC VALUES OF TOTAL FEED FLOW, RESIDENCE TIME AND GHSV, KEPT CONSTANT IN ALL RUNS OF THE METHANE OXIDATION EXPERIMENTS. ....	44
<b>4.7.</b> OVERVIEW OF CATALYTIC ACTIVITY EXHIBITED BY THE TWO CATALYSTS, EXPRESSED AS TEMPERATURE REQUIRED TO OBTAIN A CERTAIN EXTENT OF CONVERSION UNDER DIFFERENT REACTANT CONCENTRATIONS. RUN 1-8 IS PERFORMED OVER THE 2 WT.% CATALYST, WHILE RUN 9-13 IS PERFORMED OVER THE 0.2 WT.% CATALYST. THE DOTTED LINES SEPARATE SEQUENTIAL RUNS. THE FEED WAS BALANCED WITH N <sub>2</sub> . ....	46
<b>4.8.</b> ACTIVATION ENERGY COMPARED FOR DIFFERENT LOADING IN THE FOUR DIFFERENT EXPERIMENTS CONDUCTED OVER BOTH THE 2 WT.% AND THE 0.2 WT.% CATALYST. THE ACTIVATION ENERGY IS ESTIMATED FROM ARRHENIUS PLOTS, CONSTRUCTED FOR CONVERSIONS BELOW 50%. ....	50
<b>4.9.</b> CALCULATED CONVERSIONS AND REACTION RATES AT 450 °C IN TWO COMPARABLE SETS OF METHANE OXIDATION EXPERIMENTS OVER THE 2 WT.% CATALYST. THE RESULTS ARE	

COMPARED FOR METHANE TO OXYGEN RATIOS OF 1:5 AND 1:2, WITH METHANE CONCENTRATIONS OF 2% AND 0.5% IN THE TWO SETS, RESPECTIVELY. ....	51
<b>4.10.</b> CALCULATED CONVERSION, REACTION RATE AND TOF AT 430 °C COMPARED FOR DIFFERENT REACTANT CONCENTRATIONS. THE DOTTED LINE SEPARATES THE COMPARED OXYGEN RICH EXPERIMENTS FROM THE STOICHIOMETRIC ONES. ....	54
<b>B.1.</b> CALCULATED AMOUNT OF CHLOROPLATINIC ACID NECESSARY TO GET THE CORRECT AMOUNT OF PT FOR THE RESPECTIVE CATALYST, SUPPORTED ON 10 G OF ALUMINA .....	V
<b>C.1.</b> CHEMISORPTION PROCEDURE USED FOR H <sub>2</sub> AND CO CHEMISORPTION OF THE 0.2 WT.% PT AND 2 WT.% PT CATALYST SAMPLES .....	VII
<b>C.2.</b> SAMPLE MASSES OF THE 0.2 WT.% PT CATALYST SAMPLES (TOP THREE) AND THE 2 WT.% PT CATALYST SAMPLES (BOTTOM THREE) SUBJECTED TO CHEMISORPTION .....	VIII
<b>D.1.</b> OVERVIEW OF THE DIFFERENT COMBINATIONS OF FEED GAS COMPOSITION USED IN THE METHANE OXIDATION EXPERIMENTS .....	X
<b>D.2.</b> FEED GAS COMPOSITION, CORRESPONDING VOLUMETRIC FLOW RATE OF EACH COMPONENT AND RESULTANT OPENING OF THE MASS FLOW CONTROLLERS.....	XII
<b>F.1.</b> CALCULATED RESIDENCE TIME AND GAS HOURLY SPACE VELOCITY IN THE METHANE OXIDATION EXPERIMENTS PERFORMED OVER THE THREE CATALYST SAMPLES .....	XVII

# 1 Introduction

## 1.1 Motivation

Air emissions emanating from shipping have received a lot of attention in recent years, and the shipping industry's demand for emission reducing solutions are increasing in line with stricter laws and regulations. The use of liquefied natural gas (LNG) as fuel, offers, in this context, many advantages to conventional oil-based fuels, and the marine sector is experiencing an increasing interest in ships running on LNG. In addition to the economic benefits that arise from using LNG as fuel, provided that the gas prices are kept low, the main benefit of gas run engines concerns the environment. As gas engines are known for emitting lower amounts of CO<sub>2</sub> and the main types of pollutants, such as, NO<sub>x</sub>- and SO<sub>x</sub> compounds, the focus on using LNG as fuel on ships is becoming increasingly relevant as the environmental legislation is tightening up. The advantages that arise from LNG ships do, however, deeply depend on the conditions under which the combustion process is run by, and are easily at risk of being jeopardized if the process does not proceed under carefully controlled conditions.

Catalytic combustion of natural gas is, already, a well-established process, being widely applied for an extensive range of applications, such as for energy production and air pollution abatement. Catalytic combustion serves as an attractive alternative to conventional thermal combustion, as it enables lower emission levels of harmful greenhouse gases and NO<sub>x</sub> to the atmosphere. Natural gas consists of many components, but its main constituents are C<sub>1</sub> to C<sub>4</sub> hydrocarbons, dominated by methane (85-95%) [1]. The overall reaction of methane combustion is given in Equation (1.1).



The reaction is highly exothermic with  $\Delta H_f^0 = -804$  kJ/mol [2]. Due to the large heat evolution the exothermic reaction produces, the temperature can easily get out of control and rise above 1600 °C [3]. At temperatures this high, formation of thermal NO<sub>x</sub> compounds will occur, which is highly unwanted. Additionally, incomplete combustion of methane leads to the formation of CO and can, in addition to CO emissions, cause slip of harmful methane gas to the atmosphere. Thus, attainment of complete oxidation of methane at as low as possible temperatures is essential if replacement of bunker fuel in favor of LNG is of environmental purposes.

Ship engines that provide for the combination of high efficiency, emissions that meet the NO<sub>x</sub> requirements and, at the same time, avoid methane slip to the atmosphere, has been found difficult to facilitate. If high efficiency is to be obtained, the process can be carried out in high temperature and pressure, where CH<sub>4</sub> slip is prevented, but the NO<sub>x</sub>

requirements are exceeded. In that case, a deNO<sub>x</sub> system, such as selective-catalytic reduction (SCR) system is required. Alternatively, the process can be carried out in low temperature and pressure, where the engine emissions meet the NO<sub>x</sub> requirements due to sufficiently low temperatures, but on the expense of CH<sub>4</sub> slip. Thus, in order to avoid slip of unburned methane present in the exhaust gases, a catalytic exhaust gas after-treatment system can be applied, providing for complete oxidation of methane. By catalytic combustion of methane, the remaining methane gas can be converted into CO<sub>2</sub> and H<sub>2</sub>O according to the complete oxidation reaction in Equation (1.1).

Catalytic combustion used for cleaning purposes, or secondary pollution control, is widely applied, and the most familiar application is the 3-way catalyst used to treat exhaust gases emitted from vehicle engines. More research is, however, needed in order to develop an equitable system for use in the marine sector, based on LNG as fuel. This requires the development of catalysts with enhanced low temperature activity, suitable for complete combustion of methane in conditions known to be prevailing in the exhaust gases of LNG engines.

## **1.2 Objective**

The main objective in this thesis has been to synthesize platinum-based catalysts of different loading by incipient wetness impregnation of alumina, characterize them with some of the main characterization techniques and investigate the catalysts for complete oxidation of methane. The feed gas composition will be varied, both in terms of stoichiometry and concentration, to investigate the feed conditions that enhance low temperature activity of the synthesized catalysts. The activity will also be compared with regards to the metal loading. Along with another student's corresponding research over a palladium-based catalyst, the projects aim to form a base case for future development of catalysts suitable for catalytic control of methane slip in marine machinery.

## **1.3 Previous work**

This thesis is an expansion of a Specialization Project, carried out in the fall of 2015. In that project, a 0.2 wt.% Pt/Al<sub>2</sub>O<sub>3</sub> catalyst was synthesized and characterized in the same manner as the catalysts in this project. Characterization results from this catalyst will be presented and compared to the 0.2 wt.% catalyst prepared and characterized during this project. This paper is based on the report written in context to the Specialization Project, and some of the content is reused.

## 2 Theory

### 2.1 Natural gas as fuel

There are vast world-wide resources of natural gas, making it an easy accessible source of fuel for both automotive and marine purposes. The use of compressed natural gas as fuel for automotive applications has experienced a large expansion in recent years, as it offers many environmental, as well as economical, advantages over gasoline and diesel. The marine sector is now moving in the same direction, as stricter emission regulations are becoming more comprehensive and is also starting to affect the shipping industry to a larger extent.

Engines in natural gas vehicles (NGV), which use compressed natural gas as fuel, operate under lean-burn conditions, meaning there is a high air to fuel ratio. This leads to a higher fuel efficiency compared to conventional compression ignition engines, and lower levels of CO<sub>2</sub> emissions. The methane molecule's high H:C ratio also contributes to reductions in the CO<sub>2</sub> emissions. Moreover, the high air to fuel ratio provides for a cooler combustion, which reduce the thermal formation of NO<sub>x</sub> compounds. The SO<sub>x</sub> emissions from NGVs are besides reported to be low. By using compressed natural gas as fuel in vehicles, toxic benzene present in gasoline emissions and polyaromatic compounds stemming from diesel are completely avoided, in addition to the elimination of soot and smoke regular fuel provides [1].

In the same manner as NGVs are being developed, the use of LNG run ships is being established as a more environmentally friendly alternative to ships running on bunker fuel. Stensvold [4] emphasizes that the emissions from the gas engines of LNG ships contain 25-30% less CO<sub>2</sub> and further reduces the harmful NO<sub>x</sub> emissions with approximately 85% compared to those of bunker fuel. Additionally, the LNG engines do not emit sulfur compounds (SO<sub>x</sub>) or oil derived particulates.

It is, however, critical to obtain complete combustion of methane in order to avoid unintended CO and CH<sub>4</sub> emissions resulting from incomplete combustion. The methane emissions need to be cut to a minimal in order to satisfy increasingly stringent environmental and emission standards. As methane is a greenhouse gas with 20 times the global warming potential as CO<sub>2</sub> and can remain in the atmosphere from 9 to 15 years [5], the advantages that arise from using natural gas as fuel are being jeopardized if unburned methane is present in the exhaust.

Methane slip abatement can be accomplished using catalysts for complete oxidation of unburned CH<sub>4</sub> present in the exhaust gases, to CO<sub>2</sub> and H<sub>2</sub>O, according to Equation (1.1). In order to optimize the process to keep the harmful emissions to a marginal level, the conditions in the exhaust, in which the catalyst will be operating in, need to be established. Gélin et. al [1] enlighten lean burn conditions present in the exhaust of NGVs, and it is

reasonable to believe that catalysts intended for LNG ships need to comprehend similar conditions. The following conditions are reported to be prevailing in NGV exhaust:

- Low temperatures, typically less than 500-550 °C
- Low concentrations of methane (500-1000 ppm)
- Large amounts of water vapor (10-15%) and CO<sub>2</sub> (15%)
- Large excess of oxygen (substantially more oxygen than the stoichiometric oxygen to fuel ratio of 2)
- Presence of SO<sub>x</sub> (about 1 ppm) and NO<sub>x</sub>

The conditions in the engine exhaust consequently requires catalysts to present high activity at low temperatures, in addition to show high resistance to potential poisons present in the exhaust gases.

Complete oxidation of methane can be performed over either noble metals or transition metal oxides. The highest activity is often shown by noble metal based catalysts, such as supported platinum and palladium, which have become attractive candidates for low temperature combustion of methane.



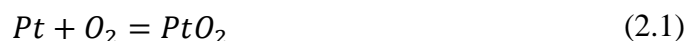
## 2.2 Catalysts for methane combustion

### 2.2.1 Platinum and Palladium

Platinum belongs to the group of noble metals and is, along with palladium, one of the most studied and used catalysts for oxidation reactions. When deposited on a high specific surface area support, like alumina, the dispersion of Pt on the support can be obtained in a high degree. Generally, a higher dispersion leads to improved catalytic activity [1].

Both supported Pt and Pd are extensively used as catalysts in automotive engines for oxidation of CO and hydrocarbons. Generally, platinum catalysts demonstrate high catalytic activity for the oxidation of alkanes and alkenes with carbon number of 3 or higher, whereas palladium catalysts are known to be more active for oxidation of methane, which is difficult to oxidize due to its low reactivity compared to higher hydrocarbons. This is, however, not always the case and could depend on the fuel composition. Burch et. al [6] reported that Pt/Al<sub>2</sub>O<sub>3</sub> catalysts have shown to exhibit higher activity than Pd/Al<sub>2</sub>O<sub>3</sub> catalysts in methane combustion under reducing, or methane-rich, conditions. Such fuel-rich mixtures may be found in several methane-containing fuel systems, making further research regarding also platinum catalysts for complete combustion of methane, highly relevant.

An important difference between the two noble metals in context to methane combustion is platinum and palladiums different reactivities toward O<sub>2</sub>. The oxidation reactions of platinum and palladium are given in Equation (2.1) and (2.2), respectively.



As can be seen from the above equations, platinum oxidizes to PtO<sub>2</sub> while palladium oxidizes to PdO in the presence of oxygen. PtO<sub>2</sub> is highly unstable, and decomposes to Pt<sup>0</sup> at around 400 °C in an ambient atmosphere. In addition to the thermal instability of PtO<sub>2</sub>, the compound is also characterized as being highly volatile. This property sometimes leads to loss of Pt and surface reconstructions, as Pt can be transported over nanometric distances as volatile PtO<sub>2</sub> under lean conditions. PdO, on the other hand, is considered a more stable compound in this context. The oxidized state of palladium is usually formed at around 300-400 °C, and is easily formed under lean conditions. The compound also has better thermal stability than the oxidized state of platinum and is stable in air at atmospheric pressure for temperatures up to around 800 °C [1, 7].

Because of the thermal instability of PtO<sub>2</sub>, it is commonly assumed that platinum mostly remains in its metallic state, as Pt<sup>0</sup>, in an oxidizing atmosphere. However, for both platinum

and palladium there are diverse opinions and an ongoing discussion regarding what phase of the respective metal that is the most active for methane oxidation. Hicks et. al. [8] observed, through his studies, that the activity of the metallic states of both platinum and palladium is way higher for methane oxidation than the activities exhibited by PtO<sub>2</sub> and PdO, respectively. Contradictory, Burch [9] claims that the metallic state of palladium is not active for methane combustion at all, and that it is the oxidized state that provides for the active phase of palladium. Lyubovski, on the other hand, concludes that the mixed PdO/Pd state is likely to be the most active form of palladium catalysts [10]. Likewise, Burch [11] came to the conclusion that a partially oxidized Pt surface exhibits the highest activity for the methane oxidation reaction and that both metallic Pt and fully oxidized Pt are inferior for C-H bond activation compared to the mixed state.

### 2.2.2 Deactivation

An inevitable issue, applying to all catalysts, is loss of catalytic activity over time, due to deactivation mechanisms. One such mechanism is poisoning.

Blockage of sites and adsorption modes is a common type of poisoning, and physical poisoning by sulfur components is especially important in the case of natural gas oxidation catalysts. As stated in Section 2.1, NGV exhaust normally contains small amounts of SO<sub>x</sub>, typically 1 ppm or less. The sulfur usually originates from either the odorizer held by the gas itself, or from the lubricating oil used on the engine [1]. Sulfur present in gas engine conditions, dominated by large excess of air, will be oxidized to SO<sub>2</sub> and SO<sub>3</sub>, and even trace amounts of these components may poison the catalyst and thus substantially decrease the catalytic activity by blocking the active noble metal sites [12]. Natural gas also contains mercury, which is known to have a poisoning effect on catalysts as well. The concentration may, however, vary significantly, depending on the location and quality of the natural gas. Natural gas has been reported to contain mercury in as different amounts as 450-5000 µg/Nm<sup>3</sup> to 0,01 µg/Nm<sup>3</sup>, depending on where the gas is extracted from [13]. With LNG as basis, these potential poisoning substances are, however, less of concern. In order to be able to cool natural gas to 77 K to obtain it in its liquid form, the gas needs to go through extensive purification operations. Hence, LNG is considered to be of high purity, containing virtually no contaminants to possibly poison the catalyst.

Chlorine traces present on the catalyst, may, however, pose a danger of poisoning the catalysts. Platinum-based catalysts are often prepared from a Cl containing precursor such as Chloroplatinic acid (H<sub>2</sub>PtCl<sub>6</sub>), and studies have proposed that chlorine, remaining from the synthesis, has a poisoning effect on the catalyst [14]. Gélin et. al [1] refers to studies where complete oxidation of methane are performed under oxidizing conditions, and where chlorine seems to inhibit the catalytic activity of platinum particles supported on alumina. The full mechanism, however, by which Cl ions act as inhibitors on the catalytic activity, is not yet evidently established. This is, nevertheless, an issue that should be kept in mind

when preparing Pt based catalysts from chlorine containing precursors and which could influence the catalytic activity exhibited by the catalyst.

Recalling the conditions prevailing in exhaust gas, listed in section 2.1, the oxidation reaction will, under normal conditions, occur in the presence of large quantities of H<sub>2</sub>O. This may cause challenges for oxidation catalysts in context to deactivation and degradation. Gholami et.al [15] have studied the effect of H<sub>2</sub>O on CH<sub>4</sub> oxidation over Pd catalysts, and found that presence of water has a deactivating effect on the catalysts. The deactivation was found to be due to formation of Pd(OH)<sub>2</sub>, resulting in suppression of the catalytic activity by reason of adsorbed hydroxyl groups preventing O exchange between the support and the active sites. It was also found that reaction inhabitation caused by H<sub>2</sub>O adsorption takes place, which is particularly of interest at temperatures below 500 °C. In this temperature range, the inhabitation increases with decreasing temperature, and with increasing H<sub>2</sub>O concentration. For temperatures above 500 °C, H<sub>2</sub>O assisted sintering was found to be the biggest issue. Hence, thermal sintering, which already poses a threat to the activity, may seem to be provoked by the presence of water.

## 2.3 Preparation of supported catalysts

A supported catalyst consists of a catalytically active phase dispersed over a support. Most noble metal catalysts are manufactured by the means of impregnation or precipitation, where the aim is to get nanometer-sized particles of the catalytically active metal spread uniformly on the support [16]. Incipient wetness impregnation is one of the most simple and direct methods of deposition [17], and is the method by which the catalysts in this project were prepared by. This is thus the only preparation method that will be explored in this report.

Proper dispersion of the active phase on the support is important for the performance and cost of the catalyst, and can be achieved by dissolving the active metal precursor in a liquid before impregnation. The solution is then introduced into the pores of the support, before the sample is thermally treated through drying and calcination to dehydrate and stabilize the catalyst [18].

An overview of the incipient wetness impregnation and drying procedure is illustrated in Figure 2.1.

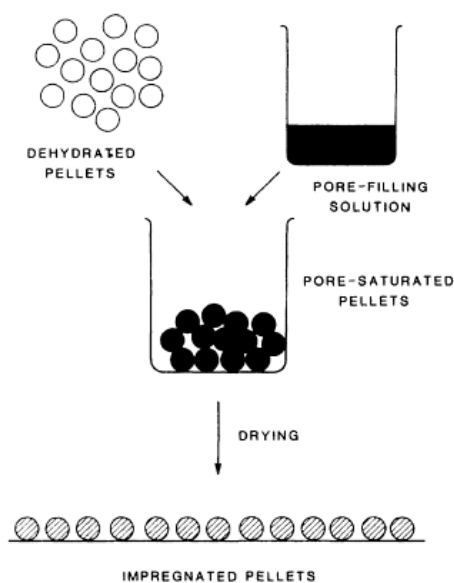


**Figure 2.1.** Schematic overview of incipient wetness impregnation and drying [17]. The precursor solution is added to the support in amounts just sufficient to fill the pores of the support. The sample is then dehydrated through drying and the solid phase precipitates onto the support.

### **2.3.1 Incipient wetness impregnation**

Incipient wetness impregnation is a method used to fill the pores of the support with a solution containing the metal salt providing for the active phase of the catalyst.

In incipient wetness impregnation, the precursor solution is drawn into the pores of the support by capillary action. The volume of the precursor solution added to the support should equal the pore volume of the support. In that way, the amount of liquid added, is just sufficient to fill the pores and wet the outside of the particles. In the case of proper incipient wetness impregnation, no excess solution will remain outside the pore space [18].

The support is often heated or evacuated prior to impregnation to remove pore moisture, making the diffusion of the solute into the pores more efficient [17]. Additionally, it is important that the precursor salt introduced by impregnation, is both soluble and have properties that make it easy transformable to an oxidic or metallic phase upon decomposition by heating [18].

### **2.3.2 Drying**

After impregnation, the sample is thermally treated through drying and calcination. Drying is performed to eliminate any solvent added to the support in the impregnation step, and is necessary to achieve supersaturation and precipitation of the solid phase on the pore surface. The sample is typically heated in an oven to the boiling point of the solvent, allowing for complete evaporation of the solvent. The removal of water from the pores of the support causes the precursor concentration to increase until saturation is reached, and crystallization of the salt on the pore surface will eventually take place [18].

The rate of drying can influence the distribution of the active phase on the support, which again affects the catalytic properties. Thus, the drying process needs to be performed under studied and controlled conditions. An improper drying process can cause intermittent concentration distributions, as the rate affects both the pore- and the particle profiles. In order to obtain uniform deposits and prevent gradients from arising, the crystallization process should proceed at a rate that is neither too fast nor too slow [17].

A too slow rate may cause evaporation to take place at the meniscus. Most of the solute will then be concentrated down the pore, and at the end of the crystallization process, the salt will, for the most part, be positioned at the bottom of the pore or at the particle center, as shown in Figure 2.2a. The opposite turn out, illustrated in Figure 2.2c, happens if the drying take place too fast. Contradictory to the slow-drying case, the evaporation process will, in this situation, mainly occur deep in the pore. Due the rapid temperature changes, a temperature gradient will arise and the solution will be driven toward the outside of the particle. At the end of the crystallization process, most of the salt will then be positioned at the top of the pore, or at the outer part of the particle. An ideal drying rate, resulting in

uniformly dispersed particles on the surface, will give a pore- and particle profile as in Figure 2.2b. This rate is, however, hard to predict, and needs to be established experimentally.

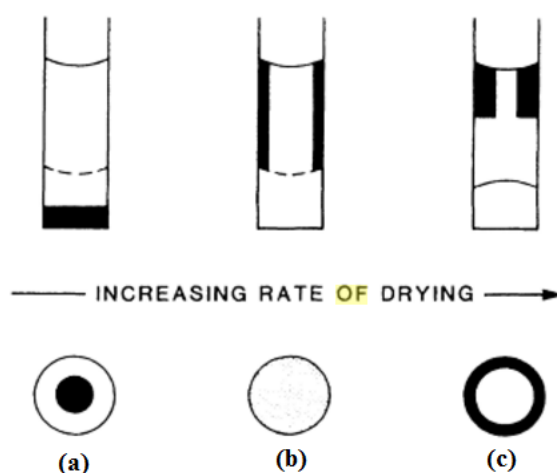


**Figure 2.2.** Pore and particle profiles as function of drying rate [17]. (a) A too slow rate causes crystallized salt to be located at the bottom of the pore or at the particle center. (b) An ideal drying rate results in uniformly dispersed particles. (c) A too fast drying rate causes crystallized salt to be located at the top of the pore or at the outer part of the particle.

### 2.3.3 Calcination

As all of the liquid is eliminated in the drying process, the system's solid/liquid interface will now be replaced by a solid/gas interface [18]. However, if the dehydrated catalyst is exposed to a moist atmosphere after being dried, the crystallized salt may re-dissolve, as the catalyst still exists in an unstable state. By performing calcination, the salt is converted into an oxide or metal and thereby the dispersion, obtained after drying, is halted and the distribution develops into a stable state [17].

### 2.3.4 Electrostatic adsorption

There are other ways to manipulate the precipitation process of a catalyst during the synthesis, next to controlling the rate of drying. By controlling the pH of the precursor solution during impregnation, the manner in which the support surface and the dissolved catalyst precursor interacts with one another can be controlled, which may affect the precipitation process, and thereby the final obtained dispersion of the catalyst.

In this project, alumina is used as support for the platinum-based catalysts. Alumina contains several types of hydroxyl groups, with linear hydroxyl groups of anionic nature being among the main types. These groups are the key to describe what happens when alumina interacts with a metal containing precursor, as they act as anchoring sites for the

metal particles. In contact with water, the linear hydroxyl groups will react with protons and OH<sup>-</sup> groups, which creates a surface charge on the support [16]. These surface charges give rise to electrostatic adsorption of metal ions of opposite charge from a precursor, and is fundamental for creating catalysts. What kind of charge the support surface obtains, depends on the acidity of the impregnating solution and the isoelectric point of the support. Alumina has an isoelectric point of about 8.5, which means that at this pH, the oxide surface is neutral and of no charge [18]. As the alumina is mixed with a liquid, the terminal hydroxyl groups on the oxide surface of the support will be either protonated and become positively charged, or deprotonated and become negatively charged, depending on whether the pH of the impregnation solution is below or above the point of zero charge for the support, respectively.

To make a Pt/Al<sub>2</sub>O<sub>3</sub> catalyst, chloroplatinic acid, H<sub>2</sub>PtCl<sub>6</sub>, is a common precursor to use to obtain negatively charged platinum ions. An aqueous solution of chloroplatinic acid dissociates into H<sup>+</sup> and PtCl<sub>6</sub><sup>-</sup> ions, and the acidic solution will have a low pH. Because of the acidity, the hydroxyl groups on the alumina will be protonated and become positively charged OH<sub>2</sub><sup>+</sup>-ions. The surface can then electrostatically adsorb the anionic metal complexes, PtCl<sub>6</sub><sup>-</sup>, from the precursor, and the active metal phase connects to the support [18]. Such anchoring of metal complexes to the support through electrostatic adsorption, facilitates obtainment of high dispersion after drying and calcination.

## 2.4 Catalyst characterization

Catalyst characterization is used to target information about both the catalyst support and the active metal phase. There are numerous different techniques available for determining a catalyst's physical and chemical properties, where the ones explored in this project include Nitrogen Physisorption, Volumetric Chemisorption, X-ray Diffraction (XRD) and X-ray Fluorescence (XRF). Theory regarding these methods and techniques will be presented in the following sections.

### 2.4.1 Nitrogen Physisorption

Nitrogen gas adsorption is a method used to obtain information about the surface area, the pore distribution and the pore volume of a catalyst.

In general, it is advantageous to have a high surface area in order to maximize the dispersion of the active component. This can be accomplished by having a large number of small pores [19]. The surface area is determined by letting an inert gas, such as nitrogen, physisorb on the surface of a porous material. When the porous material is a catalyst, the gas can physisorb on both the support and on the active material of the catalyst. By determining the amount of gas needed to form a complete monolayer on the surface, and with knowledge of how much area one adsorbate-molecule requires at the experiment conditions, the total surface area can be estimated [16].

In nitrogen adsorption, this is done by physisorption of  $N_2$  at the liquid nitrogen temperature (77 K) and by applying an adsorption isotherm. One such isotherm, commonly used to estimate surface areas, is the Brunauer, Emmet and Teller (BET) isotherm. The BET theory describes physical adsorption of gas molecules on a solid surface, and concerns multilayer adsorption. The molecules in the first layer is assumed to act as sites for the molecules in the second layer, which in turn act as sites for molecules in the third layer and so on. The BET-model is thus an extension of the Langmuir isotherm, which is based on the assumption of monolayer adsorption. However, with the introduction of several layers, some further assumptions need to be established [16, 19]. The BET isotherm is only valid under the following assumptions:

- Equal rates of adsorption and desorption in any layer
- In the first layer, molecules adsorb on equivalent adsorption sites
- The adsorption energy for the second and following layers are the same and equals the condensation energy
- The adsorption energy for the first layer is independent of, and larger than, that of the higher layers
- The multilayer grows into infinite thickness at saturation pressure

The BET isotherm is expressed in Equation (2.3).



$$\frac{P}{v_a(P_0 - P)} = \frac{1}{V_0 \cdot \chi} + \frac{(\chi - 1) P}{V_0 \cdot \chi P_0} \equiv \eta + \alpha \frac{P}{P_0} \quad (2.3)$$

In the above equation,  $P$  and  $P_0$  is the adsorption pressure and equilibrium pressure of the condensed gas,  $v_a$  denotes the total adsorbed gas quantity while  $V_0$  is the monolayer adsorbed gas quantity. The constant  $\chi$  denotes the BET-constant, and is the ratio between the adsorption heats of the first and next molecular layer, respectively.

The volume  $V_0$  can be found from Equation (2.3) by plotting  $\frac{P}{v_a(P_0 - P)}$  versus  $\frac{P}{P_0}$ . This yields a straight line that intersects the y-axis in  $\eta = \frac{1}{V_0 \cdot \chi}$  and has a slope given by  $\alpha = \frac{(\chi - 1)}{V_0 \cdot \chi}$ . The gas quantity adsorbed in the first monolayer can be found by combining the intersection- and slope expressions, resulting in  $V_0 = \frac{1}{\alpha + \eta}$ .

The surface area per mass of catalyst,  $S_{BET}$ , can then be calculated according to Equation (2.4).

$$S_{BET} = \frac{P \cdot V_0 \cdot A_0}{T \cdot m_{cat} \cdot k_B} \quad (2.4)$$

In Equation (2.4),  $A_0$  is the area one adsorbate molecule occupies on the surface,  $T$  is the temperature,  $m_{cat}$  is the mass of the catalyst and  $k_B$  is the Boltzmann constant [16].

Even though the BET-method is a valuable technique in finding the surface area, it has some limitations. Due to the assumption of monolayer being formed on the pore walls of the catalysts, the BET equation is in principle only applicable to non-porous and macro- and mesoporous materials. For microporous materials, it is hard to separate the monolayer formation process from the micro pore filling process, and hence, the method does not provide a reliable way of finding the surface area of microporous materials [20].

The pore size distribution and the pore volume can be determined using the same equipment as for determination of the surface area [19]. The properties can be found by applying the Barrett-Joyner-Halenda (BJH) method, which is based on the Kelvin equation and is corrected for multilayer adsorption. The theory uses the principle of capillary condensation in the pores, and can be applied to find the pore sizes of meso- and small macro pores, with diameters ranging from 2 nm to over 50 nm [21].

The model is applied to a hysteresis loop in the adsorption and desorption isotherms, which becomes apparent by extending the pressure beyond the conditions required for adsorption of an average monolayer on a sample. The point at which a monolayer is completely formed is denoted by “point B” in Figure 2.3. By further increasing the adsorptive gas pressure, a build-up of multilayers will occur and the gas will start to condense in the pores. The pores will gradually be filled with liquid as the pressure increases, until the saturation point, at

which all of the pores are filled with liquid. After this point, the adsorptive gas pressure is gradually reduced and the condensed gas will steadily evaporate off the system. This subsequent removal of gas from the pores provides for a hysteresis effect; the gas will leave the pores at lower equilibrium pressures than what it entered at, because of the capillary forces that have to be overcome [16, 22]. Information about the pore size and the pore volume can be found by evaluating the adsorption and desorption branches of the isotherms and the hysteresis between them. An illustration of the isotherms, and the resulting hysteresis loop, is shown in Figure 2.3 [16].

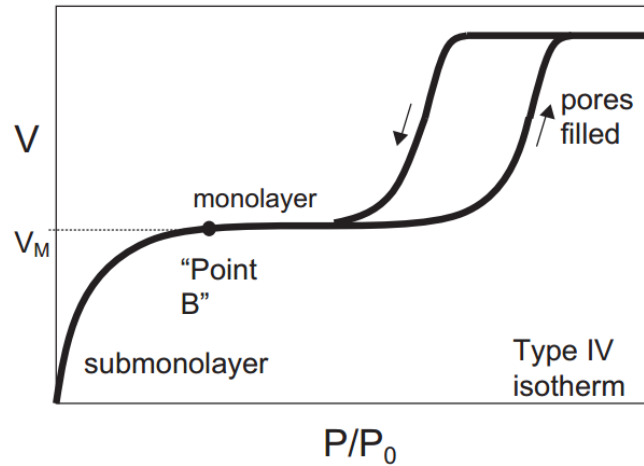


**Figure 2.3.** Hysteresis effect resulting from capillary condensation and evaporation of  $N_2$  in the pores [16]. High relative pressures are used to fill the pores with liquid, producing the ascending part of the isotherm. Subsequent lowering of relative pressure, causes evaporation of the liquid, reflected by the descending part of the isotherm.

In the BJH-method, the Kelvin equation is used to obtain the pore filling, and the pore size and pore volume can subsequently be found. The relative vapor pressure,  $P/P_0$ , at which capillary condensation takes place, is related to the Kelvin equation in accordance with Equation (2.5).

$$\ln\left(\frac{P}{P_0}\right) = -\frac{2\sigma V_m \cos\varphi}{rRT} \quad (2.5)$$

In Equation (2.5)  $P$  is the actual vapor pressure,  $P_0$  is the saturation pressure,  $\sigma$  and  $V_m$  is the surface tension and molar volume of liquid nitrogen, respectively,  $r$  is the pore radius, and  $R$  and  $T$  denotes the gas constant and the measuring temperature. The symbol  $\varphi$  represents the contact angle between capillary condensate and the pore walls, and is usually assumed to be zero [23].

## 2.4.2 Volumetric Chemisorption

Selective chemisorption is one of the most frequently used technique for characterizing metallic catalysts [24]. Whereas multilayer nitrogen physisorption is used to determine the total surface area, including both the support and the metal, selective chemisorption gives information of the active metal's surface area alone, and the dispersion of it on the catalyst.

It is usually desirable to have as much of the active metal as possible deposited on the surface, where it is the most accessible. The method is thus used to determine the total amount of surface atoms accessible for adsorption, and the catalytic surface area is assumed to be proportional to the number of active sites on the surface. The dispersion,  $D$ , is defined as the ratio of number of metal atoms on the surface,  $n_s$ , to the total number of metal atoms in the sample,  $n_t$ , as given in Equation (2.6).

$$D = \frac{n_s}{n_t} \times 100\% \quad (2.6)$$

In selective chemisorption, a gas that chemisorbs selectively only on the metal, and not on the support, is used. Common gases that behave this way, and that are used as selective adsorbates for many different supported catalysts, are CO and H<sub>2</sub>.

In volumetric chemisorption, the quantity of gas adsorbed to form monolayer coverage is measured by increasing the pressure, ideally resulting in the Langmuir isotherm. The Langmuir isotherm is based on the assumption of a homogeneous surface and absence of interactions between the adsorbed molecules. As most real surfaces are heterogeneous and there often exist repelling forces between neighboring adsorbed molecules, few chemisorption processes actually obey these assumptions over the whole area of adsorbed molecules [25].

The ideal Langmuir isotherm is illustrated in Figure 2.4. Extrapolation from the saturation pressure to zero pressure gives the H<sub>2</sub> or CO volume adsorbed on the metal,  $v_{ads}$ , required to form monolayer coverage.

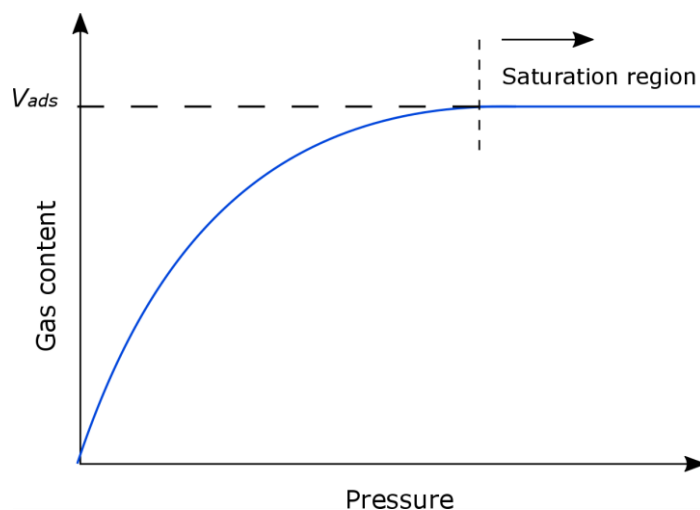


**Figure 2.4.** The ideal Langmuir isotherm with quantity of gas adsorbed as a function of pressure. Ideally, a flattening of the isotherm is obtained when monolayer coverage is reached. The figure was made using Inkscape.

Once the required volume to form monolayer coverage is found, the dispersion can be calculated from Equation (2.7).

$$D = \frac{v_{ads}M_wF}{x_m} \quad (2.7)$$

In Equation (2.7),  $v_{ads}$  is the uptake of chemisorbed molecules,  $M_w$  is the molecular weight of the metal,  $x_m$  is the weight fraction of the metal in the catalyst and  $F$  is adsorption stoichiometry [25].

As hydrogen adsorbs dissociatively on metals [25], the stoichiometric adsorption factor can be assumed to equal two in the case of hydrogen on platinum; one hydrogen molecule will cover approximately two platinum sites, as shown in Figure 2.5.

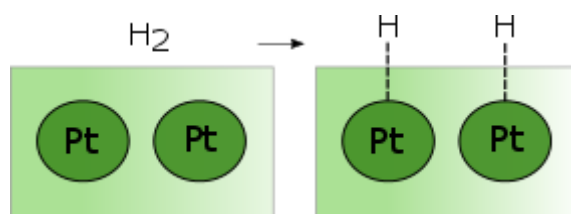


**Figure 2.5.** Dissociative adsorption of hydrogen on platinum. One hydrogen molecule will cover approximately two platinum sites, assuming a stoichiometric adsorption factor of 2 for  $H_2$  on Pt. The figure was made using Inkscape.

In the case of CO, this compound can chemisorb on metals in several different ways, i.e. linearly, bridge bound or dissociatively [25]. It is, however, commonly assumed that for

the case of CO chemisorbed on platinum, the chemisorption is single-sited with a stoichiometric adsorption factor equal to one; one CO-molecule will cover approximately one platinum site [26]. This is illustrated in Figure 2.6.

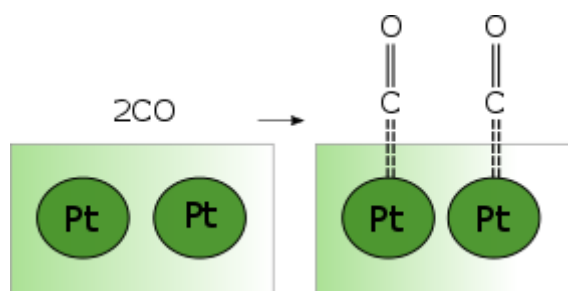


**Figure 2.6.** Single-sited chemisorption of CO on platinum. One CO molecule will cover approximately one platinum site, assuming a stoichiometric adsorption factor of 1 for CO on Pt. The figure was made using Inkscape.

### 2.4.3 X-ray Diffraction

X-ray diffraction is a technique used to identify crystalline phases from diffraction patterns and can also be used to obtain an indication of the crystal's particle size. As the method is based on periodic structural parameters, the technique only allows for phase identification of crystalline materials, and amorphous and too small particles cannot be detected.

In XRD, the sample is “attacked” by waves consisting of high-energy photons. For interference to occur, a wave must encounter a series of regularly spaced obstacles, i.e. atoms in the crystal's periodic lattice planes, which are able to scatter the X-ray photons. Beams of elastically scattered X-rays will interfere with one another as they leave the crystal, and X-rays scattered in the same phase will produce constructive interference. It is this event that causes diffraction peaks observed in XRD.

Constructive interference only happens when Bragg's relationship is fulfilled. The lattice spacing, which is characteristic for a specific compound, can be found by measuring the angles at which constructive interfering X-rays leave the crystal and applying Bragg's law, presented in Equation (2.8).

$$n\lambda = 2d\sin\theta; \quad n = 1,2,3 \dots \quad (2.8)$$

Here,  $\lambda$  is the wavelength of the X-rays,  $d$  is the distance between two lattices,  $\theta$  is the angle between the incoming X-ray and the normal to the reflecting lattice plane and  $n$  is the diffraction order [27]. From Equation (2.8) it can be seen that there is an inverse proportional relationship between  $\sin\theta$  and the lattice spacing,  $d$ , for a given wavelength and diffraction order. Thus, the largest spacings will occur at the smallest angles.

In XRD fundamentals, Bragg's law is accompanied by Ewald's sphere theory. Ewald's sphere is a construction developed with the intention of explaining the geometric

relationship between the components in a sample subjected to diffraction, and to define where the points of constructive interference will be found in the 3D space. One of the key purposes with the construction was to illustrate how desired parts of a diffraction pattern can be logged by systematically changing the alignment of the crystal [28]. When a sample consists of many, randomly oriented crystallites, there is, however, no need for rotation of the sample and one angular scan of the sample is sufficient to capture all the diffraction peaks.

XRD can also be used to calculate the average particle size by Scherrer's equation, which relates the particle size to XRD diffraction peaks. Scherrer's equation is given in Equation (2.9).

$$D_v = \frac{k'\lambda}{\beta \cos\theta} \quad (2.9)$$

In Equation (2.9),  $D_v$  is the volume weighted average crystallite size,  $\lambda$ , is the radiation wavelength,  $\beta$  is the peak integral breadth and  $k'$  is the Scherrer constant, normally taking a value between 0.89-1. The value of the Scherrer constant is variable and depends on how the peak width and the crystallite size and shape are defined. The equation builds on the assumption of a single size for all of the crystallites and can thereby be a poor model for asymmetric and multimodal size distributions [29].

#### **2.4.4 X-ray Fluorescence**

X-ray Fluorescence is a characterization technique used to obtain quantitative and qualitative information about species present in a catalyst. The method hence provides for precise determination of a sample's chemical composition, and can be used to target contaminants.

In XRF, the sample to be tested is irradiated with X-rays and the composition is determined by the fluorescence the sample emits. The fluorescence has wavelengths that are characteristic to the relevant elements the sample comprises, and hence allows for component identification.

In Figure 2.7, the process is illustrated on an atomic level.

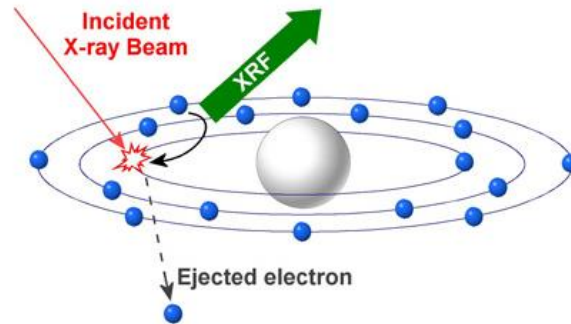


**Figure 2.7.** Principle of XRF [30]. An incoming X-ray knocks out an electron of an atom. To regain stability, an electron from an outer orbital takes over the position, and the excess energy the electron holds is emitted as fluorescent X-rays.

When an incoming X-ray hits an atom in a material, an electron in one of the orbitals surrounding the nucleus within the atom gets knocked out. This causes a hole to occur in the respective orbital, and puts the atom in an unstable, high-energy state. To regain a stabilized configuration, an electron from one of the outer orbitals drops into the hole. Because the injected electron adopts to a lower energy position, the excess energy the electron holds is emitted as a fluorescent X-ray. The energy difference between the knocked out electron and the replacement electron is characteristic to the atom at which got hit, and the emitted fluorescent X-ray is thereby directly related to a specific element being analyzed [30].

## 2.5 Gas Chromatography

### 2.5.1 Principle

Gas Chromatography (GC) is a method used to separate the components in a mixture, making it possible to obtain information about the sample's molecular composition and the amount of each specie present in the sample. A typical gas chromatograph consists of an injector, columns, flow control valves and a detector [31]. A schematic presentation of a chromatographic system is illustrated in Figure 2.8.

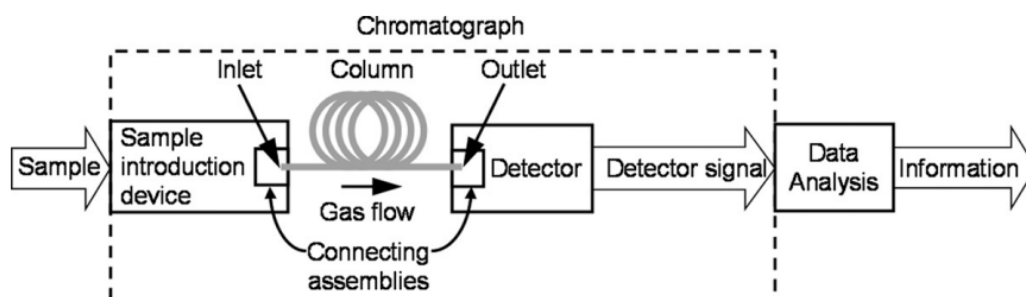


**Figure 2.8.** Block diagram of a typical chromatographic system [31]. The sample enters the system through an introduction device before it flows through a column where separation of the different components take place. At the end of the column, the separated species pass through a detector that generates an electrical signal, providing information about the sample's character and composition.

Chromatography is based on the principle of two different phases, a mobile phase and a stationary phase, where the components to be separated are distributed between the two. The mobile phase could be either a gas or a liquid, depending on the type of chromatography in question. In the case of gas chromatography, the mobile phase is a gas, commonly referred to as the carrier gas. The mobile phase, carrying the sample, filter gradually through a glass or a metal tube, known as the column, in which the stationary phase is located [32]. Separation of the components in a mixture is possible because different volatile molecules have unique equilibrium distributions between the stationary and the mobile phase. The components will thus move through the column with dissimilar velocities, reaching the end of the column at different times [33]. Consequently, the compounds in the mixture will be recognized by their characteristic retention times, which is the time a specific compound uses to pass through the column from the time it is injected. The column outlet is connected to a detector, in which the separated species in the mixture pass through. The detector senses the presence of a compound different from the carrier gas and translates this into an electrical signal, visualized as a chromatogram on the computer. As the positioning and the area of the peaks in a chromatogram are related to the identity and the molar amount of the molecular species present in the sample, the character and composition of a mixture can be known. An example of how a chromatogram may look like is illustrated in Figure 2.9.





difficulties in separating the thermal conductivities of hydrogen and helium from one another. This causes the produced peaks of hydrogen to have irregular shapes, and the element can consequently not be detected [32].

### 3 Experimental

In this chapter, a presentation of the experimental work performed in the project is given. The performed risk assessment in context to the experimental work executed in the project is given in section 3.1. This is followed by descriptions of how the synthesis and characterization of the catalysts were carried out, found in section 3.2 and 3.3, respectively. Finally, an outline of the experimental work done in context to the testing of the catalysts, is given in section 3.4.

#### 3.1 Risk Assessment

A risk assessment was done prior to starting any of the experimental work performed in this study. The likelihood and consequences of a potential, undesired incident was evaluated in terms of a standard risk matrix, as the one shown in Figure 3.1. If an incident is evaluated to be in the green area, the risk is considered acceptable. If it lies in the yellow area, risk-reducing measures should be considered, while the red area denotes an unacceptable risk where safety measures must be implemented.

LIKELIHOOD	5	Yellow	Red	Red	Red	Red
	4	Green	Yellow	Red	Red	Red
	3	Green	Green	Yellow	Red	Red
	2	Green	Green	Green	Yellow	Red
	1	Green	Green	Green	Green	Yellow
		1	2	3	4	5
		CONSEQUENTIAL				

**Figure 3.1.** Risk matrix used in the risk assessment [34]. The green area denotes an acceptable risk, while the red area represents an unacceptable risk where safety measures must be implemented. If the risk is in the yellow area, risk-reducing measures shall be considered.

Essential training concerning apparatus and chemical handling, along with a briefing regarding appropriate safety equipment in the respective lab, was given for all the relevant experiments that were to be performed in this project. Additionally, the NTNU HSE Handbook and the relevant safety data sheets for all chemical substances that were to be handled in the project were read carefully when performing the risk assessment and before entering the lab.

In this project, the main risks are associated with working with extremely flammable gases, such as H<sub>2</sub>, CH<sub>4</sub> and CO. CO is also toxic by inhalation, and can cause damage to organs by repeated exposure. When working with combustible gases under pressure, the greatest

risk involves an explosion. In this project, however, only low pressures and small amounts of gases were in use, and a fire or health concerning hazards consequently represents the greatest risk. To reduce these risks, a leak test was performed prior to all experiments involving the mentioned gases. The use of hand held detectors in the areas where the reactor is connected to pipelines, in addition to a central gas alarm system, cross sensitive to CO and H<sub>2</sub>, ensures that leaks are detected at an early stage. For the methane oxidation experiments, inert gas mixed with small amounts of H<sub>2</sub> was used to test for a leak-free system before it was exposed to methane. In addition to the risks concerning the gases, the precursor salt is characterized as both corrosive and health hazardous, and was thus handled with care, using gloves, goggles, lab coat and a face mask when contacting.

The complete risk assessment can be found in Appendix A.

## 3.2 Catalyst Preparation

Two different Pt/Al<sub>2</sub>O<sub>3</sub> catalysts were made in this project; one containing 2 wt.% Pt and one containing 0.2 wt.% Pt. A Pt/Al<sub>2</sub>O<sub>3</sub> catalyst with Pt loading of 0.2 wt.% was also synthesized and characterized during the specialization project, performed in the fall of 2015. The intention of repeating the synthesis and the experiments over a catalyst with the same loading, was to validate formerly obtained results and to get a better indication of the quality of the preparation method.

The syntheses of the catalysts were performed by applying the incipient wetness impregnation method, described in section 2.3. Chloroplatinic acid was used as a precursor of platinum, while  $\gamma$ -alumina was used as support.

Prior to the platinum impregnation, deionized water was added to the support with a pipette in order to determine the amount of liquid required to saturate the alumina. Chloroplatinic acid, in amounts sufficient to obtain the correct amount of Pt on the support for the respective catalyst, was then mixed with the pre-determined amount of deionized water and stirred well before the solution was added to the alumina support. After impregnation, the sample was dried at 120 °C for 3 hours in a ventilated drying cabinet followed by calcination in air at 500 °C for 5 hours.

The synthesis was based on an experimental procedure outlined by Sarbak et. al [35]. A detailed step-by-step recipe can be found in Appendix B, along with calculations of the necessary amount of salt needed to obtain the desired platinum content.

The weighed amount of salt and deionized water used in the precursor solutions for incipient wetness impregnation of 10 g of alumina, are given in Table 3.1.

**Table 3.1.** Weighted amount of salt and deionized water in the precursor solutions used for incipient wetness impregnation of 10 g of alumina.

Catalyst [wt.% Pt]	$m_{\text{H}_2\text{PtCl}_6,act.}$ [g]	$m_{\text{H}_2\text{O},act.}$ [g]
2	0.4226	12.066
0.2	0.0428	12.070
0.2 <sup>a</sup>	0.0425	12.066

<sup>a</sup> Catalyst synthesized during specialization project

### **3.3 Catalyst Characterization**

The apparatus and experimental method of the characterization techniques performed in this study are presented in the following sections. Nitrogen physisorption, volumetric chemisorption, XRD and XRF are the techniques presented in section 3.3.1 to 3.3.4, respectively.

#### **3.3.1 Nitrogen Physisorption**

The N<sub>2</sub> adsorption was performed in a Micrometrics tri Star 3000 Surface Area and Porosity Analyzer apparatus, in order to find the surface area, pore size distribution and pore volume as described in section 2.4.1. All catalysts, as well as a reference sample containing only the support, were subjected to N<sub>2</sub> physisorption. Between 50-100 mg of the samples was weighted out and used in the experiment. Prior to the measurement, the samples were degassed with a VacPrep 061 Degasser. The degassing was performed at 200 °C until the pressure in the degas unit was below 100 mTorr.

#### **3.3.2 Volumetric Chemisorption**

The chemisorption apparatus ASAP 2020 NTNU was used to obtain the dispersion of the catalysts, as described in section 2.4.2. Both H<sub>2</sub> and CO chemisorption were performed on the 2 wt.% sample, while the 0.2 wt.% sample only underwent H<sub>2</sub> chemisorption.

About 150-200 mg catalyst was placed in a U-tube reactor with a gently packed layer of quartz wool placed below and above the samples. The samples were heated at 120 °C for 1 hour prior to the chemisorption experiments to remove any entrained liquid from the samples. The samples were subsequently weighted again to see if the mass had changed as a result of evaporation, and the new sample weight was registered as the reactor was installed to the instrument.

The system was first exposed to a flow of helium and evacuated before the samples were reduced with hydrogen at 400 °C. The system was then exposed to another evacuation followed by a leak test integrated in the procedure before the system was exposed to hydrogen or CO during the analysis. The analysis took place at 35 °C with an equilibration interval of 20 seconds and the pressure ranging from 50 to 500 mmHg.

The 2 wt.% catalyst was subjected to two H<sub>2</sub> chemisorptions and one CO chemisorption, while the 0.2 wt.% was subjected to three H<sub>2</sub> chemisorptions. A detailed procedure description and the weighted sample masses used in each run are given in Appendix C.

### 3.3.3 X-ray Diffraction

The XRD analyzes were performed using a Bruker D8 Advanced DaVinci Diffractometer to identify the phases present in the catalysts, as described in section 2.4.3. A reference sample of only support was analyzed, in addition to the catalyst samples. The samples were analyzed for 30 minutes with the chosen  $2\theta$  angles ranging between  $10^\circ$  and  $75^\circ$ . The settings of the slit opening were set to V6, meaning that the divergence slit automatically were being opened during the scan and the length of the test area, exposed to X-rays, were kept constant at 6 mm at all times. The phases were furthermore identified using DIFFRAC<sup>Plus</sup> EVA software.

### 3.3.4 X-ray Fluorescence

A Wavelength Dispersive X-Ray Fluorescence (WDXRF) Supermini200 analyzer was used to analyze the catalysts in terms of chemical composition, as described in section 2.4.4. The X-rays in the apparatus were generated from a Pd-source interacting with the catalysts sending the fluorescent X-rays.

The analysis requires the samples to be in pellet form, and the sample preparation is an important part of the measurement as it needs to be performed in a correct manner in order to obtain a homogeneous sample and avoid contaminations.

Pellets of 40 mm in diameter were prepared by mixing about 200 mg of catalyst with 2.8 g boric acid, acting as a binder. The powder mixture was further pulverized in a mortar to get a homogeneous and fine grained blend. Once this was obtained, the mixture was placed in a carefully cleaned container of right size, and put pressure on by a press machine. The finished pellets were subsequently placed in a pellet holder and covered by 6  $\mu\text{m}$  polypropylene film before they were positioned in the analyzer.

Repeated analyzes were performed for both batches of 0.2 wt.% catalyst, where the first analysis of the catalyst from the specialization project was performed in the fall, prior to the apparatus being recalibrated.

## 3.4 Catalyst Testing

The catalysts were tested in several complete methane oxidation experiments, performed at an adapted reaction rig set up by Jia Yang, Research Scientist at SINTEF Materials and Chemistry.

The purpose of the experiments was to compare the catalytic performance of the 0.2 wt.% Pt/Al<sub>2</sub>O<sub>3</sub> catalyst to that of the 2 wt.% Pt/Al<sub>2</sub>O<sub>3</sub> catalyst, and to investigate how the catalytic activity of the synthesized catalysts depended on the reactant concentrations and the stoichiometry of methane and air, present in the feed. It was also of interest to investigate if deactivation of the catalysts occurred, and if any undesired by-products were produced during the reaction.

### 3.4.1 Experimental set-up

The catalytic activity measurements were performed by conducting complete methane oxidation experiments, increasing the reactor temperature satisfactory to achieve 100% conversion of methane.

Methane, air, nitrogen and hydrogen was supplied to a fixed bed reactor through pipelines from the respective gas tanks. The hydrogen was not used in the methane oxidation experiment itself, but for leak testing the system prior to letting methane enter the reactor. Mass flow controllers (MFC) were used to control the flow of each gas and ensure that the established feed concentrations were kept in compliance at all times. Additionally, pressure controllers were installed for each flow before entering the reactor in order to keep track of the pressure and, if necessary, automatically cut of the flow to avoid accidents.

Part of the flow exiting the reactor was sent through a gas chromatograph, detecting and quantifying the different compounds present in the stream. The gas analysis was performed in an Agilent 3000 Micro Gas Chromatograph, with the mobile and stationary phase being helium and HP-AL/M, respectively. Two different columns leading to the detector were used in the set-up; channel A and channel B. Channel A was a Molsieve 5A PLOT (10 m x 0.32 mm) column, used to quantify nitrogen and methane. Channel B was a Plot U (8 m x 0.32 mm) column, used to quantify carbon dioxide. The detector itself was of type TCD.

A flowsheet of the reaction rig is shown in Figure 3.2.



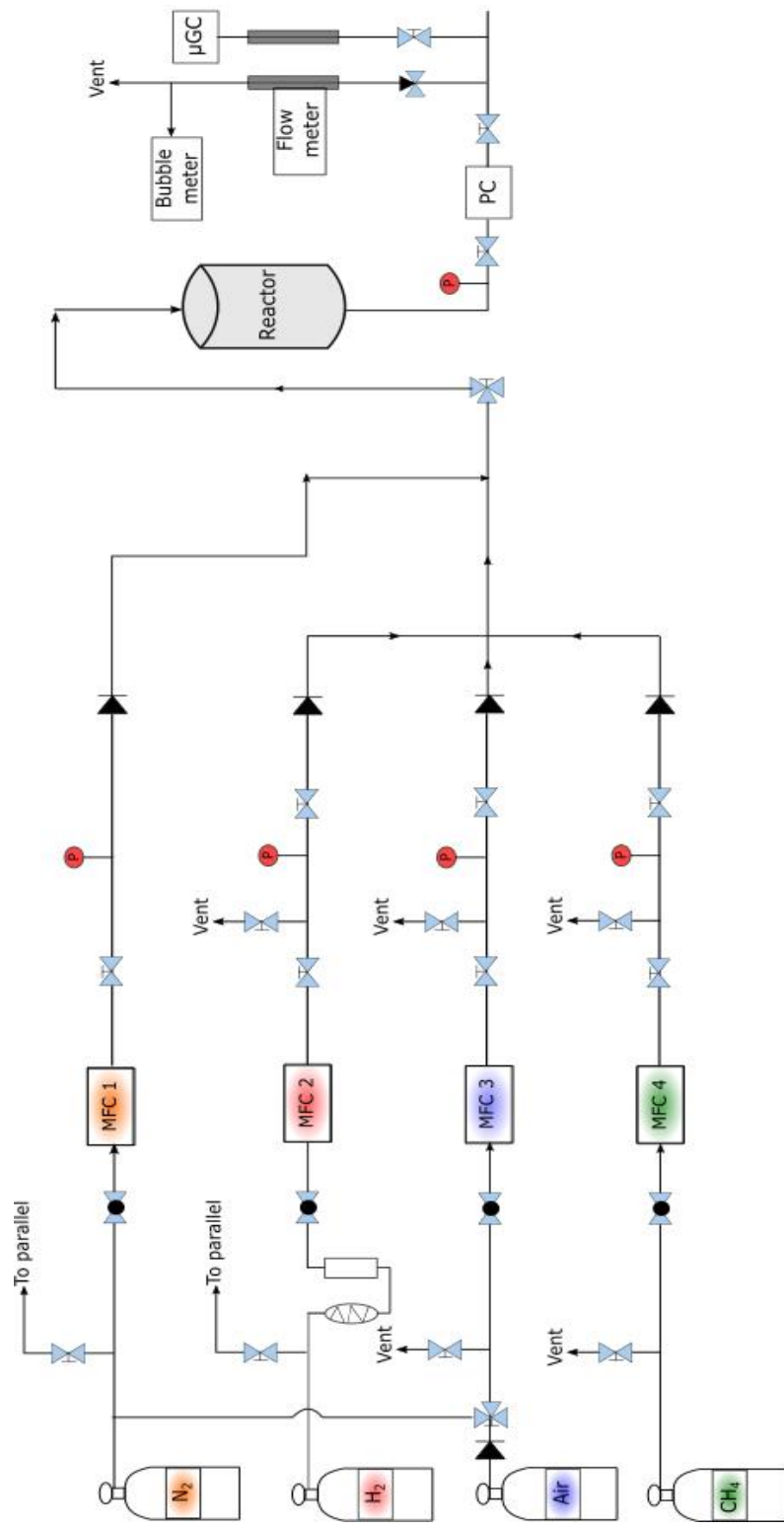


**Figure 3.2.** Flow sheet of the reaction rig, set up for methane oxidation experiments. MFC signify mass flow controllers, P denotes pressure controllers and  $\mu$ GC is the gas chromatograph. The flow sheet was made using Inkscape.

### 3.4.2 Reactor

A laboratory scale fixed bed reactor made of quartz was used to perform the methane oxidation experiments. The reactor had an inner diameter of 1 cm and a total length of 55 cm. The catalysts were placed on a porous layer, located approximately in the middle of the reactor, which had a hole in the center. A 3 mm outer diameter thermowell went from the bottom of the reactor, and through this hole, containing a moveable thermocouple to measure the temperature throughout the catalyst bed. The bottom of the reactor was enclosed by a teflon cap with a screw. The shape and dimensions of the quartz fixed bed reactor is illustrated in Figure 3.3.

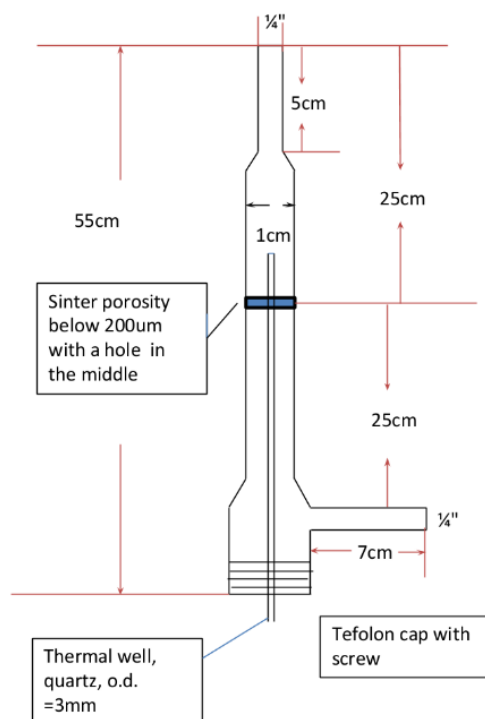


**Figure 3.3.** Shape and dimensions of the quartz fixed bed reactor, used in the methane oxidation experiments for measurements of the catalytic activity.

### 3.4.3 Methane oxidation

The synthesized catalysts had particle sizes ranging between 75-150  $\mu\text{m}$ , due to the size of the supplied alumina that was used to make the catalysts. For the catalyst of that size range that was tested during the specialization project, a pressure drop of 0.9 bar was observed. In order to minimize the pressure drop in the experiments performed in this project, the catalysts were pressed to pellets, before being crushed and fractionated to have particle sizes ranging between 250-425  $\mu\text{m}$ .

Three different samples of catalyst diluted with a 1:10 ratio of silicon carbide were prepared in this project; two containing 2 wt.% Pt catalyst (sample 1 and 2) and one containing 0.2 wt.% Pt catalyst (sample 3). The purpose of mixing the catalyst with an inert material, such as silicon carbide, is to minimize temperature gradients arising during the experiment, as the combustion reaction is highly exothermic. In addition to improve the isothermicity of the bed, the dilution ensures better packing distribution and a more uniform flow pattern. Thus, unwanted bypass effects are more likely to be avoided.

In total 13 runs of methane oxidation experiments were performed. The respective runs each sample were used in are reported in Table 3.2, along with the amount of catalyst and SiC used to prepare the different samples and each sample's bed height. The first run for each sample denotes a fresh catalyst, i.e. run 1, 7 and 9. The following runs are subsequent experiments over the same catalyst.

**Table 3.2.** Composition of the different samples of diluted catalyst used in the experiments, the bed height and an overview of the runs the different samples were used in.

Sample	Catalyst [-]	$m_{\text{cat}}$ [mg]	$m_{\text{SiC}}$ [g]	Bed height [mm]	Run [#]
1	2 wt.% Pt	196.1	1.978	21	1-6
2	2 wt.% Pt	196.2	1.972	21	7-8
3	0.2 wt.% Pt	196.1	2.034	21,5	9-13

Before starting an experiment containing a new sample, a leak test was performed by flowing the system with 20%  $\text{H}_2$  in  $\text{N}_2$ . This was followed by a cleaning of the system with pure  $\text{N}_2$  to remove any  $\text{H}_2$  left in the system before the reactants were introduced to the system.

The total feed flow was 200 Nml/min in all of the oxidation experiments. The feed consisted of  $\text{N}_2$ ,  $\text{CH}_4$  and  $\text{O}_2$ , and the feed gas composition, in terms of fuel to air ratios and reactant concentrations, varied for each run according to Table 3.3. The fuel to air ratio was varied between oxygen rich (1:5) and stoichiometric (1:2) conditions. Calculations and numeric values of the volumetric flowrates and percentage opening of the mass flow controllers for the different feed compositions, are given in Appendix D. The mass flow

controllers were calibrated by Jia Yang, Research Scientist at SINTEF Materials and Chemistry, in the spring of 2015.

**Table 3.3.** Air to fuel ratio and reactant concentrations in the different methane oxidation experiments performed. The order in which the experiments were performed in is also reported, expressed as runs. Due to the low methane concentration in run 7 and 8, the CH<sub>4</sub> gas tank was switched out by a 5% CH<sub>4</sub> in N<sub>2</sub> gas tank when these experiments were performed, in order to have the flow conform with the MFC.

Run		Ratio	Feed concentration		Comment
2 wt.%	0.2 wt.%	CH <sub>4</sub> : O <sub>2</sub>	CH <sub>4</sub> [mol%]	O <sub>2</sub> [mol%]	
1,3	10	1:5	2	10	Reference experiment
2,6	9,13	1:2	2	4	
4	11	1:2	0.5	1	
5	12	1:5	0.5	2.5	
7	-	1:2	0.25	0.5	5% CH <sub>4</sub> in N <sub>2</sub>
8	-	1:5	0.1	0.5	5% CH <sub>4</sub> in N <sub>2</sub>

For each run, the reactor was heated in steps of 50 °C until complete conversion of methane was obtained. The system was kept isothermal for 30 minutes at each temperature step, in order to obtain a steady state value of the methane conversion. The system was subsequently cooled down, stepwise, in the same manner as the heating was performed. The heating and cooling rate was set to 5 °C/min, and all experiments were performed at ambient pressure. Profiles of the temperature throughout the catalyst bed were made for each run during the heating of the reactor, and the temperature was measured at the time the furnace temperature stabilized at 300, 400 and 500 °C. For the 0.2 wt.% catalyst, temperature profiles were also obtained at 600 °C. The bed temperature was measured by moving a thermocouple throughout the bed, using a ruler to predict the positioning within the bed.

For sample 1, which was the first of the samples to be tested, the experiment with oxygen rich conditions, containing 2% CH<sub>4</sub> and 10% O<sub>2</sub>, was repeated after having one run in between, as seen in Table 3.3. This was done to ensure that the synthesized catalyst did not deactivate and was suited for sequential testing, which was the case. The experiment with stoichiometric conditions, containing 2% CH<sub>4</sub> and 4% O<sub>2</sub>, was, however, decided to be used as a reference experiment for the sequential experiments over both sample 1 and sample 3, as a lower temperature was necessary to reach complete conversion of methane under this condition. This experiment was thus repeated as the last experiment of both sequences.

For the experiments performed with sample 2 (run 7 and 8), the methane concentration was so low that the methane gas tank had to be substituted by a gas tank containing 5% methane

in N<sub>2</sub>. A correction factor of 0.72 for methane was thus used to get the correct concentration of methane with the calibrated mass flow controller. The calculations are given in Appendix D.

### 3.4.4 Processing of analysis data

As can be seen from the flow sheet in Figure 3.2, the setup is connected to a gas chromatograph. This device detects and analyzes the product stream or the feed stream, making it possible to calculate the conversion of a given compound. The conversion of component *i* can be defined as in Equation (3.1), where  $X_i$  is the conversion of component *i*, and  $F_i$  is the molar flow rate of component *i*.

$$X_i = \frac{F_{i,in} - F_{i,out}}{F_{i,in}} \quad (3.1)$$

The molar flow rate of a component can be expressed through the mole fraction of that component in the gas mixture,  $y_i$ , and the total molar flow rate,  $F_{tot}$ , according to Equation (3.2).

$$F_i = y_i \cdot F_{tot} \quad (3.2)$$

When the GC analyses a gas stream, it senses the presence of a component different from the carrier gas and translates this into an electrical signal. The area of the peak resulting from the GC analysis and the component's response factor,  $k_i$ , is related to the concentration of that component according to Equation (3.3).

$$y_i = A_i \cdot k_i \quad (3.3)$$

By inserting the correlations in Equation (3.2) and (3.3) into (3.1), the conversion of a given component can be expressed as in Equation (3.4), or Equation (3.5).

$$X_i = \frac{A_{i,in} k_i F_{tot,in} - A_{i,out} k_i F_{tot,out}}{A_{i,in} k_i F_{tot,in}} \quad (3.4)$$

$$X_i = \frac{y_i F_{tot,in} - y_i F_{tot,out}}{y_i F_{tot,in}} \quad (3.5)$$

Nitrogen can be used as an internal standard since it is inert, and thereby is neither consumed nor formed during the reaction. An internal standard is used to compensate for, or correct, the concentration of the target compound, and since it does not take part in the

reaction it is possible to use inert N<sub>2</sub> to relate the total molar feed flow to the total molar product flow. This is shown in Equation (3.6), (3.7) and (3.8).

$$F_{N_2,in} = F_{N_2,out} \quad (3.6)$$

$$y_{N_2,in} \cdot F_{tot,in} = y_{N_2,out} \cdot F_{tot,out} \quad (3.7)$$

$$F_{tot,out} = \frac{y_{N_2,in} F_{tot,in}}{y_{N_2,out}} \quad (3.8)$$

By inserting the relation in Equation (3.8) into the conversion expression in Equation (3.5), the conversion of methane can be calculated from Equation (3.9).

$$X_{CH_4} = 1 - \frac{y_{CH_4,out}}{y_{CH_4,in}} \cdot \frac{y_{N_2,in}}{y_{N_2,out}} \quad (3.9)$$

The conversion calculations can be verified by performing a mass balance over carbon. If methane undergoes complete combustion and no CO is formed, all the carbon entering the system as methane should be detected by the GC in the product stream as CO<sub>2</sub>.

$$F_{CH_4,in} = F_{CO_2,out} \quad (3.10)$$

Before 100 % conversion is reached, carbon in the form of unconverted methane will be found in the product stream in addition to the carbon existing as CO<sub>2</sub>.

$$F_{CH_4,in} = F_{CH_4,out} + F_{CO_2,out} \quad (3.11)$$

The error in the carbon balance can be calculated according to Equation (3.12).

$$E = 100\% \left( 1 - \frac{F_{CH_4,in}}{F_{CH_4,out} + F_{CO_2,out}} \right) \quad (3.12)$$

By inserting the relations from Equation (3.2) and (3.8), this can be expressed by the mole fractions of CH<sub>4</sub>, CO<sub>2</sub> and N<sub>2</sub> in the feed and product stream, obtained from the GC results.

$$E = 100\% \left( 1 - \frac{y_{CH_4,in}}{y_{N_2,in}} \cdot \frac{y_{N_2,out}}{y_{CH_4,out} + y_{CO_2,out}} \right) \quad (3.13)$$

The error in the carbon balance calculated for the different methane oxidation experiments can be found in Appendix E.

### 3.4.5 Calculation of activation energy

Kinetics of the methane combustion reaction are reported in previous studies to be first order with respect to methane and independent of the oxygen concentration [36, 37]. The reaction rate for consumption of methane can hence be expressed as in Equation (3.14), where  $k$  is the rate constant and  $C_A$  is the methane concentration.

$$-r_A = kC_A \quad (3.14)$$

The methane concentration can be expressed through the entering concentration and the methane conversion,  $X_A$ , according to Equation (3.15)

$$C_A = C_{A,0}(1 - X_A) \quad (3.15)$$

The temperature dependence of the rate constant is furthermore given by Arrhenius equation, given in Equation (3.16). Here,  $A$  is a pre-exponential factor,  $E_A$  is the activation energy,  $R$  is the gas constant and  $T$  is the absolute temperature.

$$k(T) = Ae^{-\frac{E_A}{RT}} \quad (3.16)$$

Equation (3.17) is obtained by taking the natural logarithm of Equation (3.16).

$$\ln(k) = \ln A - \frac{E}{R} \left( \frac{1}{T} \right) \quad (3.17)$$

The design equation of a packed bed, can be expressed as in Equation (3.18), where  $W$  is the weight of the catalyst.

$$\frac{dF_A}{dW} = r_A \quad (3.18)$$

With the molar flow rate being related to concentration and volumetric flow rate,  $q$ , according to Equation (3.20)

$$F = C \cdot q \quad (3.19)$$

The residence time, which describes the amount of time a fluid spends inside the reactor, is related to the volume of the reactor,  $V$ , and the volumetric flow rate of the fluid according to Equation (3.20).

$$\tau = \frac{V}{q} \quad (3.20)$$

Volume is related to weight and density according to Equation (3.21)

$$V = \frac{W}{\rho} \quad (3.21)$$

Using the relations in the above equations, the design equation can be expressed as in Equation (3.22)

$$\frac{dC_A}{d\tau} = -kC_A \quad (3.22)$$

Rearranging Equation (3.22) yields Equation (3.23) and Equation (3.24) is obtained by integration.

$$\int_{C_{A,0}}^{C_A} \frac{dC_A}{C_A} = \int_0^\tau -k d\tau \quad (3.23)$$

$$\ln[C_A] - \ln[C_{A,0}] = -k\tau \quad (3.24)$$

Inserting Equation (3.15), one obtains,

$$-\ln(1 - X_A) = k\tau \quad (3.25)$$

Inserting the Arrhenius Equation and taking the natural logarithm of both sides, results in Equation (3.26).

$$\ln(-\ln(1 - X_A)) = \ln(A) - \frac{E_A}{R} \left(\frac{1}{T}\right) \quad (3.26)$$

An Arrhenius plot can thus be made, in order to estimate the activation energy of a reaction. The slope of the curve equals  $-\frac{E_A}{R}$ , and the activation energy is consequently found by multiplying with the gas constant. An example of an Arrhenius plot is illustrated in Figure 3.4.

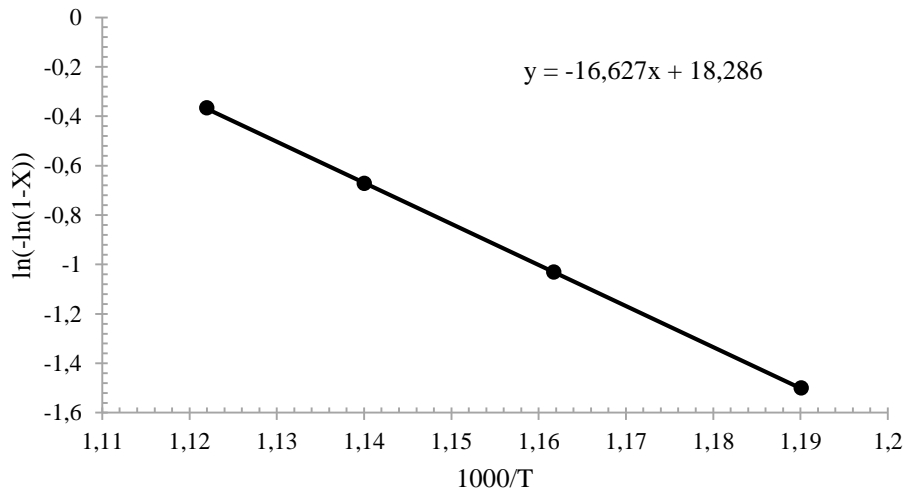


**Figure 3.4.** Example of Arrhenius plot, where the slope yields the activation energy divided by the gas constant.



## 4 Results

### 4.1 Catalyst Characterization

The characterization results of the different batches of Pt/Al<sub>2</sub>O<sub>3</sub> catalysts are given in the following sections. The results of the 0.2 wt.% catalyst, prepared and characterized during the specialization project, is also included for comparison with the catalyst containing the same amount of Pt, synthesized during this project.

#### 4.1.1 Nitrogen Physisorption

The BET surface area, pore volume and pore size of the different batches of catalysts and of the alumina support, as a reference sample, are given in Table 4.1.

**Table 4.1.** BET surface area, pore volume and pore diameter of the 2 wt.% Pt/Al<sub>2</sub>O<sub>3</sub> catalyst, two different 0.2 wt.% Pt/Al<sub>2</sub>O<sub>3</sub> catalysts and of the alumina support. The surface areas and the pore volumes and pore sizes are determined from the BET- method and the BJH-method, respectively.

Batch	BET Surface area [m <sup>2</sup> /g]	Pore volume [cm <sup>3</sup> /g]	Pore size [nm]
2 wt.% Pt	161	0.71	13-16
0.2 wt.% Pt	161	0.72	13-16
0.2 wt.% Pt <sup>a</sup>	142	0.65	13-16
γ-alumina	152	0.68	13-16

<sup>a</sup> Catalyst synthesized during the specialization project

The largest surface area is observed for the 2 wt.% catalyst and the 0.2 wt.% catalyst synthesized during this project. Both of these catalysts possess a larger surface area than that of the support, while the surface area of the 0.2 wt.% catalyst prepared during the specialization project appears to be somewhat smaller than that of the alumina. All of the measured surface areas are, however, in the same size range.

The pore volume follows the same trend for the samples as the surface area, and nor do they differ significantly from one another. The pore sizes are found to be the same for all samples, being in the mesoporous size range, with sizes ranging between 13-16 nm.

## 4.1.2 Volumetric Chemisorption

Volumetric chemisorption was performed 3 times for each of the catalysts prepared in this project. For the 2 wt.% Pt catalyst, two H<sub>2</sub> chemisorption experiments and one CO chemisorption experiment were performed. The purpose of using CO as adsorbate in addition to H<sub>2</sub>, was to see if the obtained results were consistent for both adsorbates. For the 0.2 wt.% Pt catalyst, equivalent H<sub>2</sub> chemisorption experiments were performed three times, and the results were compared to the best obtained results from the H<sub>2</sub> chemisorption experiments performed on the 0.2 wt.% catalyst synthesized and tested during the specialization project.

The obtained dispersions and particle sizes from each experiment are listed in Table 4.2. Both the total and the difference results are reported, and a further discussion regarding the implication of the two will be given in section 5.1.2.

**Table 4.2.** Dispersion and crystallite size obtained from chemisorption experiments performed on the 2 wt.% Pt/Al<sub>2</sub>O<sub>3</sub> catalyst and 0.2 wt.% Pt/Al<sub>2</sub>O<sub>3</sub> catalysts.

Catalyst	Sample number	Adsorbate	Dispersion		Crystallite size	
			Total [%]	Diff. [%]	Total [nm]	Diff. [nm]
2 wt.% Pt	1	H <sub>2</sub>	94	53	1.2	2.2
2 wt.% Pt <sup>a</sup>	2	H <sub>2</sub>	87	49	1.3	2.3
2 wt.% Pt	3	CO	91	72	1.2	1.6
0.2 wt.% Pt	1'	H <sub>2</sub>	185	117	0.61	0.97
0.2 wt.% Pt <sup>a</sup>	2'	H <sub>2</sub>	127	65	0.89	1.7
0.2 wt.% Pt <sup>a</sup>	3'	H <sub>2</sub>	3.15	2.78	36	41
0.2 wt.% Pt <sup>b</sup>	4'	H <sub>2</sub>	105	79	1.1	1.4

<sup>a</sup> Repeated chemisorption experiment

<sup>b</sup> Catalyst synthesized during the specialization project

The estimated dispersions of the 2 wt.% catalyst resemble, to some extent, in all three experiments, indicating reasonable reproducibility of the results. The dispersion from the total results ranges between 85-95%, while the difference results give a dispersion ranging between 50-75%. The crystallite size is estimated to be virtually the same in all experiments, being of 1-2 nm.

As can be seen from Table 4.2, the dispersion is found to be extremely high for the first two H<sub>2</sub> chemisorption experiments performed on the 0.2 wt.% catalyst, and resembles the results obtained for the catalyst synthesized during the specialization project. One repetition does, however, stand out as giving remarkable different results from the other experiments, both in term of dispersion and crystallite size. The dispersion of sample 3' is found to be 3% in comparison to over 100% for the other two experiments performed on the same

catalyst, and a crystallite size of 36 nm was estimated, compared to less than 1 nm for the equivalent experiments.

The adsorption isotherms for the 2 wt.% Pt/Al<sub>2</sub>O<sub>3</sub> catalyst and the 0.2 wt.% Pt/Al<sub>2</sub>O<sub>3</sub> are illustrated in Figure 4.1 and Figure 4.2, respectively, with the average difference between the two isotherms reported. Comparing the isotherms in Figure 4.2c to the other isotherms in the two figures, could enlighten why the results are so different. A further discussion regarding this, will be given in section 5.1.2.

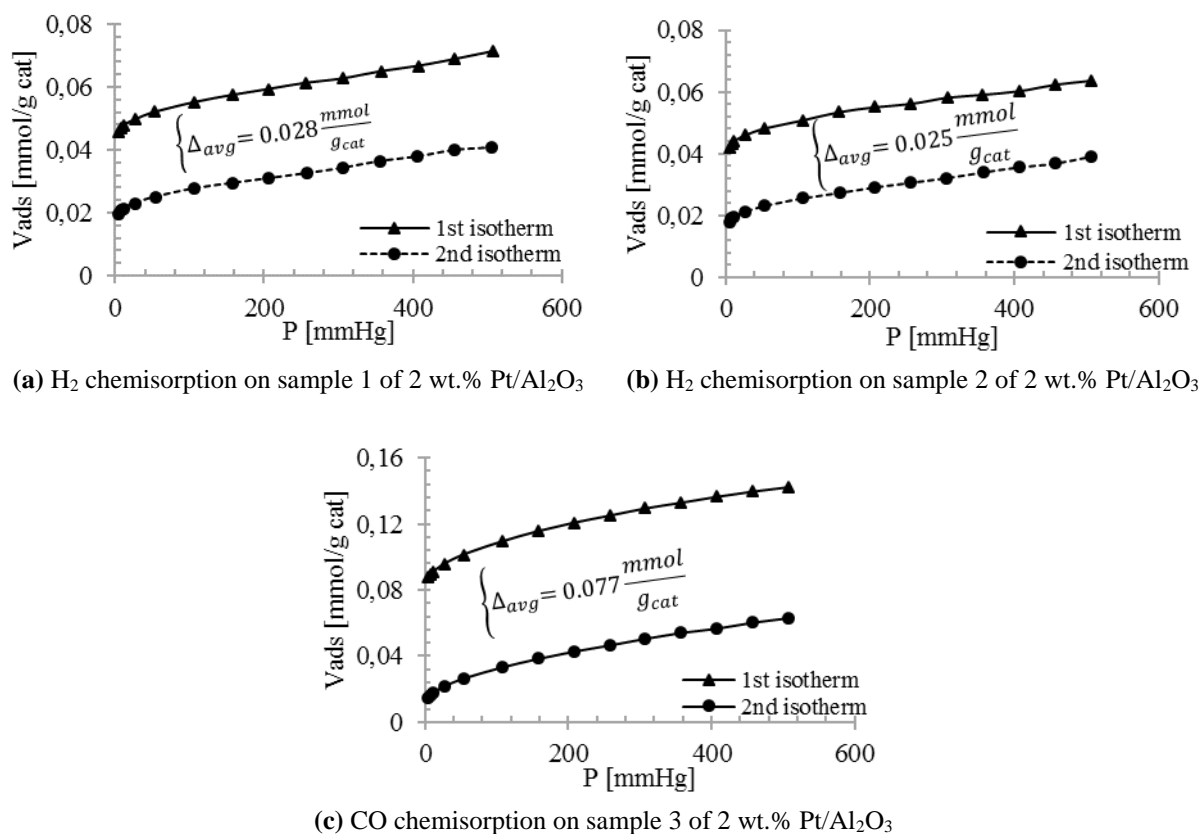


**Figure 4.1.** Adsorption isotherms from H<sub>2</sub> chemisorption (a-b) and CO chemisorption (c) of 2 wt.% Pt/Al<sub>2</sub>O<sub>3</sub> catalyst. All isotherms, and thereby the dispersion and crystallite size calculations, are estimated for pressures between 5-500 mmHg. The average difference between the first and the second isotherms are also given for each case.

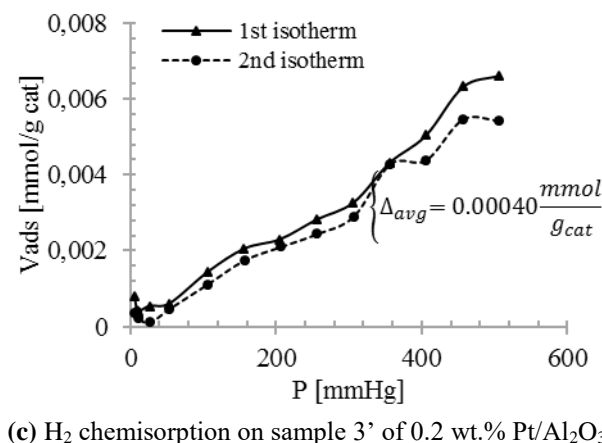
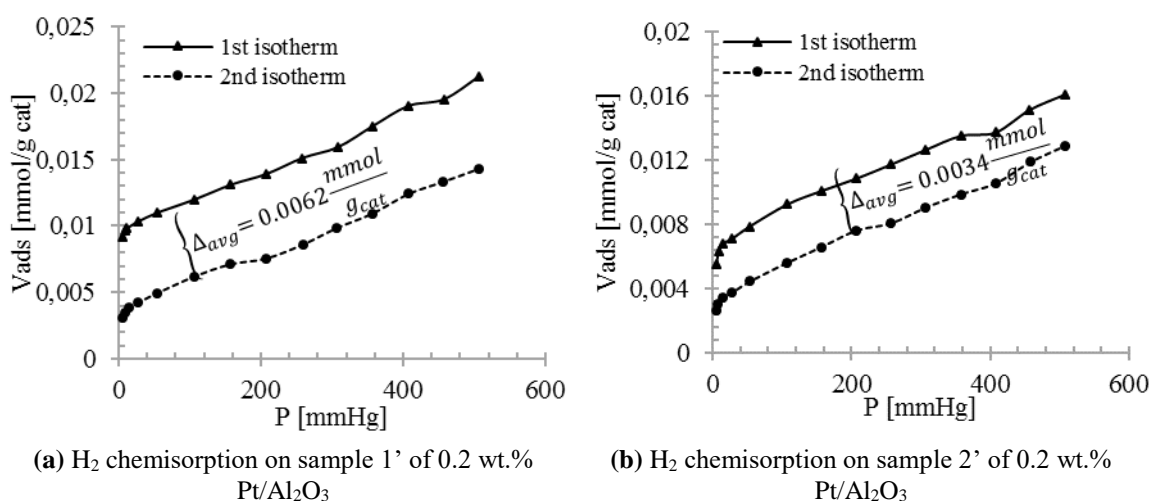


**Figure 4.2.** Adsorption isotherms from three different H<sub>2</sub> chemisorption experiments (a-c) of the 0.2 wt.% Pt/Al<sub>2</sub>O<sub>3</sub> catalyst. All isotherms, and thereby the dispersion and crystallite size calculations, are estimated for pressures between 5-500 mmHg. The average difference between the first and the second isotherms are also given for each case.

The ASAP 2020 chemisorption apparatus calculates the crystallite size according to Equation (4.1).

$$d_p = 6.00 \cdot \frac{V}{A_t} \quad (4.1)$$

In the above equation, A and V is the total surface area and the total volume of the dispersed metal, respectively, estimated during the analysis.

The crystallite size of Pt particles can also, however, be calculated from Equation (4.2).

$$d_p = \frac{108}{D [\%]} \quad (4.2)$$

Equation (4.2) is based on the assumption of spherical Pt crystallites with the Pt atom having a planar area of 0.084 nm<sup>2</sup>/site. This value is based the average of the three most common surface planes, which is (100), (110) and (111) for face centered cubic metals, such as Pt [38].

In Table 4.3, the crystallite size estimated by the chemisorption apparatus, denoted by ASAP, is compared to the calculated value, obtained by applying Equation (4.2). The values are based on the difference results from the chemisorption experiments, and could give an indication of the accuracy of the apparatus, in context to Pt being the active metal.

**Table 4.3.** Comparison between crystallite size obtained from chemisorption measurements, denoted by ASAP, and calculated crystallite size from equation adapted for Pt particles. The values are based on the difference results from the chemisorption experiments.

Sample number	Crystallite size	
	ASAP <sup>a</sup>	Calculated <sup>b</sup>
1	2.18	2.04
2	2.33	2.20
3	1.57	1.50

<sup>a</sup> Estimated from  $d_p [nm] = 6.00 \cdot \frac{V}{A}$

<sup>b</sup> Estimated from  $d_p (Pt) [nm] = \frac{108}{D[\%]}$  [38]

### 4.1.3 X-ray Diffraction

The XRD diffractograms of the different batches of Pt/Al<sub>2</sub>O<sub>3</sub> catalysts and the alumina support, as reference, are shown in Figure 4.3. The suggested phases, matching the diffraction peaks the best, are shown by different labels in the diffractogram. The phases were matched using the DIFFRAC<sup>plus</sup> EVA software.

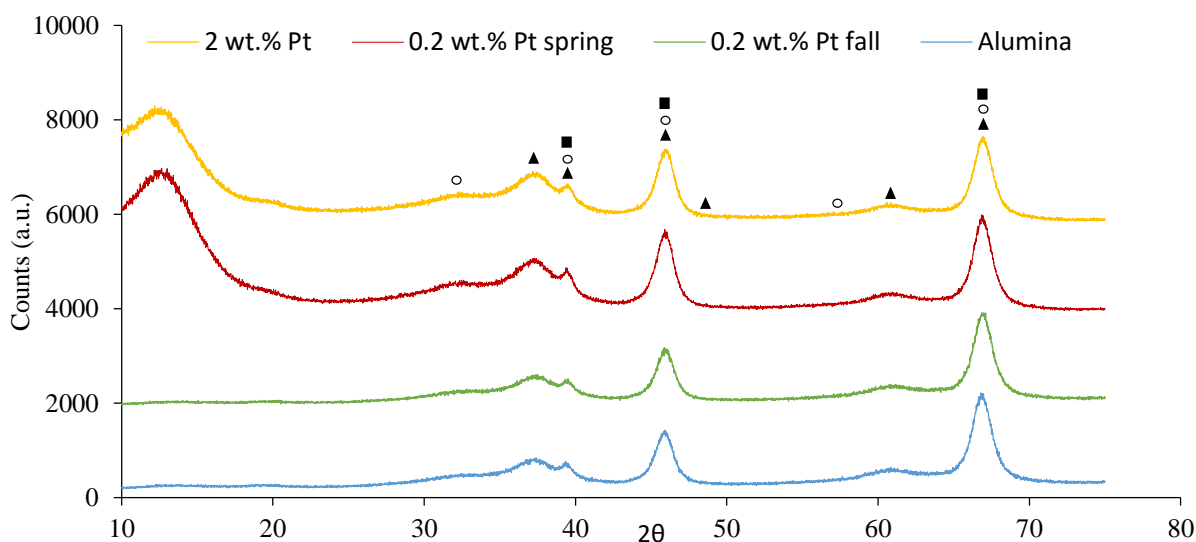


**Figure 4.3.** XRD patterns of 2 wt.% Pt/Al<sub>2</sub>O<sub>3</sub> catalyst shown in yellow, 0.2 wt.% Pt/Al<sub>2</sub>O<sub>3</sub> catalyst shown in red, 0.2 wt.% Pt/Al<sub>2</sub>O<sub>3</sub> catalyst synthesized during the specialization project shown in green and alumina shown in blue. The labels represent reference peaks matched to the diffraction pattern using DIFFRAC<sup>plus</sup> EVA software. The label ▲ denotes γ-alumina, ■ is Pt and ○ is PtO<sub>2</sub>.

As can be seen from Figure 4.3, the diffractograms of the different catalysts and the support are close to identical. The phase matching and labelling only suggests what phases the peaks might correspond to, and will be further discussed in section 5.1.3.

### 4.1.4 X-ray Fluorescence

The sample composition of the samples, obtained from XRF analyzes, is given in Table 4.4. The analysis of both batches of 0.2 wt.% catalysts were repeated to ensure the reproducibility of the instrument. The repetition of the experiment performed on the 0.2 wt.% catalyst from the specialization project was done after the apparatus had been recalibrated in order to see if this had any impact on the detected compounds, and to improve the basis of comparison between the two 0.2 wt.% catalysts.

**Table 4.4.** Sample composition of the different catalysts and the support, obtained from XRF analysis. The repetition of the analysis concerning the catalyst from the specialization project, was performed in this project after the instrument had been recalibrated.

Sample	Mass %					
	Al <sub>2</sub> O <sub>3</sub>	PtO <sub>2</sub>	Cl	Fe <sub>2</sub> O <sub>3</sub>	SiO <sub>2</sub>	K <sub>2</sub> O
2 wt. %	97.0	1.76	0.727	-	-	0.470
0.2 wt. %	98.7	0.244	0.155	0.0735	0.298	0.508
0.2 wt. % <sup>a</sup>	98.8	0.224	0.121	0.110	0.377	0.413
0.2 wt. % <sup>b</sup>	98.8	0.149	-	0.0661	1.000	-
0.2 wt. % <sup>a,b</sup>	99.5	0.165	-	0.0603	-	0.318
$\gamma$ -alumina	99.5	-	-	0.0666	-	0.411

<sup>a</sup> Repeated XRF experiment

<sup>b</sup> Catalyst synthesized during specialization project

The platinum content, calculated based on the detected PtO<sub>2</sub> content, along with the deviations from the nominal loading of platinum in each of the catalyst samples, are listed in Table 4.5.

**Table 4.5.** Calculated platinum content in each of the catalyst samples, based on the results from the XRF analysis. The deviation from the nominal loading of platinum is also reported for each sample.

Sample	Pt content	Deviation <sup>c</sup>
[-]	[mass %]	[%]
2 wt. %	1.51	- 25
0.2 wt. %	0.210	+ 5
0.2 wt. % <sup>a</sup>	0.192	- 4
0.2 wt. % <sup>b</sup>	0.128	- 36
0.2 wt. % <sup>a,b</sup>	0.142	- 29

<sup>a</sup> Repeated XRF experiment

<sup>b</sup> 0.2 wt. % Pt catalyst from specialization project

<sup>c</sup> Deviation from nominal loading

As can be seen from Table 4.5, the 2 wt. % Pt catalyst seems to only contain 1.5 wt. % Pt, according to the XRF results, which is a negative deviation of about 25% from the nominal loading. The 0.2 wt. % Pt catalyst synthesized during this project appears to contain platinum in amounts very close to the nominal value, only deviating with about  $\pm 5\%$ . The 0.2 wt. % Pt catalyst synthesized during the specialization project, however, appears to contain about 30% less than the nominal loading.

## 4.2 Catalytic Activity

The activity of the 2 wt.% Pt and the 0.2 wt.% Pt catalyst was investigated at different feed conditions, as described in section 3.4.3. The results of the reference experiments as well as the temperature profiles throughout the catalyst beds will be presented in section 4.2.1 and 4.2.2, respectively, as these findings may highlight if deactivation has taken place. Furthermore, the effect the metal loading has on the catalytic activity was investigated by comparing the performance of the 2 wt.% catalyst to that of the 0.2 wt.% catalyst under the same conditions, which results are presented in section 4.2.3. Moreover, the effect of the molar feed ratio of methane to oxygen was studied as well as the effect of the reactant concentrations, and the respective results are presented in section 4.2.4 and 4.2.5. The results of the 2 wt.% catalyst are chosen to be presented with regards to these results, as this catalyst generally shows better performance, and the concentration was reduced to the lowest amount over this catalyst, providing for a wider basis of comparison.

As outlined in section 3.4.3, a total of 13 runs of methane oxidation experiments were performed. Since this has been a comparable study of catalysts with different loading and their performance at different feed concentrations, other parameters have intentionally been held constant in each run. The total feed flow, residence time and gas hourly space velocity (GHSV), applying to all runs, are summarized in Table 4.6. The calculations of the residence time and the gas hourly space velocity can be found in Appendix F.

**Table 4.6.** Numeric values of total feed flow, residence time and GHSV, kept constant in all runs of the methane oxidation experiments.

Parameter	Abbreviation	Value	Unit
Total feed flow	$q_{\text{tot}}$	200	Nml/min
Residence time	$\tau$	2	s
Gas hourly space velocity	GHSV	61200	Nml/h·g <sub>cat</sub>

In each run, the reactor was heated stepwise until complete conversion of methane was obtained, and the system was subsequently cooled back down to room temperature. The conversion as a function of the temperature has been plotted during the heating and the cooling process for all runs, and a resultant, representative graph is shown in Figure 4.4.



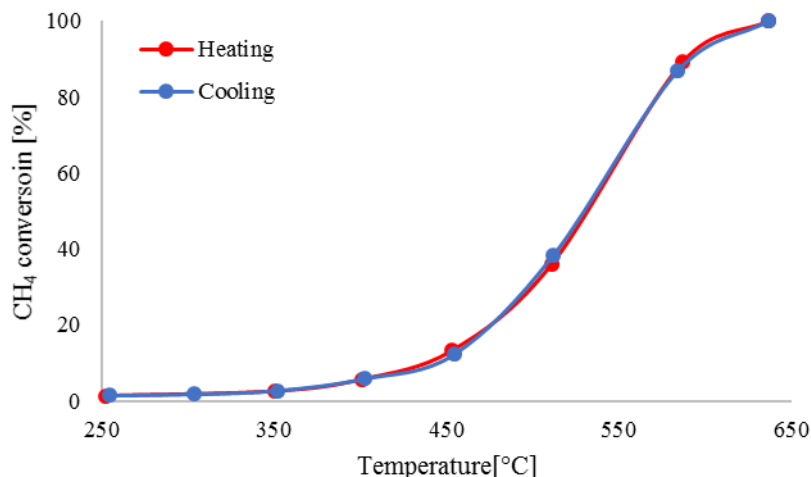


**Figure 4.4.** Methane conversion as a function of temperature during heating of the reactor, shown in red, and cooling, shown in blue. The temperature was measured by a thermocouple at the inlet of the catalyst bed. The illustrative graph is obtained with CH<sub>4</sub> and O<sub>2</sub> concentrations of 2% and 10%, respectively.

In Figure 4.4, an overlap between the heating and the cooling curve is observed. This was more or less observed for all runs, and indicates that the temperature in the system is kept under firm control. Only the heating curve will, however, be taken into account in the figures presented in the following sections, in order to keep it orderly as the figures have comparative purposes.

No CO was detected by the GC during the any of the experiments, neither with oxygen rich nor stoichiometric feed. It is therefore reasonable to assume that CO<sub>2</sub> is the only carbon containing compound present in the product stream, apart from unconverted methane. The limit of detection of a TCD is, however, on the order of 100 ppm [39], which means that in practice, there may be small amounts of CO or other carbon containing compounds present in the product stream, that are too low to be detected by the GC.

As stated in section 3.4.3, the catalysts were pressed to pellets and crushed in order to increase the particle size to minimize the pressure drop during the reaction. For the catalyst with a particle size of 75-150  $\mu\text{m}$ , tested during the specialization project, a pressure drop of 0.9 bar was observed. Increasing the particle size to 250-425  $\mu\text{m}$  did, however, result in avoidance of pressure drop for all experiments performed during this project.

For each of the 13 runs of methane oxidation experiments performed, the temperature required to obtain a certain extent of conversion during the heating was calculated. This was done by approximating a 6<sup>th</sup> degree polynomial, fitting the temperature versus conversion curve such as the one illustrated in red in Figure 4.4. The Matlab script, used to approximate the 6<sup>th</sup> degree polynomials and to calculate temperatures at desired conversions, is given in Appendix G.

The temperature required to obtain a certain degree of conversion for different feed concentrations and metal loading is presented in Table 4.7.

**Table 4.7.** Overview of catalytic activity exhibited by the two catalysts, expressed as temperature required to obtain a certain extent of conversion under different reactant concentrations. Run 1-8 are performed over the 2 wt.% catalyst, while run 9-13 are performed over the 0.2 wt.% catalyst. The dotted lines separate sequential runs. The feed was balanced with N<sub>2</sub>.

Run	Loading [wt%]	CH <sub>4</sub> :O <sub>2</sub> ratio	Feed gas [mol %]		Catalytic activity				
			CH <sub>4</sub>	O <sub>2</sub>	T <sub>10</sub>	T <sub>30</sub>	T <sub>50</sub>	T <sub>70</sub>	T <sub>90</sub>
1	2	1:5	2	10	457	502	530	552	575
2	2	1:2	2	4	434	484	513	537	562
3	2	1:5	2	10	437	500	534	561	588
4	2	1:2	0.5	1	422	468	493	511	526
5	2	1:5	0.5	2.5	432	482	512	535	560
6	2	1:2	2	4	434	486	515	539	565
7	2	1:2	0.25	0.5	387	471	501	523	540
8	2	1:5	0.1	0.5	390	467	493	511	526
9	0.2	1:2	2	4	510	561	587	610	633
10	0.2	1:5	2	10	536	588	618	644	670
11	0.2	1:2	0.5	1	511	546	568	587	606
12	0.2	1:5	0.5	2.5	523	566	596	621	649
13	0.2	1:2	2	4	538	572	593	611	629

#### 4.2.1 Reference experiments

The methane oxidation experiment with reactant concentrations of 2% CH<sub>4</sub> and 4% O<sub>2</sub> was set as a reference experiment for the sequential runs over the 2 wt.% catalyst and the 0.2 wt.% catalyst, and was thus repeated at the end of the sequences. The results from these reference experiments could say something about whether or not the catalyst have tended to deactivate.

As can be seen when comparing run 2 to run 6 and run 9 to run 13 in Table 4.7, there are marginal differences between the runs in the beginning and at the end of each sequence. The temperatures are nearly identical in the case of the 2 wt.% catalyst, while there are some differences between run 9 and run 13 at low conversions for the 0.2 wt.% catalyst. These are, however, evened out as the conversions exceeds 50%.

The experiment with feed containing 2% CH<sub>4</sub> and 10% O<sub>2</sub> was also repeated once over the 2 wt.% catalyst, and was performed in run 1 and 3, respectively. From Table 4.7, it can be seen that oxygen rich and stoichiometric experiments were performed alternately

throughout the sequences, and it has been speculated in whether the conditions in the previous experiment has had an impact on the following experiment. The results from these runs can thus advantageously be compared, to see if having a stoichiometric experiment in between the runs impacts the results.

As seen when comparing run 1 and 3 in Table 4.7, the required temperature to obtain low conversions is initially lower in run 3 than in run 1. As the conversion exceeds 50%, however, a somewhat higher temperature is required in run 3 compared to run 1. Overall, the catalyst seems to show a, to some extent, better performance in the first run, but the differences are not remarkable. It should be taken into consideration that the first run is performed over a fresh catalyst, and hence may represent a special case. As it may take some time for a catalyst to stabilize, the observed differences should not exclusively be assigned to be due to the stoichiometric experiment in the preceding run.

## 4.2.2 Temperature profiles

Temperature profiles across the catalytic bed was measured at 300, 400 and 500 °C during the heating process of each experiment. For the 0.2 wt.% catalyst, temperature profiles were also obtained at 600 °C.

The measured bed temperatures as a function of position within the fixed bed reactor for the six sequential runs over the 2 wt.% catalyst are shown in Figure 4.5. The displayed profiles are obtained from when the furnace temperature stabilized at around 400 °C in (a) and 500 °C in (b). The dashed lines in the figure, represents the end of the catalytic bed, which height was measured to be 21 mm.

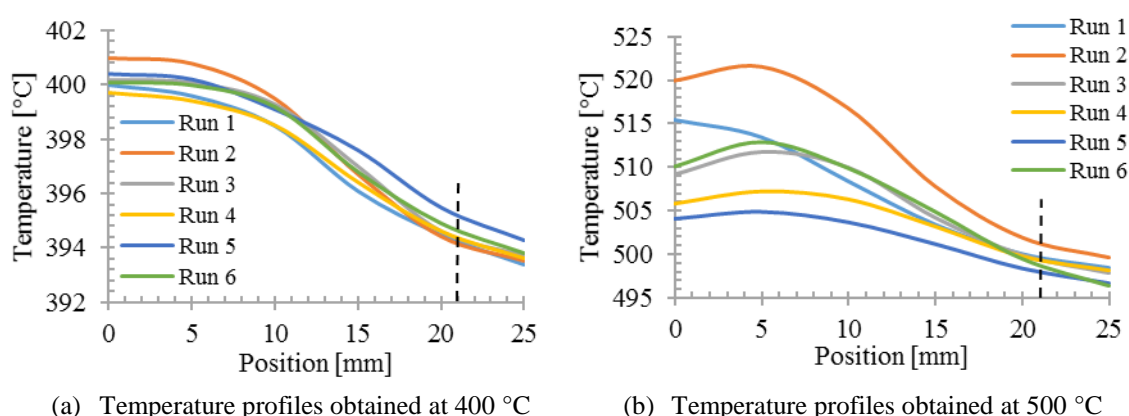


**Figure 4.5.** Measured bed temperature as a function of position within the catalyst bed, obtained during each run of the six sequential methane oxidation experiments, performed over the 2 wt.% Pt/Al<sub>2</sub>O<sub>3</sub> catalyst. The dotted lines represent the end of the bed, which had a height of 21 mm. The profiles are obtained when the furnace temperature stabilized at around 400°C in (a) and at 500 °C in (b).

The profiles do follow the same trend for each run, and there are no remarkable differences from the profile of the first to the last run, other than some variations in initial bed temperature when the furnace temperature stabilized at 500 °C for some of the runs, seen in Figure 4.5b. It can also be noted that the peak temperature through the catalyst bed seems to be shifted from the beginning of the bed, assigned as 0 mm, at 400 °C to around 5 mm at 500 °C.

The measured bed temperatures as a function of position within the bed for the sequential runs over the 0.2 wt.% catalyst are shown in Figure 4.6. The displayed profiles are obtained from when the furnace temperature stabilized at around 500 °C in (a) and 600 °C in (b). The dashed lines in the figure, represents the end of the catalytic bed, which height was measured to 21.5 mm.

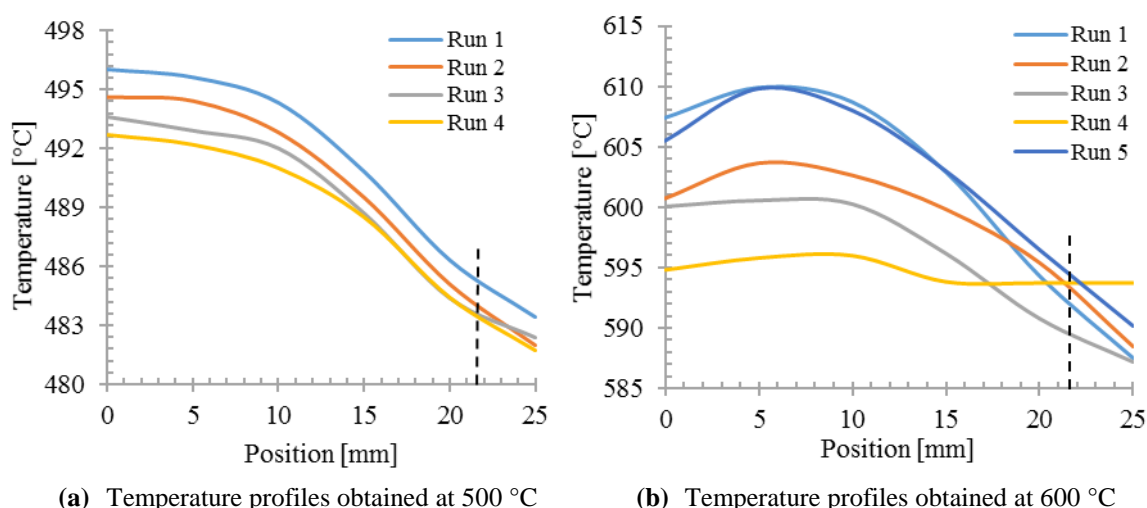


**Figure 4.6.** Measured bed temperature as a function of position within the catalyst bed obtained during each of the sequential methane oxidation experiments, performed over the 0.2 wt.% Pt/Al<sub>2</sub>O<sub>3</sub> catalyst. The dotted lines represent the end of the bed, which had a height of 21.5 mm. The profiles are obtained when the furnace temperature stabilized at around 500°C in (a) and at 600 °C in (b).

Similar as for the temperature profiles obtained over the 2 wt.% catalyst, the profiles seem to follow the same trend for each run, with the smallest differences in the profiles being observed at the lowest temperature. The shift in peak temperature that was observed at 500 °C over the 2 wt.% catalyst, is observed at 600 °C for the 0.2 wt.% catalyst. The differences in measured bed temperature between the runs are, similarly as for the 2 wt.% catalyst, larger at the highest temperature (maximum 20 K).

### 4.2.3 Effect of loading

Four different experiments were performed equivalently over both the 2 wt.% and the 0.2 wt.% catalysts and hence forms the basis of comparison of activity with regards to metal loading. Plots of temperature versus conversion for the comparable experiments are illustrated in Figure 4.7.

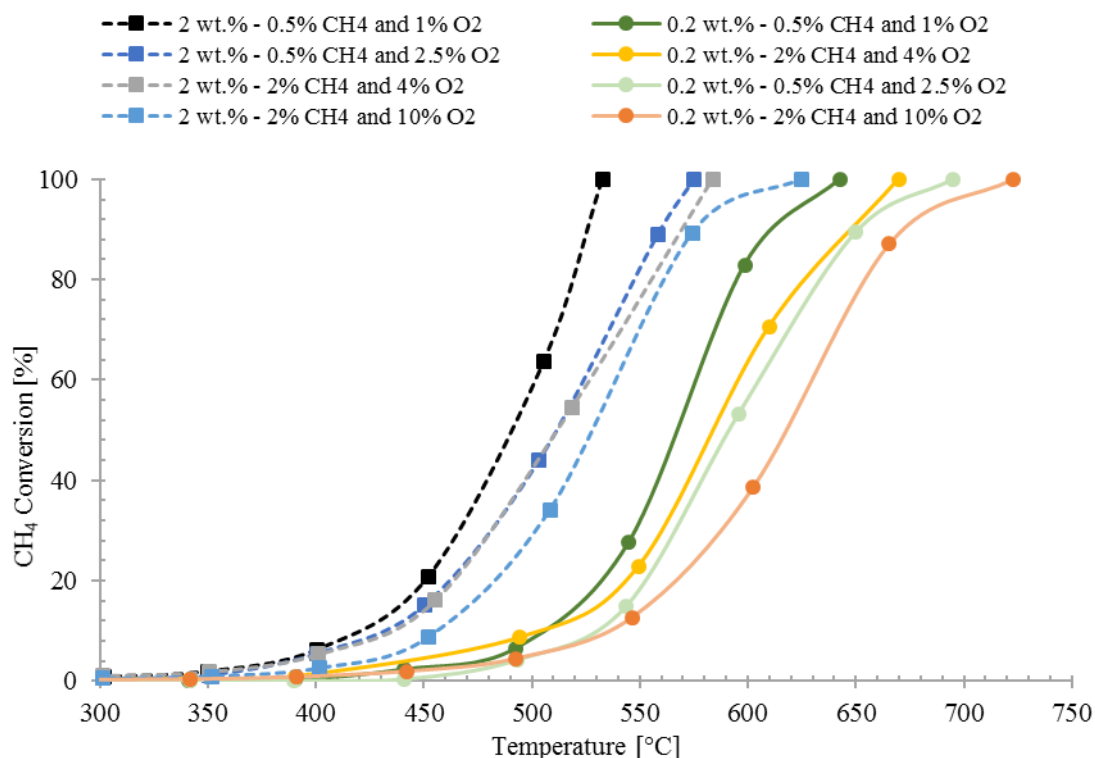


**Figure 4.7.** Comparison of temperature versus CH<sub>4</sub> conversion curves of the 2 wt.% Pt/Al<sub>2</sub>O<sub>3</sub> catalyst and the 0.2 wt.% Pt/Al<sub>2</sub>O<sub>3</sub> at matching conditions in four different experiments performed over each catalyst. The temperature corresponds to the inlet of the catalyst bed.

As can be seen from Figure 4.7, the 2 wt.% catalyst exhibit higher catalytic activity than the 0.2 wt.% catalyst, for all the tested conditions. The “poorest” reaction conditions tested for the 2 wt.% catalyst, still outperforms the “best” conditions tested for the 0.2 wt.% catalyst.

In Table 4.7, the compared conditions and results are listed in run 2-5 over the 2 wt.% catalyst, and correspondingly in run 9-12 over the 0.2 wt.% catalyst. From the results in Table 4.7, the 0.2 wt.% catalyst appears to require a temperature about 70-90 °C higher than the 2 wt.% catalyst in order to obtain the same degree of methane conversion, irrespective of the level of conversion of interest.

The activation energy, compared for the 2 wt.% catalyst and the 0.2 wt.% catalyst under equal reactant conditions, are reported in Table 4.8. The activation energies were estimated

by Arrhenius plots, as explained in section 3.4.5. The plots were made for conversions below 50%, and can be found in Appendix H.

**Table 4.8.** Activation energy compared for different loading in the four different experiments conducted over both the 2 wt.% and the 0.2 wt.% catalyst. The activation energy is estimated from Arrhenius plots, constructed for conversions below 50%.

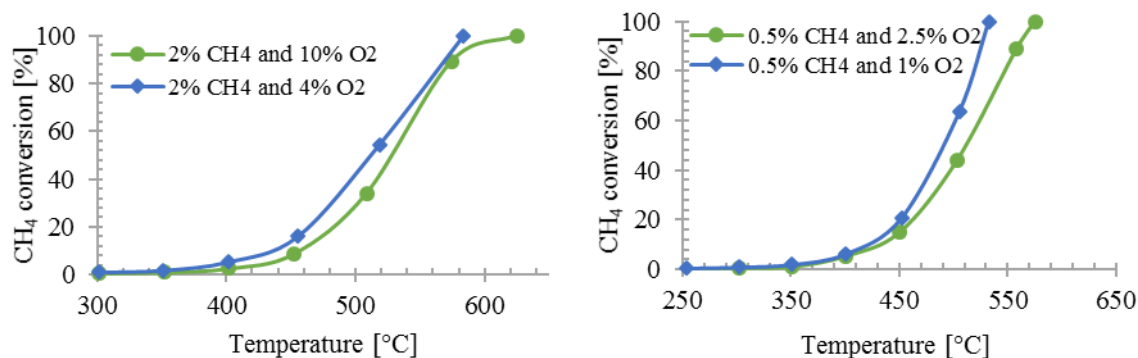
CH <sub>4</sub> :O <sub>2</sub> ratio	Feed conc. [mol %]		E <sub>A</sub> [kJ/mol]	
	CH <sub>4</sub>	O <sub>2</sub>	2 % Pt	0.2 % Pt
1:5	2	10	126	138
1:2	2	4	110	148
1:5	0.5	2.5	109	141
1:2	0.5	1	117	176

The activation energy, which represents an energy barrier that has to be overcome to attain a completed reaction, appears to be higher when the reaction is performed over the 0.2 wt.% catalyst, compared to the catalyst with higher loading.

#### 4.2.4 Effect of stoichiometry

The effect the stoichiometry of the reactants has on the catalytic activity, was investigated by conducting methane oxidation experiments with both stoichiometric and oxygen rich feed gas conditions, respectively. Two different sets of experiments were compared, and for each set, the methane concentration, and thus the partial pressure of methane, was kept constant, while the oxygen concentration was altered. CH<sub>4</sub>:O<sub>2</sub> ratios of 1:5 and 1:2 were compared, with methane concentrations of 2% and 0.5%.

The results from each set are presented graphically in Figure 4.8, expressed with plots of temperature versus conversion obtained for each condition. A CH<sub>4</sub> concentration of 2% and O<sub>2</sub> concentrations of 10% and 4%, respectively, are shown in (a), while a CH<sub>4</sub> concentration of 0.5% and O<sub>2</sub> concentrations of 2.5% and 1%, respectively, are shown in (b).



(a) 2% CH<sub>4</sub> in oxygen rich (10% O<sub>2</sub>) and stoichiometric (4% O<sub>2</sub>) conditions.

(b) 0.5% CH<sub>4</sub> in oxygen rich (2.5% O<sub>2</sub>) and stoichiometric (1% O<sub>2</sub>) conditions.

**Figure 4.8.** Inlet temperature versus conversion compared for oxygen rich and stoichiometric conditions in methane oxidation experiments over the 2 wt.% Pt/Al<sub>2</sub>O<sub>3</sub> catalyst. Oxygen rich conditions are shown in green, while stoichiometric conditions are shown in blue. (a) CH<sub>4</sub> concentration of 2% and O<sub>2</sub> concentrations of 10% and 4%, respectively. (b) CH<sub>4</sub> concentration of 0.5% and O<sub>2</sub> concentrations of 2.5% and 1%, respectively.

The rate of oxidation of CH<sub>4</sub> over the 2 wt.% catalyst was calculated at 450 °C for the different conditions, and is presented in Table 4.9 along with the obtained conversions at this temperature. At 450 °C, the reaction can be approximated as differential, as the conversion is below 20% for all cases [35]. The calculations can be found in Appendix F.

**Table 4.9.** Calculated conversions and reaction rates at 450 °C in two comparable sets of methane oxidation experiments over the 2 wt.% catalyst. The results are compared for methane to oxygen ratios of 1:5 and 1:2, with methane concentrations of 2% and 0.5% in the two sets, respectively.

CH <sub>4</sub> :O <sub>2</sub> Ratio	Feed gas [mol %]		$X_{CH_4, 450^\circ C}$ [%]	$r_{CH_4}$ [mol CH <sub>4</sub> / g <sub>cat</sub> h]
	CH <sub>4</sub>	O <sub>2</sub>		
1:5	2	10	8.31	0.0045
1:2	2	4	14.4	0.0079
1:5	0.5	2.5	15.2	0.0021
1:2	0.5	1	19.9	0.0027

In both sets, the catalyst appears to exhibit a higher catalytic activity under stoichiometric conditions than in oxygen rich conditions. Figure 4.8 displays how a lower temperature is required to obtain complete conversion of methane under stoichiometric conditions, and the improved activity is also reflected by the reaction rates in Table 4.9. At 450 °C, the highest extent of conversion is obtained under stoichiometric conditions, for both sets, and the reaction rate is correspondingly higher than for the oxygen rich conditions. Overall, the 2 wt.% catalyst appears to require a temperature of 10-30 °C more under oxygen rich

conditions, in order to obtain the same conversion as under stoichiometric conditions. This is found by comparing run 1 and 2 to each other, and run 4 and 5 to each other, in Table 4.7.

An interesting observation, when comparing the curves of stoichiometric and oxygen rich conditions in Figure 4.8, is the difference in the shape of the curves. Under oxygen rich conditions, the temperature-conversion curve seems to obtain an “S-shape”, while it, under stoichiometric conditions, appears to have a more uniform slope in the period of time after ignition. For the comparison with 2% CH<sub>4</sub> in the feed, the temperature necessary to obtain 90% conversion is almost the same for the two conditions. Under oxygen rich conditions, the catalytic activity seems to slow down after this point, and requires a steeper temperature increase in order to obtain 100% conversion. Under stoichiometric conditions, however, the temperature increase necessary to obtain a higher degree of conversion, seems to be constant, also towards the end of the reaction, where the conversion increases from 90-100%.

The “S-shaped” curve is less prominent in the case of the lower methane concentration compared, i.e. 0.5% CH<sub>4</sub>. There is still an intimation of an S-shape for the oxygen rich curve, but it resembles the curve of the stoichiometric conditions a lot more. This will be touched some more in the following section, where concentration differences are compared.

#### **4.2.5 Effect of concentration**

The catalytic activity's dependence on the reactant concentration was investigated over the 2 wt.% Pt/Al<sub>2</sub>O<sub>3</sub> catalyst by comparing experiments with different amounts of reactants present in the feed, under equal conditions in terms of stoichiometry. For the case of oxygen rich conditions, CH<sub>4</sub> concentrations of 2%, 0.5% and 0.1%, with respective O<sub>2</sub> concentrations to comply with a 1:5 ratios of CH<sub>4</sub> to O<sub>2</sub>, were compared. For the case of stoichiometric conditions, CH<sub>4</sub> concentrations of 2%, 0.5% and 0.25% with respective O<sub>2</sub> concentrations were compared.

The temperature versus conversion graphs for the different reactant concentrations in the case of stoichiometric and oxygen rich conditions, are illustrated graphically in Figure 4.9 (a) and (b), respectively.



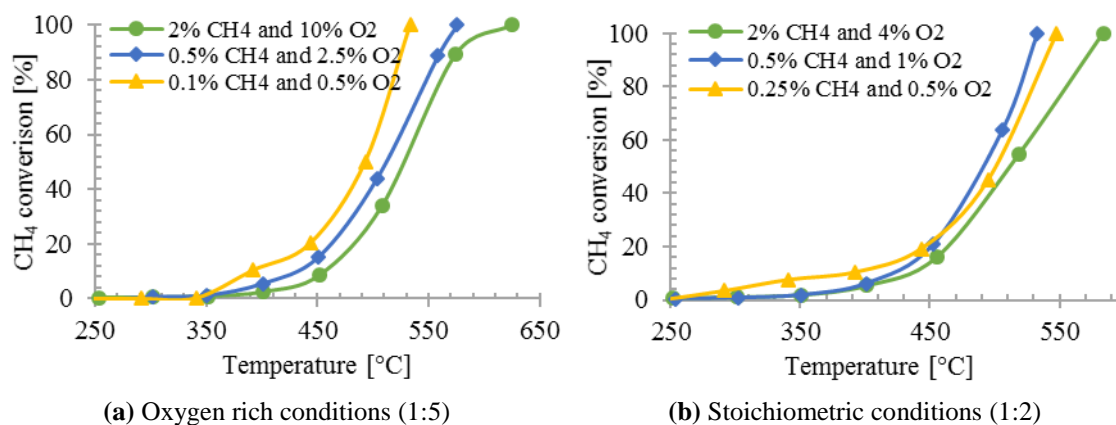


**Figure 4.9.** Inlet temperature of the catalytic bed, versus conversion compared for different reactant concentrations in methane oxidation experiments over the 2 wt.% Pt/Al<sub>2</sub>O<sub>3</sub> catalyst. (a) Comparison of concentrations under oxygen rich conditions, with CH<sub>4</sub> concentrations of 2%, 0.5% and 0.1%, and corresponding O<sub>2</sub> concentrations of 10%, 2.5% and 0.5%, respectively. (b) Comparison of concentrations under stoichiometric conditions, with CH<sub>4</sub> concentrations of 2%, 0.5% and 0.25%, and corresponding O<sub>2</sub> concentrations of 4%, 1% and 0.5%, respectively.

In Figure 4.9a, it can be seen that the “S-shaped” curve, characteristic for the temperature-conversion curve under oxygen rich conditions, becomes less s-shaped and more uniformly sloped as the reactant concentrations decrease. For the lowest concentrations tested, the shape of the curve is almost identical as the curves obtained under stoichiometric conditions, seen in Figure 4.9b, which appears to always be straight, with a, to some degree, increasingly steeper slope as the concentrations are reduced.

In Figure 4.9 it can also be seen that the general trend is that a lower reaction temperature is needed in order to obtain the same extent of conversion, as the reactant concentration decreases. In the case of oxygen rich conditions, an average temperature reduction of about 20 °C is observed when the concentrations are reduced from 2% to 0.5% CH<sub>4</sub> and an average temperature reduction of another nearly 30 °C is observed when the concentrations are further reduced from 0.5% to 0.1% CH<sub>4</sub>, according to Table 4.7 (run 1,5 and 8).

However, as different concentrations with regards to both CH<sub>4</sub> and O<sub>2</sub> are compared in Figure 4.9, the conversion level at different temperatures is not a valid basis to comment on the catalytic activity on. The kinetics of methane combustion have to be taken into consideration, which are previously established to be approximately first order in methane and zero order in oxygen.

The reaction rate and turnover frequency (TOF), calculated at 430 °C for the different conditions, are presented in Table 4.10, along with the conversions obtained at this temperature.

**Table 4.10.** Calculated conversion, reaction rate and TOF at 430 °C compared for different reactant concentrations. The dotted line separates the compared oxygen rich experiments from the stoichiometric ones.

CH <sub>4</sub> :O <sub>2</sub> Ratio	Feed gas [mol %]		$X_{CH_4, 430^\circ C}$ [%]	$r_{CH_4}$ [mol CH <sub>4</sub> / g <sub>cat</sub> h]	TOF [s <sup>-1</sup> ]
	CH <sub>4</sub>	O <sub>2</sub>			
1:5	2	10	4.77	0.003	0.73
1:5	0.5	2.5	9.56	0.001	0.37
1:5	0.1	0.5	16.9	0.0005	0.13
1:2	2	4	9.15	0.005	1.4
1:2	0.5	1	12.3	0.002	0.47
1:2	0.25	0.5	15.7	0.001	0.30

In compliance with Figure 4.9, Table 4.10 shows how the extent of conversion increases with decreasing reactant concentration. The catalytic activity, however, expressed through reaction rate or TOF, decreases with decreasing reactant concentration. The turnover frequency as a function of the methane concentration is illustrated graphically in Figure 4.10, where a linear trend is observed in stoichiometric conditions.

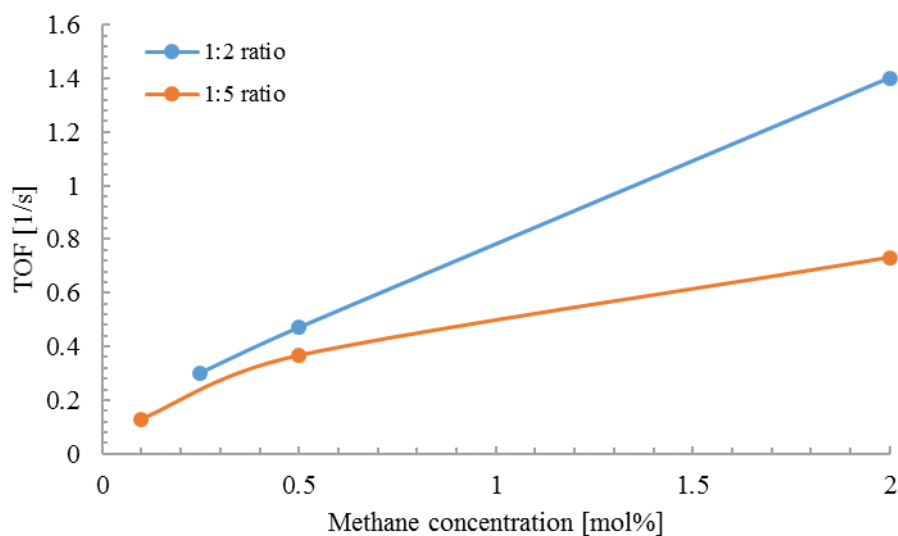


**Figure 4.10.** Turnover frequency as a function of methane concentration, under stoichiometric conditions (1:2), shown in blue, and oxygen rich conditions (1:5), shown in orange.

# 5 Discussion

## 5.1 Catalyst Characterization

### 5.1.1 Nitrogen Physisorption

The results from the analyzes of the impregnated catalysts and that of only the alumina support, displayed in Table 4.1, reveal that there are some small differences between the samples with regards to the physical properties investigated in the experiment.

Using the alumina sample as a reference, it is seen that the surface area increases slightly as a result of impregnation, in the case of the 2 wt.% catalyst and the 0.2 wt.% catalyst synthesized in this project. Alumina is a high surface area support, and it is usually advantageous to have an as high surface area as possible. An increase in surface area as a result of impregnation of finely dispersed platinum particles on the surface is hence desirable.

The opposite is, however, commonly observed, and appears to be the case for the 0.2 wt.% catalyst sample, synthesized during the specialization project. A decrease in the surface area of about  $10 \text{ m}^2/\text{g}$  is observed for this catalyst and could be due to catalyst particles blocking the smaller pores of the support. Another possible scenario that can lead to decrease in surface area is sintering. Argyle [40] describes some effects of catalyst variables on sintering rates of supported metal catalysts and states that the thermal stability of a catalyst exposed to  $\text{O}_2$  is a function of the volatility of the metal oxide. As mentioned in section 2.2, platinum oxide is a highly volatile compound and could thus provoke sintering of the supported catalyst. Additionally, the calcination process, performed in air at  $500 \text{ }^\circ\text{C}$ , could also have led to growth of the metal particles. Whether or not this temperature is high enough to cause sintering is uncertain, emphasized with Argyle's statement that in most cases, metals supported on alumina possesses better thermal stability than metals supported on other common supports, like  $\text{SiO}_2$  and carbon. If sintering during the synthesis had occurred, it would, however, most likely have been reflected by the other catalysts, which was not the case.

Even though the variations in surface area between the two batches of 0.2 wt.% catalyst are rather small, it is still discuss-worthy. It is speculated in whether the larger surface area is associated with chlorine present in the samples, as both the 2 wt.% catalyst and the 0.2 wt.% catalyst synthesized during this project, contain chlorine and possesses a higher surface area than the chlorine free 0.2 wt.% catalyst. Conventional oxy-chlorination is a common way to regenerate catalysts to re-disperse larger crystallites formed as a result of sintering. Argyle [40] remarks, however, that re-dispersion of alumina-supported platinum crystallites also may be conceivable when exposed to a chlorine-free  $\text{O}_2$  atmosphere, provided that chlorine is present on the catalyst. He refers to an experiment on a  $\text{Pt}/\text{Al}_2\text{O}_3$

catalyst, also impregnated with chloroplatinic acid, where a maximum increase in dispersion was observed when exposed to O<sub>2</sub> for 1 hour at around 550 °C. This process could be comparable to the calcination process, performed during the synthesis of the catalysts in this project. Hence, it is possible that the difference in surface area between the 0.2 wt.% catalysts originates from the chlorine, causing re-dispersion of clustered platinum particles when exposed to O<sub>2</sub> at high temperatures and consequently resulting in a larger surface area.

Taking into consideration that the 0.2 wt.% catalyst with the lowest surface area was the first of the catalysts to be synthesized, it is also possible that the difference with regards to the other catalysts is due to inaccuracies during the preparation. The accuracy when preparing the catalysts may have improved with experience, which may be reflected by the similarities between the two catalysts synthesized during this project. Nevertheless, the variations between the physical properties of the catalysts tested in the experiments do not appear to be very significant, and both the observed surface areas and pore volumes are all in the same size range.

### **5.1.2 Volumetric Chemisorption**

For the chemisorption results, presented in section 4.1.2, both the total and the difference results are presented in Table 4.2, and the first and second isotherms, produced over each sample, are illustrated in Figure 4.1 and Figure 4.2. In the first isotherm, the total amount of gas that is both chemisorbed and physisorbed on the surface is included, whereby the chemisorbed molecules are bound to the surface by strong chemical bonds, causing a potentially irreversible adsorption, while the physisorbed molecules are bound by weak Van der Waal's forces and the adsorption can be considered reversible. This total amount of adsorbed gas forms the basis of the "total" results, presented in Table 4.2. The second isotherm is only based on reversible physisorption of gas molecules. Thus, the difference between the two isotherms results in involving only the strong, chemical bonding, and forms the basis of the "difference" results presented in Table 4.2.

Whether it is the total results or the difference results that give the most correct dispersion and crystallite size for the catalysts, depends on the definition and the nature of the bonding between the active phase and the adsorbates. Oudenhuijzen et. al [41] have studied the nature of the Pt-H bonding for strongly and weakly bonded hydrogen on platinum through a series of H<sub>2</sub> chemisorption experiments, and found that the H/Pt values used to determine the accessible metal surface area, and hence the dispersion, should be based on the total amount of hydrogen adsorbed. The difference results will, according to Rioux and Vannice [42], provide for the most correct information in the case of CO chemisorption.

The CO chemisorption on the 2 wt.% catalyst was performed both to validate the results obtained from H<sub>2</sub> chemisorption and as an attempt to give an indication of whether the results from the total analysis or the difference results provides for the most physically

relevant values. The results from the CO chemisorption indicates the same size range of obtained dispersion as H<sub>2</sub> chemisorption, with regards to both the total and the difference results. For the 2 wt.% catalyst, the dispersion based on the total amount of gas adsorbed is found to be 85%-95%, while it, from the difference results, is found to be about 50-70%. For the 0.2 wt.% catalyst, however, the dispersion, based on the total results, is found to be over 100% in several of the analyses, which is not theoretically possible. This taken into consideration, in addition to the datum that the difference results are associated with strongly bounded adsorbate, the difference results are suggested to be providing for the most meaningful and relevant results in these experiments.

The results from all of the chemisorption experiments indicate that the catalysts possess a really high dispersion and that the particles are of small size, around 1-2 nm. There is one repetition, however, which stands out. The H<sub>2</sub> chemisorption performed on sample 3' of the 0.2 wt.% catalyst, results in a dispersion of about 3% and a particle size of 36 nm, as seen in Table 4.2. When comparing the adsorption isotherms of the different samples, however, the isotherms for this experiment, shown in Figure 4.2c, differs suggestively from the ones produced for all of the other experiments. An "ideal" Langmuir isotherm was illustrated in Figure 2.4 (section 2.4.2). With regards to this figure, the isotherms for sample 3' are the one most far off, and the experiments performed on the other samples are thus assumed to provide for more correct results.

The isotherms produced over the 2 wt.% catalyst are in general more flawless than the ones produced over the 0.2 wt.% catalyst, which is assumed to be due to the higher metal loading. Low metal loading, potential equipment errors and small leakages are considered the most important factors that may influenced the results from chemisorption experiments. Several chemisorption experiments performed during the specialization project over the 0.2 wt.% catalyst showed that the signal provided by the catalyst is at risk of being weak, and that the system seems to be more exposed to leakages at such low metal loading. Long enough evacuation time is hence important to avoid this, in particular for samples with low loadings.

Based on the difference results, an average dispersion of 58% and 87% is obtained for 2 wt.% Pt and the 0.2 wt.% Pt, respectively, not taking sample 3' into consideration. The respective, average particle sizes are found to be 2.0 nm and 1.4 nm. This coincides well with a previous study, where a dispersion of 53% and 84% was reported for 2 wt.% Pt and 0.5 wt.% Pt, respectively, both supported on Al<sub>2</sub>O<sub>3</sub>. The respective particle sizes were found to be 2.2 nm and 1.4 nm [37]. The crystallite size, estimated by the ASAP apparatus, is assumed to be precise for Pt particles, due to the similarities between the values reported in Table 4.3. Hence, from the chemisorption experiments performed, it can be concluded that the 2 wt.% catalyst appears to have a dispersion of around 50% with an average particle size of about 2 nm. The 0.2 wt.% catalyst seems to have a larger dispersion, suggestively close to 100%, and contains smaller particles, with an average diameter around 1 nm.

### 5.1.3 X-ray Diffraction

An unidentified peak is found in the beginning of the top two diffractograms in Figure 4.3. No elements were identified to fit this peak, and it is assumed to be caused by disturbances in the apparatus. The lack of it in the bottom two diffractograms is assumed to be due to that these analyzes were performed during the specialization project.

Except from this, the diffraction patterns of the four different samples, shown in Figure 4.3, are more or less identical, having peaks of similar shape and size at seemingly the exact same angles. The  $\gamma$ -alumina phase matches pretty well with the diffraction peaks, being identified at all the major peaks. The peaks fitted for Pt and PtO<sub>2</sub> are, however, present at nearly the same angles as some of the peaks identified as alumina. Based on the similarities between the diffractogram of alumina, and those of the catalysts that for sure contain platinum, it is, with great certainty, safe to assume that the alumina phase is the only phase detected for all samples.

The fact that alumina is detected, do, however, establish that the alumina support is semi-crystalline, which is reflected by the broad peaks in the XRD pattern. Amorphous structures are not detectable by the apparatus, and a highly crystalline material would have given much sharper peaks. That  $\gamma$ -alumina is the detected alumina phase, also confirms that alumina remains in the  $\gamma$  phase, and has not gone through a phase transformation to  $\alpha$ -alumina as a result of the calcination during the synthesis.

The analysis does, as mentioned, not give any conclusive indications of detecting Pt or PtO<sub>2</sub> in the catalyst samples. A material needs to be present in amounts greater than 1% to be detectable in an XRD analysis [43]. As the Pt content in the 0.2 wt.% catalysts is below the detection limit, the Pt phase is not expected to be identified by the XRD for these catalysts. The fact that the diffraction pattern of the 2 wt.% catalyst and the 0.2 wt.% catalysts are so similar, are in this context a good sign. The absence of a detected platinum phase for the 2 wt.% catalyst, could hence indicate the presence of finely dispersed platinum particles, which is in compliance with the chemisorption results, showing high dispersion of the particles on the catalysts, and small crystallite sizes.

### 5.1.4 X-ray Fluorescence

The Pt content in the three different catalysts compared in this project, was calculated based on the XRF results and displayed in Table 4.5. For both the 2 wt.% catalyst and the 0.2 wt.% catalyst synthesized during the specialization project, the measured platinum content was lower than expected, compared to the nominal loading. There are several possible explanations for this. The deviation from the nominal loading could be due to inaccuracies in the apparatus or, in the case of the 0.2 wt.% catalyst, that the device was not calibrated properly, as this analysis was performed in the fall. The apparatus have, however, been

recalibrated before the reproduction was executed, and the observed content still seems to deviate with about 30% from the nominal amount.

Another possible explanation for the lower amount of Pt could be that some Pt were lost during the preparation of the catalyst. Due to the preparation method of the catalysts being incipient wetness impregnation, there are, however, few circumstances that would cause platinum to disappear, as the method “forces” the material to stay on the catalyst. The exception is formation of volatile platinum oxide, which is a recurrent issue with platinum at high temperatures. This is known to lead to weight losses of Pt in catalysts, as the solid platinum can react with oxygen and leave the sample as gaseous PtO<sub>2</sub>. This is, for instance, a common issue in ammonia oxidation where the lost Pt often is recovered by traps, comprised by a gauze pack of palladium [44]. This is, however, mainly an issue occurring at high temperatures, and Powell [45] emphasizes that rapid weight loss of Pt usually is observed at temperatures above 1000 °C. As the calcination in the preparation of the catalyst only took place at 500 °C, this does most likely not contribute to a significant loss in the sample weight.

For catalysts with low dispersion, the measured Pt content, obtained from XRF, could present itself as lower than it really is, due to unevenly distributed Pt and low levels present at the XRF part of the sample. This is most likely not the case for the catalysts investigated in this project, as the dispersions appear to be obtained in a high degree for all catalysts. The repeated analysis substantiates this, indicating similar Pt content for both trials. Hence, the deviations are probably caused by inaccuracies in the scale or other apparatus used during the synthesis, resulting in a lower amount of hexachloroplatinic acid being impregnated on the support than intended. Despite the deviations, the obtained mass fractions of Pt are still in the same size range as the nominal loading, and is not suspected to have had a large impact on the performance of the catalysts.

A noteworthy aspect of the sample composition results presented in Table 4.4 is the chlorine content, found in both the 2 wt.% catalyst and the 0.2 wt.% catalyst synthesized during this project. The chlorine is lacking in both the original analysis of the 0.2 wt.% catalyst synthesized and analyzed during the specialization project, and in the reproduction performed after recalibration of the instrument. The chlorine originates from chloroplatinic acid used to impregnate the catalysts, and the catalysts are found to contain 0.7 wt.% and 0.1 wt.% Cl for the 2 wt.% and the 0.2 wt.% catalysts, respectively. Previous studies have reported that chlorine, originating from Pt precursors, may strongly inhibit the catalytic activity of platinum particles, supported on alumina, in the complete oxidation of methane in excess O<sub>2</sub> [1]. Due to this poisoning effect, it is advantageous to keep the chlorine content in the samples to an as low as possible level.

Apart from the platinum content, the samples contain, as expected, mostly Al<sub>2</sub>O<sub>3</sub>. Small amounts of SiO<sub>2</sub>, Fe<sub>2</sub>O<sub>3</sub> and K<sub>2</sub>O are, however, also detected. According to the analysis, SiO<sub>2</sub> in amounts of 1% of the total sample weight is found in the 0.2 wt.% catalyst synthesized during the specialization project, which is more than one would expect a mere

contamination to contribute to. The silica could have entered the sample through either the sample holders used for the XRD analysis or from equipment used during the preparation of the pellets. Another possibility is that it entered the sample already during the synthesis. Alumina dominates the sample composition, and if traces of silica is present in the support, this could result in a higher  $\text{SiO}_2$  content relative to silica stemming from another source, such as the sample holders. There is also a chance that some silica, originating from the material of the quartz reactor, got mixed with the sample during calcination. However, as the results from the repeated analysis completely lack detection of  $\text{SiO}_2$ , it is most likely to stem from calibration errors or equipment impurities.

As far as the  $\text{K}_2\text{O}$  and  $\text{Fe}_2\text{O}_3$  content are concerned, also these compounds were assumed to be originating from equipment impurities, and not from the introduction of platinum during the synthesis. By reason of other students having used the XRF equipment getting similar peaks and content for both compounds, despite analyzing different catalysts and support, there is a compelling chance that both impurities originate from either the sample holders or the boric acid, used as binder during the preparation of the sample pellets.

Overall, the samples seem to be pretty pure and contain, for the most part, what they are supposed to contain. This could imply that the used preparation method has been a good way to synthesize the catalysts, and that deviations from the nominal content is mainly caused by equipment impurities or inaccuracies.



## 5.2 Catalytic Activity

### 5.2.1 Deactivation and “hot spots”

The catalysts do not seem to show any significant signs of deactivation through the sequential experiments performed. The reference experiments show that the catalytic activity remains more or less the same in the experiment performed in the beginning and at the end of the sequences for both catalysts.

The temperature profiles could also have given an indication of deactivation if the position of the peak temperature within the catalyst bed had shown signs of movement as the catalysts were used throughout the sequential runs. For a fresh catalyst with uniform distribution of catalytic and inert material, the highest temperature, or the “hot spot”, is usually found close to the reactor inlet, where the degree of conversion is the highest. If the peak temperature had moved along the bed, progressively for each run towards the reactor outlet, this could have been a sign of deactivation of particles located close to the inlet.

A shift in the peak temperature is not observed as a result of several runs, but it is, however, observed as a result of increasing temperature in each specific run. For the 2 wt.% catalyst, the peak temperature is positioned further down the bed at 500 °C in comparison to 400 °C, as seen in Figure 4.5. The same is observed for the 0.2 wt.% catalyst, where the peak temperature has experienced a shift at 600 °C compared to at 500 °C, seen in Figure 4.6. The conversion of methane increases when the temperature increases, which results in more evolved heat. The “hot spot” seems to be transferred from the inlet to a position further down the bed as the conversion increases and approaches 100%. This heat transfer is suspected to be caused by axial heat conduction. In conduction, contacting materials are causing the heat transfer. Metals are good conductors, and the heat may be transferred by conduction when heated particles at the inlet, contacts cooler particles positioned further down the bed. The heated particles have gained more energy, and thus vibrates more, and can transfer the heat by bumping into neighboring particles.

According to the results of effect of loading, reported in section 4.2.1, a temperature of 70-90 °C more was found to give the same conversion for 0.2% Pt as 2% Pt. Hence, the temperature profiles obtained at 600 °C for the 0.2 wt.% catalyst, are comparable to the temperature profiles obtained at 500 °C for the 2 wt.% catalyst, and the observed shift is thus in compliance between the two catalysts.

### 5.2.2 Effect of loading

From Figure 4.7, it is visibly evident that the catalytic activity increases with amount of Pt added. The catalytic activity of the 2 wt.% catalyst was shown to be better than that for the 0.2 wt.% catalyst in all of the conducted experiments. This was anticipated, as a catalyst with higher loading is likely to have more active sites available on the surface, although the dispersion was found to be higher for the catalyst with the lowest loading. The correlation between activity and loading was tested by Gèlin [1], who investigated the influence of the Pd loading on the temperature at which the methane conversion reached 50% in oxidation of CH<sub>4</sub> experiments. He tested for metal loadings between 0.1 and 20 wt.%, and found that the temperature decreased in line with increasing metal loading. The temperature variations did, however, seem to stagnate when increasing from 10 to 20% Pd, where it becomes increasingly difficult to maintain the dispersion.

Comparing the results to a similar study, performed by Sarbak [35], shows clear similarities between the obtained results. He investigated the effect of loading on oxidation of methane, comparing a 3 wt.% Pt/Al<sub>2</sub>O<sub>3</sub> catalyst to a 0.3 wt.% Pt/Al<sub>2</sub>O<sub>3</sub> catalyst among others. In his experiments, complete conversion was reached at about 600 °C and 700 °C for the 3 wt.% and 0.3 wt.% catalyst, respectively. The experiments were conducted under oxygen rich feed conditions with 1% CH<sub>4</sub> and 21% O<sub>2</sub>, balanced with N<sub>2</sub>. The most comparable feed conditions tested in this project contained 2% CH<sub>4</sub> and 10% O<sub>2</sub>, where full conversion was reached at about 625 °C and 725 °C for the 2 wt.% and the 0.2 wt.% catalyst, respectively.

When comparing the experiments performed over both loadings at equivalent feed conditions, presented in Table 4.7, the general trend show that a temperature of 70-90 °C higher was necessary for the 0.2 wt.% catalyst to reach the same level of conversion as the 2 wt.% catalyst. The activation energy was also found to be higher in the reactions performed over the 0.2 wt.% catalyst, which emphasizes the higher degree of difficulty in completing the reaction over the lower loading catalyst.

### 5.2.3 Effect of stoichiometry

The methane oxidation experiments performed under stoichiometric conditions, turned out to have an enhancing effect on the catalytic activity of the catalysts, compared to oxygen rich conditions. In Table 4.7, the results of experiments performed under stoichiometric- and oxygen rich conditions with the partial pressure of methane kept constant, clearly shows the superior catalytic activity exhibited under stoichiometric conditions. This is seen by a comparison between run 2 to 3 and run 4 to 5.

Based on the kinetics of the methane oxidation reaction, being approximately first order with respect to the methane concentration and zero order in oxygen [36, 37], one would assume the reaction rate to be constant when altering the O<sub>2</sub> concentration. The reaction rate still, however, seems to be influenced by the amount of oxygen present in the feed.

The rate of reaction, reported in Table 4.9, was found to be higher at 450 °C under less oxidizing conditions, for both comparable sets of stoichiometric versus oxygen-rich conditions.

The excess oxygen present in experiments run with CH<sub>4</sub>/O<sub>2</sub> ratios of 1:5 therefore seem to inhibit the catalysts, and may be due to formation of PtO<sub>2</sub>. If the inferior catalytic activity is due to formation of PtO<sub>2</sub>, this could imply that platinum, in fact, is more active in its metallic form than in the oxidized form. With stoichiometric feed conditions, less oxygen will be available for surface oxide formation, and more active sites will hence be available for adsorption, increasing the catalytic activity. Recalling section 2.2.1, there are diverse opinions and an ongoing discussion regarding what phase of the metal that is the most active for methane oxidation. Based on the assumption of metallic Pt being the most active state of platinum, the results in this study could imply that more platinum is likely to be present in its metallic form under stoichiometric conditions, providing for a higher catalytic activity than under conditions where platinum allegedly will be oxidized to a greater extent. The same has been observed in a previous study [37], where the catalytic activity, on equal terms as in this study, was compared for oxygen-rich (1:5) versus stoichiometric (1:2) feed conditions. Also here, the Pt/Al<sub>2</sub>O<sub>3</sub> catalyst was found to be more active when the reactant mixture was altered from oxygen-rich to stoichiometric. The superior activity was, likewise, suggested to be due to a less oxidized surface being more active than a more oxidized surface.

Under stoichiometric conditions, a smooth increase in conversion as a function of temperature is observed, while oxygen-rich conditions produce a “S-shaped” conversion curve at higher reactant concentrations. The S-shape is suggested to be due to ignition of the catalyst, which is more prominent in excess O<sub>2</sub>. For the conversion curves plotted and compared under oxygen rich conditions (Figure 4.9a), the curve noticeably becomes less “S-shaped” as the O<sub>2</sub> concentration in the feed decreases, indicating a smaller necessary temperature increase to reach complete conversion of methane. It could seem like the catalyst behaves more and more like it does under stoichiometric conditions, as a smaller amount of O<sub>2</sub> is present to ignite the catalyst when the concentrations are reduced. It is possible that stoichiometric conditions also would have produced an S-shape if more steady state conversions had been monitored. The logged methane conversion for these runs did, however, rapidly increase from a steady state conversion of about 60% to 100% in 10 minutes. This was also the case for the lowest tested oxygen-rich concentration, shown in yellow in Figure 4.9a, which produced a strikingly similar conversion curve as of low stoichiometric concentrations. In the two runs where an S-shape is indicated, shown in green and blue in Figure 4.9a, the conversion also stabilized at 90% conversion. The “S-shape” is, however, a lot less prominent with 2.5% O<sub>2</sub> present (blue) than with 10% O<sub>2</sub> present (green), despite both runs having steady state conversions monitored at more or less the same levels. This substantiates that less O<sub>2</sub> leads to a less prominent ignition.

## 5.2.4 Effect of concentration

The catalytic activity appears to decrease with decreasing methane concentration. This is in compliance with the rate expression for methane combustion, as the reaction is identified to be first order with respect to the methane concentration [36]. The decreasing catalytic activity as a function of decreased methane concentration is reflected by the decreasing reaction rates, calculated at 430 °C, and the turnover frequencies.

The turnover frequency plotted as a function of the methane concentration in Figure 4.10, shows a linear relationship in the case of stoichiometric feed conditions, and as expected, the turnover frequency increases with increasing methane concentration. The relationship exhibited under oxygen-rich conditions is, however, not linear, and the increase in TOF is smaller as the methane concentration is increased from 0.5% to 2%, relative to when it is increased from 0.1% to 0.5%. The gentler slope indicates that the increase in CH<sub>4</sub> molecules converted per unit time is reduced, as the CH<sub>4</sub> concentration, and hence the oxygen concentration, is increased. The oxygen amount gets substantially larger as the methane concentration increases, due to the 1:5 ratio of CH<sub>4</sub> to O<sub>2</sub>. It could seem like the increasing concentration of oxygen is what inhibits the TOF from keeping the linear trend, as seen under stoichiometric conditions. The oxygen-rich curve is furthermore generally positioned below the curve of stoichiometric conditions. The lower positioning, indicates that fewer methane molecules are converted when the oxygen amount is 5 times that of the methane, compared to when it is only twice the amount. The lower specific activity exhibited by the catalyst in excess O<sub>2</sub>, is suggested to be caused by a higher degree of PtO<sub>2</sub> formation, which seem to influence the activity to a larger extent when the reactant concentrations increase.

No CO was detected by the GC during the any of the experiments, and it has been assumed that CO<sub>2</sub> is the only carbon containing compound present in the product stream, apart from unconverted methane. The error in the carbon balance, plotted for each run in Appendix E, shows that the error never exceeds 8%, except from in run 7 and 8, involving the lowest tested reactant concentrations. In these runs, the carbon balance is found to negatively deviate with as much as 40% and 70%, respectively. The GC has been calibrated for concentrations down to 1% CH<sub>4</sub> and CO<sub>2</sub>, and in these experiments the CH<sub>4</sub> concentrations was as low as 0.25% and 0.1%. The error is thus most likely caused by improper calibration of the GC in the experiments involving such low concentrations. From the GC data, it has been observed that the proper inlet concentration of CH<sub>4</sub> is detected, and that it steadily decreases until it reaches zero when complete conversion is obtained. The CO<sub>2</sub> concentration is, however, not detected in amounts sufficient to match the CH<sub>4</sub> inlet concentration at complete conversion, and it is here the error is suspected to be originating from. The error in the balance is hence not suspected to have impacted the conversion calculations to a large degree, as it appears to mainly origin from the detected amount of CO<sub>2</sub>, not included in these calculations. As no other carbon compound was detected by the GC, it is considered unlikely that other carbon compounds were formed during the experiment, especially in amounts large enough to compensate for the great error.

The lowest tested methane concentration, was tested in run 8 (Table 4.7). The fact that the catalyst is able to obtain complete conversion of methane at the lowest observed temperature in this run, containing 0.1% CH<sub>4</sub> and 0.5% O<sub>2</sub>, is promising, as this reactant mixture is the one that resembles application relevant conditions the most, among the tested conditions. 0.1% CH<sub>4</sub> corresponds to 1000 ppm, and as listed in section 2.1, low concentrations of methane (500-1000 ppm) and large excess of oxygen are the conditions known to be prevailing in NGV exhaust, and are thus considered comparable to LNG engine exhaust. The exhaust gas does, however, contain several other species that influences and complicates the process, which has not been included in this study and should be further looked into in subsequent studies.



## 6 Conclusion

In this project, alumina-supported platinum catalysts, with metal loading of 2 wt.% and 0.2 wt.%, have been synthesized by incipient wetness impregnation, characterized with some of the main characterization techniques and investigated for complete oxidation of methane. The feed gas-composition has been varied, both in terms of stoichiometry and concentration, to investigate the feed conditions that enhance low temperature activity of the synthesized catalysts.

The XRF analyzes revealed that the platinum content in the catalysts deviated somewhat from the nominal loading, but was, however, in the same size range. The 0.2 wt.% catalyst synthesized during the specialization project differed somewhat from the 0.2 wt.% catalyst synthesized in this project, in that it contained less platinum, no chlorine and had a smaller surface area. It is possible that the difference in surface area between the 0.2 wt.% catalysts originates from the chlorine, potentially causing re-dispersion of clustered platinum particles when exposed to O<sub>2</sub> at high temperatures, resulting in a larger surface area. A correspondingly larger surface area was also observed for the chlorine-containing 2 wt.% catalyst. The differences are, however, not huge and the BET analyzes showed that the chlorine containing catalysts possessed a surface area of about 160 m<sup>2</sup>/g, versus 140 m<sup>2</sup>/g for the non-chlorine catalyst, all having pores in the mesoporous size range.

Semi-crystalline  $\gamma$ -alumina was found to be the only compound detected in the XRD analyzes, where the diffraction patterns of the support and the catalysts were more or less identical. The absence of a detected platinum phase for the 2 wt.% catalyst, is suggested to be due to finely dispersed platinum particles with small crystallite sizes. This is in compliance with the chemisorption results, which revealed that both catalysts have high dispersion and small particle sizes. An average dispersion of 87% and 58% and was obtained for the 0.2 wt.% and the 2 wt.% catalyst, respectively, with corresponding particle sizes of 1 and 2 nm. Overall, this suggests that the applied incipient wetness impregnation procedure has been a satisfying preparation method of the catalysts.

The 2 wt.% catalyst generally exhibited better performance than the 0.2 wt.% catalyst. A temperature of about 70-90 °C more was necessary to obtain the same level of conversion with the lowest metal loading. Stoichiometric reactant concentrations (1:2) was found to enhance the low temperature activity of the catalysts, in comparison to oxygen-rich conditions (1:5). The excess oxygen seemed to inhibit the activity, and may be due to formation of PtO<sub>2</sub>. This may then substantiate that platinum tends to be more active in its metallic form than in the oxidized state, given that the concentration of metallic platinum is greater in stoichiometric reactant mixtures.

Furthermore, the catalytic activity was found to increase with increasing methane concentration, which is in accordance with the kinetics of methane combustion. The catalysts were still, however, able achieve complete conversion of methane for all tested

conditions, and the temperature necessary to obtain this, decreased with decreasing methane concentration. The lowest temperature needed to obtain complete conversion, was observed in excess O<sub>2</sub> with feed containing 1000 ppm CH<sub>4</sub>, which resembles application relevant conditions the most among the tested. This is hence promising for further development of platinum catalysts, suitable for catalytic control of methane slip in marine machinery.



## 7 Suggestions for further work

Water addition to the feed is encouraged to be looked into, in order to investigate potential deactivation of Pt catalysts during the methane oxidation reaction. Feed gas conditions that to a larger extent resembles those prevailing in exhaust gas could also be tested, to see the effect of large amounts of H<sub>2</sub>O and CO<sub>2</sub> present, in combination with excess O<sub>2</sub> and even lower concentrations of methane than were tested in this project.

More comprehensive deactivation experiments can in general be performed, and the activity of the Pt catalyst can in this respect be compared to the activity of a Pt catalyst made from a chlorine-free precursor.

Furthermore, bi-metallic catalysts containing both palladium and platinum are bright-looking catalysts with regards to methane oxidation, and tests over such catalysts are encouraged to be further investigated.



# References


1. Gélin, P. and M. Primet, *Complete oxidation of methane at low temperature over noble metal based catalysts: a review*. Applied Catalysis B, Environmental, 2002. **39**(1): p. 1-37.
2. Aylward, G.H. and T.J.V. Findlay, *Si chemical data*. 6th ed. ed. 2008, Milton: Wiley.
3. Lee, J.H. and D.L. Trimm, *Catalytic combustion of methane*. Fuel Processing Technology, 1995. **42**(2): p. 339-359.
4. Stensvold, T. *Norge har ledet an på LNG-skip. Nå kommer verden etter*. 2015 [cited 2015 17. November]; Available from: <https://tustudio.tu.no/industri/2015/02/20/norge-har-ledet-an-pa-lng-skip.-na-kommer-verden-etter>.
5. *An Exploration of Methane and Properly Managed Livestock through Holistic Management*. . 2013 [cited 2016 25. April]; Available from: [http://www.savoryinstitute.net/media/40742/Savory\\_Institute\\_Methane\\_Paper\\_April2013.pdf](http://www.savoryinstitute.net/media/40742/Savory_Institute_Methane_Paper_April2013.pdf).
6. Burch, R. and P.K. Loader, *Investigation of Pt/Al<sub>2</sub>O<sub>3</sub> and Pd/Al<sub>2</sub>O<sub>3</sub> catalysts for the combustion of methane at low concentrations*. Applied Catalysis B: Environmental, 1994. **5**(1): p. 149-164.
7. Kamiuchi, N. and K. Eguchi, *Catalytic combustion of methane*. 2012. 305-327.
8. Hicks, R.F., et al., *Structure sensitivity of methane oxidation over platinum and palladium*. Journal of Catalysis, 1990. **122**(2).
9. Burch, R. and F.J. Urbano, *Investigation of the active state of supported palladium catalysts in the combustion of methane*. Applied Catalysis A, General, 1995. **124**(1): p. 121-138.
10. Lyubovsky, M. and L. Pfefferle, *Methane combustion over the  $\alpha$ -alumina supported Pd catalyst: Activity of the mixed Pd/PdO state*. Applied Catalysis A: General, 1998. **173**(1): p. 107-119.
11. Burch, R. and M.J. Hayes, *C-H bond activation in hydrocarbon oxidation on solid catalysts*. Journal of Molecular Catalysis A: Chemical, 1995. **100**(1-3): p. 13-33.
12. Honkanen, M., et al., *Accelerated deactivation studies of the natural-gas oxidation catalyst-Verifying the role of sulfur and elevated temperature in catalyst aging*. Applied Catalysis B: Environmental, 2016. **182**: p. 439-448.
13. Catchpole, S., *Mercury removal in hydrocarbon streams*. Petroleum Technology Quarterly, 2009. **14**(2): p. 39-45.
14. Chen, J., et al., *Recent Advances in Catalysts for Methane Combustion*. previously: Catalysis Surveys from Japan, 2015. **19**(3): p. 140-171.
15. Gholami, R., M. Alyani, and K. Smith, *Deactivation of Pd Catalysts by Water during Low Temperature Methane Oxidation Relevant to Natural Gas Vehicle Converters*, in *Catalysts*. 2015. p. 561-594.
16. Chorkendorff, I. and J.W. Niemantsverdriet, *Concepts of modern catalysis and kinetics*. 2nd, rev. and enl. ed. ed. 2007, Weinheim: Wiley-VCH.
17. Richardson, J.T., *Principles of catalyst development*. Fundamental and applied catalysis. 1989, New York: Plenum Press.
18. Jong, K.P.d., *Synthesis of solid catalysts*. 2009, Weinheim: Wiley-VCH.

19. Vanhaecke, E., *Catalyst characterization. University lecture in TKP2 at NTNU*. 2015.
20. *Calculation of BET Area of Microporous Materials with Automated Software from Quantachrome*. [cited 2015 10. December]; Available from: <http://www.azom.com/article.aspx?ArticleID=9434>.
21. Groen, J.C., L.A.A. Peffer, and J. Pérez-Ramírez, *Pore size determination in modified micro- and mesoporous materials. Pitfalls and limitations in gas adsorption data analysis*. *Microporous and Mesoporous Materials*, 2003. **60**(1): p. 1-17.
22. Micromeritics. *Gas Adsorption Theory*. [cited 2015 October 28]; Available from: [http://www.micromeritics.com/Repository/Files/Gas\\_Adsorption\\_Theory\\_poster.pdf](http://www.micromeritics.com/Repository/Files/Gas_Adsorption_Theory_poster.pdf).
23. Takei, T., M. Chikazawa, and T. Kanazawa, *Validity of the Kelvin equation in estimation of small pore size by nitrogen adsorption*. *Kolloid-Zeitschrift und Zeitschrift für Polymere.*, 1997. **275**(12): p. 1156-1161.
24. *Handbook of Heterogeneous Catalysis*. 2008, Weinheim, Germany: Weinheim, Germany: Wiley-VCH Verlag GmbH.
25. Holmen, A., *Heterogen Katalyse*. 2002, Trondheim: Institutt for kjemisk prosessteknologi, NTNU.
26. Lanyon, M.A.H. and B.M.W. Trapnell, *The Interaction of Oxygen with Clean Metal Surfaces*. *Proceedings of the Royal Society of London. Series A, Mathematical and Physical Sciences (1934-1990)*, 1955. **227**(1170): p. 387-399.
27. Niemantsverdriet, J.W., *Spectroscopy in Catalysis: An Introduction*. 2007, Weinheim, Germany: Weinheim, Germany: Wiley-VCH Verlag GmbH & Co. KGaA.
28. McPherson, A., *Introduction to Macromolecular Crystallography*. 2nd ed. ed. *Introduction to Macromolecular Crystallography, Second Edition*. 2009, Hoboken: Wiley.
29. Høydalsvik, K., *XRD and structure analysis with Topas. University Lecture at NTNU*. 2015.
30. *X-Ray Fluorescence Analysis*. [cited 2015 12. November]; Available from: <http://www.horiba.com/scientific/products/x-ray-fluorescence-analysis/tutorial/x-ray-fluorescence-the-basic-process/>.
31. Poole, C., *Gas Chromatography : Gas Chromatography*. *Gas Chromatography*. 2012, Burlington: Elsevier Science.
32. McNair, H.M. and J.M. Miller, *Basic Gas Chromatography*. 2nd ed. ed. *Basic Gas Chromatography Second Edition*. 2009, Hoboken: Wiley.
33. Greibrokk, T., et al., *Kromatografi : separasjon og deteksjon*. 1994, Universitetsforlaget: Oslo.
34. *Risk Assessment and Risk Management*. 18. June 2010 [cited 2015 09. November]; Available from: [http://www.nt.ntnu.no/users/karinwig/HSE-Info-forms/Risk\\_evealuation\\_English/Risk%20assessment%20and%20risk%20management.pdf](http://www.nt.ntnu.no/users/karinwig/HSE-Info-forms/Risk_evealuation_English/Risk%20assessment%20and%20risk%20management.pdf).
35. Sarbak, Z. and S. Andersson, *Effect of support and loading on oxidation of methane over platinum catalysts*. *Reaction Kinetics and Catalysis Letters*, 2007. **92**(2): p. 231-238.
36. Xin, Y., et al., *Kinetics of catalytic oxidation of methane over palladium oxide by wire microcalorimetry*. *Journal of Physical Chemistry C*, 2013. **117**(38): p. 19499-19507.

37. Burch, R. and P.K. Loader, *Investigation of Pt/Al<sub>2</sub>O<sub>3</sub> and Pd/Al<sub>2</sub>O<sub>3</sub> catalysts for the combustion of methane at low concentrations*. Applied Catalysis B, Environmental, 1994. **5**(1): p. 149-164.
38. Bartholomew, C.H. and R.J. Farrauto, *Fundamentals of industrial catalytic processes*. 2nd ed. ed. 2006, Hoboken, N.J: Wiley-Interscience.
39. Takahashi, Y., et al., *Measurements of plasma parameters in atmospheric helium plasma detectors for gas chromatograph*. 2010. p. 1-1.
40. Argyle, M.D. and C. Bartholomew, *Heterogeneous Catalyst Deactivation and Regeneration: A Review*, in *Catalysts*. 2015. p. 145-269.
41. Oudenhuijzen, M.K., et al., *The nature of the Pt-H bonding for strongly and weakly bonded hydrogen on platinum. A XAFS spectroscopy study of the Pt-H antibonding shape resonance and Pt-H EXAFS*. Journal of Physical Chemistry B, 2001. **105**(20): p. 4616.
42. Rioux, R.M. and M.A. Vannice, *Dehydrogenation of isopropyl alcohol on carbon-supported Pt and Cu-Pt catalysts*, in *J. Catal.* 2005. p. 147-165.
43. Deng, W., *The catalytic activity of gold clusters on oxide supports for the low-temperature oxidation of carbon monoxide by dioxygen and water in hydrogen-rich gas streams*. 2008: Proquest Information and Learning Company.
44. Moulijn, J.A., M. Makkee, and A.v. Diepen, *Chemical process technology*. 2nd ed. ed. 2013, Chichester: Wiley.
45. Powell, A., *Behaviour of the Platinum Metals at High Temperatures*. Platinum Met. Rev, 1958. **2**(3): p. 95.



# Appendix A. Risk Assessment

NTNU		<b>Risk assessment</b>		Prepared by	Nummer	Date
				HSE section	HMSRV/2603	04.02.2011
HMS /KS				Approved by	Page	Replaces
			The Rector		09.02.2010	

Unit: *(Institute)* **Kjemisk prosesseteknologi** Date: **15.09.2015**  
 Line manager: *(responsible supervisor)* **Edd Blekkan**

Participants in the identification process (incl. function) **Hilde Venvik (supervisor), Rune Lodeng (co-supervisor, SINTEF), Jia Yang (PhD stipendiist), Hanna Marie Storrvik (MSc)**

Risk assessment of: **Catalysis for control of methane slip in marine machinery**

Signaturer:

ID nr.	Activity from the identification process form	Potential undesirable incident/strain	Likelihood: (1-5)	Consequence:			Risk value (human)	Comments/status Suggested measures
				Human (A-E)	Environment (A-E)	Economy/material (A-E)		
1	Use of corrosive salt H2PtCl6	(a) Spills (b) Skin burns (c) Sensitization	(a) 3 (b) 2 (c) 2	(a) B (b) B (c) B	(a) A (b) A (c) A	(a) A (b) A (c) A	(a) B3 (b) B2 (c) B2	Appropriate protection equipment, incl. dust mask and gloves
2	High Temperature Calcination oven	(a) Skin burns (b) Fire	(a) 2 (b) 1	(a) B (b) C	(a) A (b) B	(a) A (b) B	(a) B2 (b) C1	High temperature warning sign on oven
3	Changing/closing of gas bottles of non-toxic/non-combustible gases (N2, He, Ar)	(a) Leakage (b) Explosion	(a) 2 (b) 1	(a) B (b) E	(a) B (b) D	(a) B (b) D	(a) B2 (b) E1	Leak testing
4	Use of ethanol/acetone for cleaning procedures	(a) Spills (b) Fire	(a) 2 (b) 1	(a) A (b) C	(a) A (b) C	(a) A (b) C	(a) A2 (b) C1	Use of lab coat, goggles and gloves
5	Use of flammable gases CH4 and H2	(a) Leakage (b) Fire (c) Explosion	(a) 2 (b) 1 (c) 1	(a) B (b) C (c) E	(a) A (b) C (c) D	(a) A (b) C (c) D	(a) B2 (b) C1 (c) E1	Leak testing
6	Use of Aluminium Oxide	Spills	3	A	A	A	A3	Use of appropriate protection equipment

NTNU	<b>Hazardous activity identification process</b>			Prepared by	Number	Date
				HSE section	HMSRV2601	22.03.2011
HSE				Approved by	Page	Replaces
		The Rector		01.12.2006		

Unit: *(Institute)* **Kjemisk prosesseteknologi** Date: 15.09.2015  
 Line manager: *(responsible supervisor)* **Edd Blekkan**  
 Participants in the identification process (incl. function) Hilde Venvik (supervisor), Rune Lødeng (co-supervisor, SINTEF), Jia Yang (PhD stipendiist), Hanna Marie Storrvik (MSC)  
 Short description of the main activity/main process: Catalysis for control of methane slip in marine machinery  
 Signatures: \_\_\_\_\_

ID nr.	Activity/process	Responsible person	Existing documentation	Existing safety measures	Laws, regulations etc.	Comment
1	Use of corrosive salt H2PcI6	Hilde Venvik	Safety data sheet	Lab coat, goggles, gloves, dust mask	Arbeidsmiljøloven, HSE regulations	
2	High Temperature Calcination oven	Hilde Venvik	User manual	Lab coat, goggles, gloves	Arbeidsmiljøloven, HSE regulations	
3	Changing/closing of gas bottles of non-toxic/non-combustible gases (N2, He, Ar)	Hilde Venvik	User manual	Lab coat, goggles	Arbeidsmiljøloven, HSE regulations	Change of gas bottles is done by appropriate staff
4	Use of ethanol/acetone for cleaning procedures	Hilde Venvik	Safety data sheet	Lab coat, goggles, gloves	Arbeidsmiljøloven, HSE regulations	
5	Use of flammable gases CH4 and H2	Hilde Venvik	Safety data sheet YPX078A	Room detector, local detector, leak testing, lab coat, goggles, gloves	Arbeidsmiljøloven, HSE regulations	Change of gas bottles is done by appropriate staff
6	Use of Aluminium Oxide	Hilde Venvik	Safety data sheet	Lab coat, goggles, gloves, face mask	Arbeidsmiljøloven, HSE regulations	



Risk value = Likelihood (1, 2 ...) x consequence (A, B ...). Risk value A1 means very low risk. Risk value E5 means very large and serious risk

Likelihood		Consequence					
Value	Criteria	Grading		Human	Environment	Economy/material	
1	Minimal: Once every 50 year or less	E	Very critical	May produce fatality/ies	Very prolonged, non-reversible damage	Shutdown of work >1 year.	
2	Low: Once every 10 years or less	D	Critical	Permanent injury, may produce serious health damage/sickness	Prolonged damage. Long recovery time.	Shutdown of work 0.5-1 year.	
3	Medium: Once a year or less	C	Dangerous	Serious personal injury	Minor damage. Long recovery time	Shutdown of work < 1 month	
4	High: Once a month or less	B	Relatively safe	Injury that requires medical treatment	Minor damage. Short recovery time	Shutdown of work < 1week	
5	Very high: Once a week	A	Safe	Injury that requires first aid	Insignificant damage. Short recovery time	Shutdown of work < 1day	

### MATRIX FOR RISK ASSESSMENT

<b>CONSEQUENCE</b>	Very critical	E1	E2	E3	E4	E5
	Critical	D1	D2	D3	D4	D5
	Dangerous	C1	C2	C3	C4	C5
	Relatively safe	B1	B2	B3	B4	B5
	Safe	A1	A2	A3	A4	A5
		Minimal	Low	Medium	High	Very high
		<b>LIKELIHOOD</b>				

### Explanation of the colors used in the risk matrix.

Color	Description
Red	Unacceptable risk. Safety measures must be implemented.
Yellow	Measures to reduce risk shall be considered.
Green	Acceptabel risk.



## Appendix B. Synthesis of catalysts

### B.1. Calculation of salt amount

Two different catalysts, containing 2 wt.% Pt and 0.2 wt.% Pt, respectively, were to be made, each supported on 10 g of  $\gamma$ -alumina.

The amount of platinum needed to obtain the desired platinum content on 10 g support was calculated according to Equation (B.1).

$$m_{Pt} = \frac{wt.\%_{Pt} \cdot m_{Al_2O_3}}{100\%} \quad (B.1)$$

Once the necessary amount of Pt needed to make the different catalysts were found, the amount of Chloroplatinic acid,  $H_2PtCl_6$ , that provides for the platinum, was calculated. This was done according to Equation (B.2) and (B.3) given below.

$$n_{H_2PtCl_6} = n_{Pt} = \frac{m_{Pt}}{M_{wPt}} \quad (B.2)$$

$$m_{H_2PtCl_6} = n_{H_2PtCl_6} \times M_{wH_2PtCl_6} \quad (B.3)$$

The molecular weights used in the calculations are 195.1 g/mol and 409.8 g/mol for Pt and  $H_2PtCl_6$ , respectively, obtained from SI Chemical Data.

The results from the calculations are summarized Table B.1

**Table B.1.** Calculated amount of Chloroplatinic acid,  $H_2PtCl_6$ , necessary to get the correct amount of Pt for the respective catalyst supported on 10 g of alumina.

Catalyst [wt.% Pt]	$m_{Pt,theo.}$ [g]	$m_{H_2PtCl_6,theo.}$ [g]
2	0.2	0.42
0.2	0.02	0.042

## B.2. Preparation of support

About 50 g Aluminum Oxide was weighted out, placed in a ceramic beaker and dried in a High Temperature Oven at 600 °C for 6 hours at a heating rate of 5 °C/min.

After the heat treatment, the support was fractionated to 75-150 µm.

## B.3. Synthesis procedure

- About 5 g support was weighted out and placed in a ceramic beaker. The beaker containing the support was weighted. Deionized water was subsequently added dropwise with a pipette until the support became saturated. The beaker was then weighted again to see how much water that was necessary to reach this point.
- Necessary amount of  $\text{H}_2\text{PtCl}_6$  (ref. Table B.1) was weighted out and placed in a beaker. The salt was dissolved in deionized water, which amount corresponded to twice the amount found in the previous point (for 10 g support).
- The solution was mixed with 10 g  $\text{Al}_2\text{O}_3$  in a ceramic beaker and mixed well.
- The sample was dried at 120 °C for 3 hours in a ventilated drying cabinet. The sample was stirred regularly, after 30 minutes, 1 hour and 2 hours, respectively.
- The sample was then transferred to a calcination reactor and was calcinated in air at 500 °C for 5 hours.

# Appendix C. Volumetric Chemisorption

## C.1. Procedure description

The experimental procedure used in H<sub>2</sub> and CO chemisorption of the samples, is found in Table C.1.

**Table C.1.** Chemisorption procedure used for H<sub>2</sub> chemisorption or CO chemisorption of the 0.2 wt.% Pt and 2 wt.% Pt catalyst samples.

Operation	Gas	Temp [°C]	Rate [°C/min]	Time [min]
Flow	He	200	10	10
Evacuation		100	10	10
Flow	H <sub>2</sub>	400	10	30
Evacuation		400	10	30
Evacuation		35	10	120
Leak Test		35	10	
Evacuation		35	10	10
Analysis	H <sub>2</sub> /CO	35	10	

During the specialization project, there were some trial and error regarding times and temperatures of the different operations in the chemisorption procedure, as it was found difficult to perform the analysis on the catalyst with low metal loading. The variations lied in time and temperature of the first evacuation, the following flow of hydrogen through the system and the subsequent evacuation prior to the leak test. The procedure given in Table C.1. was the one found to work the best, and has been used in all of the chemisorption experiments performed in this project.

## C.2. Sample masses

The weighted sample masses used in the different chemisorption experiments are given in Table C.2. The sample name indicates the platinum content in the sample, type of adsorbate (H<sub>2</sub>/CO) and the parallel number.

About 150 mg material was used in the 2 wt.% Pt samples, while about 200 mg material was used in the 0.2 wt.% Pt samples, due to the lower metal loading.

**Table C.2.** Sample masses of the 0.2 wt.% Pt catalyst samples (top three) and the 2 wt.% Pt catalyst samples (bottom three) subjected to chemisorption. The sample name indicates the platinum content in the sample, type of adsorbate (H<sub>2</sub>/CO) and the parallel number.

Sample name [-]	Mass [mg]
0.2 wt.%-H <sub>2</sub> -1	219.1
0.2 wt.%-H <sub>2</sub> -2	216.5
0.2 wt.%-H <sub>2</sub> -3	210.7
2 wt.%-H <sub>2</sub> -1	163.6
2 wt.%-H <sub>2</sub> -2	171.9
2 wt.%-CO	165.9

# Appendix D. Mass flow controllers

## D.1. Calibration curves

Calibration of the mass flow controllers was performed by Jia Yang in the spring of 2015. The calibration curves, along with the linear regression lines for nitrogen, methane, synthetic air and hydrogen are given in a-d, respectively in Figure D.1. The calibration curves were used to calculate the necessary percentage opening of the mass flow controllers to obtain the desired concentration of the respective components.

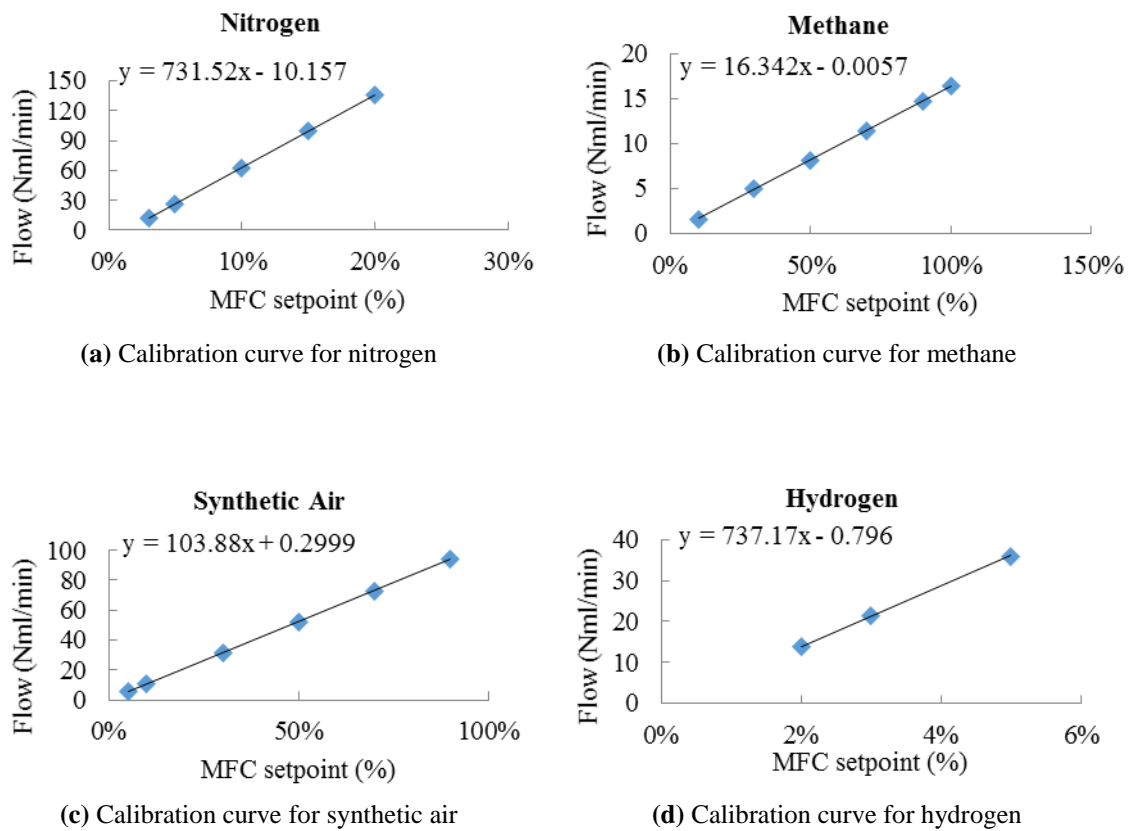


**Figure D.1.** Calibration curves for the mass flow controller of (a) Synthetic air, (b) Nitrogen, (c) Methane and (d) Hydrogen. The calibration was performed by Jia Yang in the spring of 2015.

The calibrated curves for the mass flow controller of nitrogen, methane, synthetic air and hydrogen are given in Equation (D.1)-(D.4), respectively.

$$y = 731.52x - 10.157 \quad (\text{D.1})$$

$$y = 16.342x - 0.0057 \quad (\text{D.2})$$

$$y = 103.88x + 0.2999 \quad (\text{D.3})$$

$$y = 737.17x - 0.796 \quad (\text{D.4})$$

In the above equations,  $y$  is the feed flow of the respective component and  $x$  is the opening of the mass flow controller, controlling the flow of that component.

## D.2. Calculations

Six variations of the reactant concentrations were used in the experiments, and an overview of the different feed gas compositions are given in Table D.1.

**Table D.1.** Overview of the different combinations of feed gas composition used in the methane oxidation experiments.

Feed concentrations		
CH <sub>4</sub> [mol%]	O <sub>2</sub> [mol%]	N <sub>2</sub> [mol%]
2	10	88
2	4	94
0.5	1	98.5
0.5	2.5	97
0.25 <sup>a</sup>	0.5	99.25
0.1 <sup>a</sup>	0.5	99.4

<sup>a</sup> Concentration too low for calibrated MFC, so the CH<sub>4</sub> tank was switched to a 5% CH<sub>4</sub> in N<sub>2</sub> tank.

The total feed flow,  $q_{tot}$ , was 200 Nml/min in all experiments. The corresponding methane flow,  $q_{CH_4}$ , for a given methane concentration,  $C_{CH_4}$ , was calculated from Equation (D.5), while the corresponding amount of O<sub>2</sub> was calculated in the same manner, specified in Equation (D.6).

$$q_{CH_4} = q_{tot} \cdot \frac{C_{CH_4}}{100\%} \quad (\text{D.5})$$

$$q_{O_2} = q_{tot} \cdot \frac{C_{O_2}}{100\%} \quad (\text{D.6})$$



The oxygen was supplied from a synthetic air gas tank, containing 21% O<sub>2</sub> and 79% N<sub>2</sub>. The necessary air flow needed to obtain the correct amount of O<sub>2</sub> was hence calculated from Equation (D.7).

$$1 \left( \frac{mL}{min} \right)_{air} = 0.21 \left( \frac{mL}{min} \right)_{O_2} \quad (D.7)$$

Once the required flows of CH<sub>4</sub> and O<sub>2</sub> was found, the supplementary flow of N<sub>2</sub>, in addition to that provided through the air flow, was calculated according to Equation (D.8).

$$q_{N_2} = q_{tot} - q_{CH_4} - q_{air} \quad (D.8)$$

As can be seen in Table D.1, when the concentration becomes too low for the calibrated mass flow controller of methane when the methane concentration reaches values as low as 0.25% and 0.1%. The original gas tank, containing pure CH<sub>4</sub>, was consequently switched out by a gas tank containing 5% CH<sub>4</sub> in N<sub>2</sub>. A mass flow controller gas correction factor of 0.72 was used for methane to correct for the amount of CH<sub>4</sub>, relative to N<sub>2</sub>, having a correction factor of 1.

The necessary flow of 5% CH<sub>4</sub> in N<sub>2</sub>,  $q_{5\% CH_4}$ , required to obtain the correct methane concentration in the feed, was calculated according to Equation (D.9). The calculated methane flow from Equation (D.5), is here corrected for being supplied from a tank containing only 5% CH<sub>4</sub>, and the correction factor of methane ensures that the mass flow controller is adjusted to provide for the correct amount with respect to CH<sub>4</sub>.

$$q_{5\% CH_4} = q_{CH_4} \cdot \frac{0.72}{0.05} \quad (D.9)$$

Once the required flows of N<sub>2</sub>, CH<sub>4</sub> and synthetic were established, the corresponding opening value of the mass flow controllers were calculated by rearrangements of Equation (D.1)- (D.3), respectively. In the equations, y is the feed flow of the respective component and x is the opening of the mass flow controller, controlling the flow of that component.

The obtained values of both flows and mass flow controller openings are summarized in Table D.2.

**Table D.2.** Feed gas composition, corresponding flow rate of each component and resultant opening of each mass flow controller, ensuring that the correct flow rate of the corresponding component is supplied to the reactor. The total feed flow was 200 Nml/min in all runs.

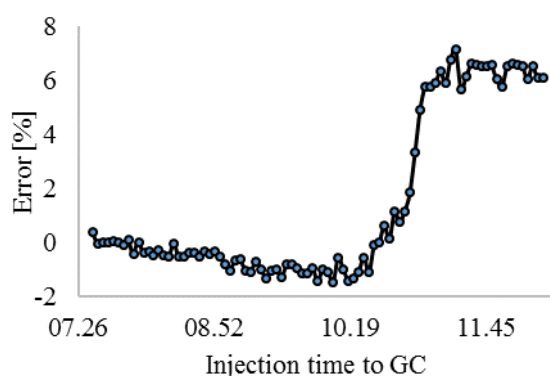
Feed concentrations [mol%]			q [Nml/min]			Opening value MFC [%]		
CH <sub>4</sub>	O <sub>2</sub>	N <sub>2</sub>	CH <sub>4</sub>	Air	N <sub>2</sub>	CH <sub>4</sub>	Air	N <sub>2</sub>
2	10	88	4	95.2	100.8	24.51	91.39	15.16
2	4	94	4	38.1	157.9	24.51	36.38	22.97
0.5	1	98.5	1	9.5	189.5	6.15	8.88	27.29
0.5	2.5	97	1	23.8	175.2	6.15	22.63	25.34
0.25 <sup>a</sup>	0.5	99.25	7.2 <sup>a</sup>	4.8	188.0	44.09 <sup>a</sup>	4.30	27.09
0.1 <sup>a</sup>	0.5	99.4	2.9 <sup>a</sup>	4.8	192.3	17.66 <sup>a</sup>	4.30	27.68

<sup>a</sup> 5% CH<sub>4</sub> in N<sub>2</sub>

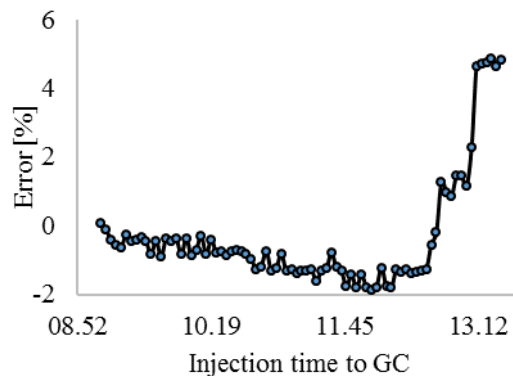
## Appendix E. Carbon balances

The mass error in the mass balance with respect to carbon was calculated according to Equation (3.13). The amount of carbon coming into the system was assumed to be constant, and the carbon balance was checked at every point of injection to the GC during the analysis until full conversion was reached. The purpose of the calculations was to get an indication of the variations in the carbon balance and to verify that the conversion calculations makes sense.

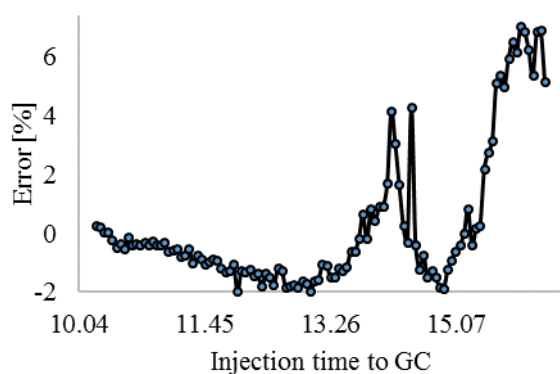
The errors in the carbon balances as a function of injection time to the GC for all the runs over the 2 wt.% catalyst are illustrated in Figure E.1.



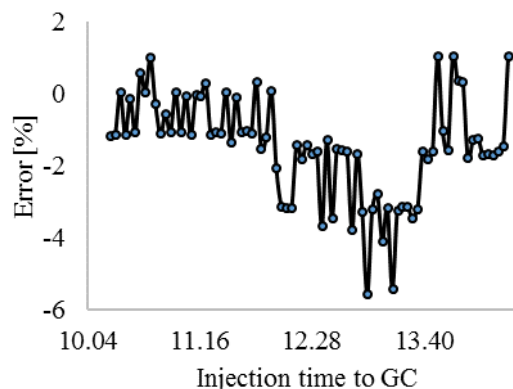
(a) 2% CH<sub>4</sub> and 10% O<sub>2</sub> (Run 1)



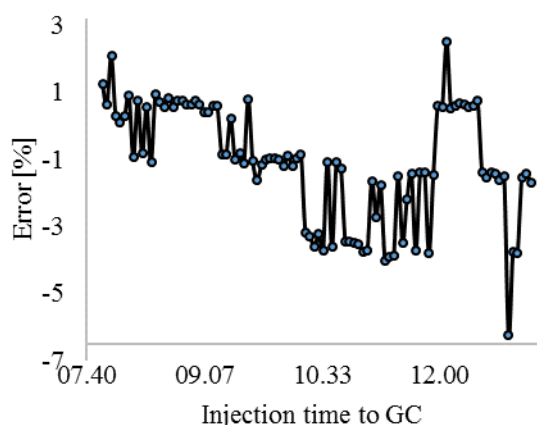
(b) 2% CH<sub>4</sub> and 4% O<sub>2</sub> (Run 2)



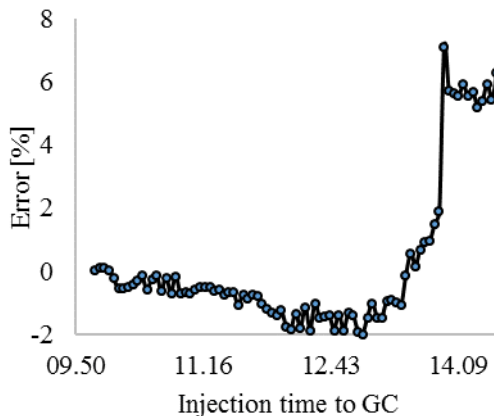
(c) 2% CH<sub>4</sub> and 10% O<sub>2</sub> (Run 3)



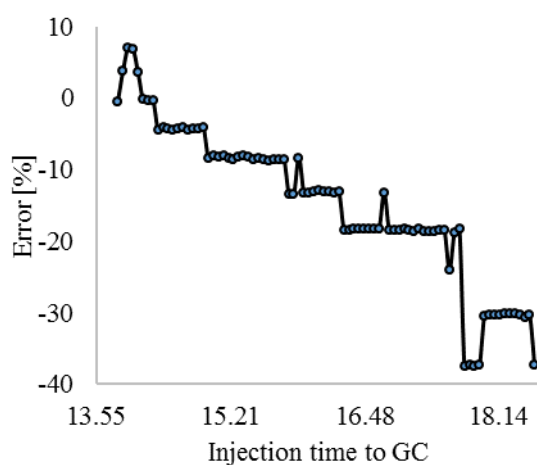
(d) 0.5% CH<sub>4</sub> and 1% O<sub>2</sub> (Run 4)



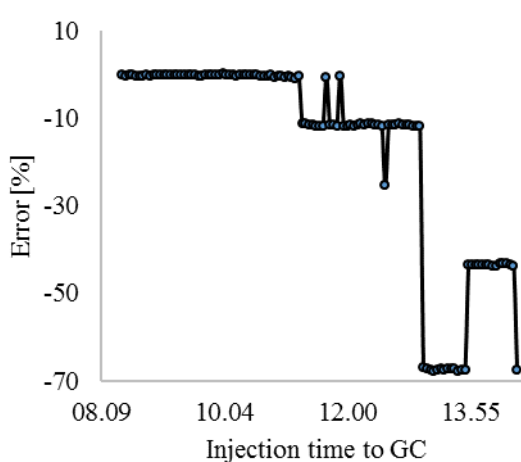
(e) 0.5% CH<sub>4</sub> and 2.5% O<sub>2</sub> (Run 5)



(f) 2% CH<sub>4</sub> and 4% O<sub>2</sub> (Run 6)



(g) 0.25% CH<sub>4</sub> and 0.5% O<sub>2</sub> (Run 7)



(h) 0.1% CH<sub>4</sub> and 0.5% O<sub>2</sub> (Run 8)

**Figure E.1.** The error in the mass balance with respect to carbon as a function of injection time to GC. The mass balance error of the different methane oxidation experiments over the 2 wt.% catalyst is given in (a)-(h). the carbon balance was checked at every point of injection to the GC during the analysis until full conversion was reached.

The deviations in the mass balance observed in Figure E.1 (a)-(f) are considered fairly normal with respect to uncertainty levels. The error is more or less steady over time, but appears to increase as the conversion approaches 100%. Nevertheless, the error in the mass balance does not exceed 8% in these experiments, which is considered acceptable. For the lowest methane concentrations, however, this do not seem to be the case. As seen in Figure E.1 (g)-(h), the error in the carbon balance is found to reach levels as low as -40% and -70%, respectively. The CG has been calibrated for concentrations down to 1% CH<sub>4</sub> and CO<sub>2</sub>, and in these experiments the CH<sub>4</sub> concentrations was as low as 0.25% and 0.1%. The error is thus most likely caused by improper calibration of the GC in the experiments involving such low concentrations. A negative error theoretically means that there is more carbon in the feed than in the product flow. This observation could be due to the assumption

of the amount of carbon coming into the system being constant, or the GC not being able to detect all the CO<sub>2</sub> formed. As no other carbon compound was detected by the GC, there is reason not to believe other carbon compounds were formed during the experiment.

The errors in the carbon balances as a function of injection time to the GC for all the runs over the 0.2 wt.% catalyst are illustrated in Figure E.2.

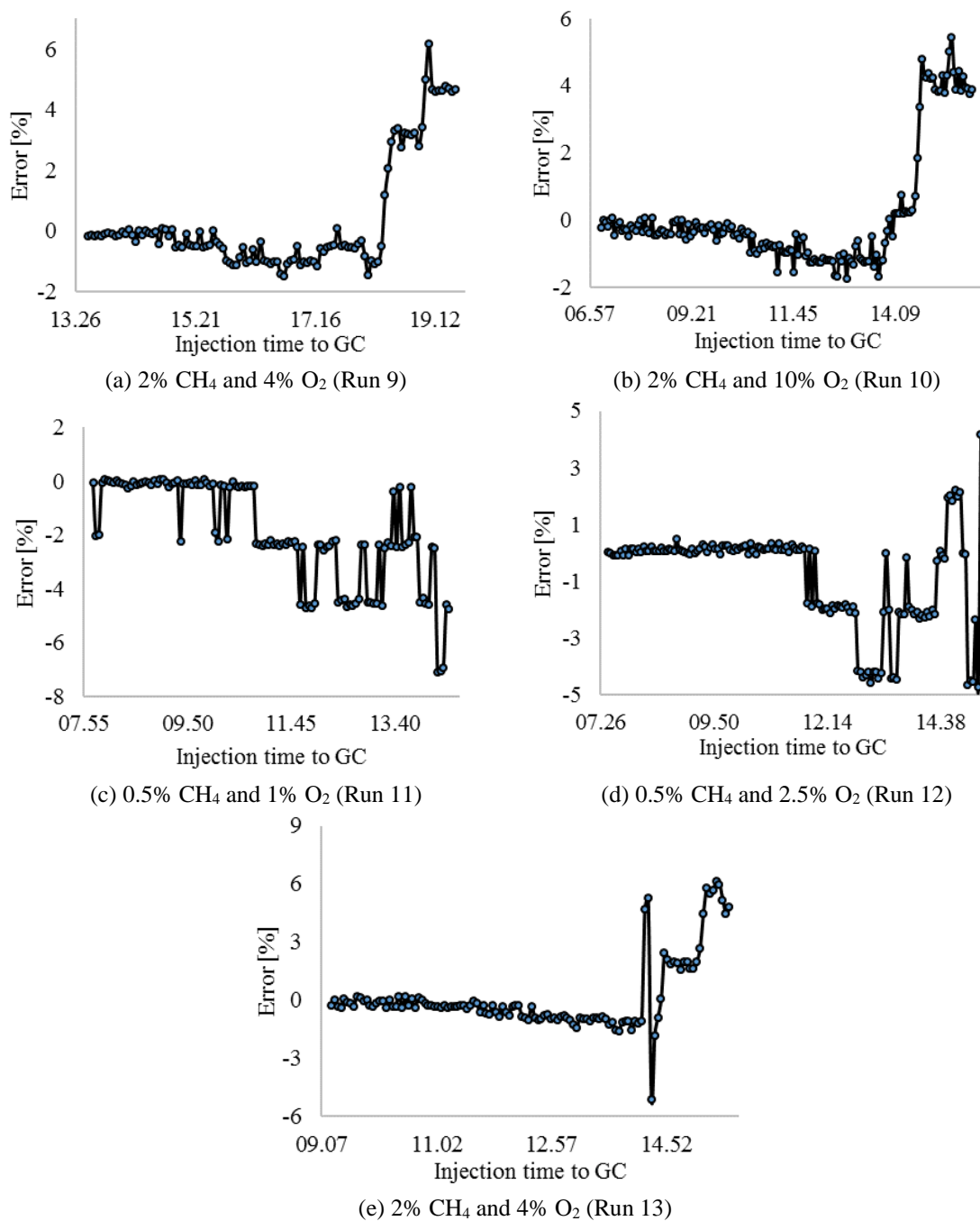


**Figure E.2.** The error in the mass balance with respect to carbon as a function of injection time to GC. The mass balance error of the different methane oxidation experiments over the 0.2 wt.% catalyst is given in (a)-(e). the carbon balance was checked at every point of injection to the GC during the analysis until full conversion was reached.

## Appendix F. Kinetics Calculations

The gas hourly space velocity (GHSV) was calculated according to Equation (F.1), where  $q_{tot}$  is the total volumetric feed flow and  $m_{cat}$  is the amount of catalyst in the reactor.

$$GHSV = \frac{q_{tot}}{m_{cat}} \quad (F.1)$$

The residence time,  $\tau$ , was calculated from Equation (F.2), with the volume of the bed,  $V_{bed}$ , being calculated from Equation (F.3).

$$\tau = \frac{V_{bed}}{q_{tot}} \quad (F.2)$$

$$V_{bed} = \pi r^2 h \quad (F.3)$$

Equation (F.3),  $r$  is the radius of the reactor, and hence of the catalytic bed, and  $h$  is the height of the bed.

The calculated GHSV and residence times for the methane oxidation experiments performed over the three catalyst samples, are given in Table F.1.

**Table F.1.** Calculated residence time and gas hourly space velocity in the methane oxidation experiments performed over the three catalyst samples.

Sample	$\tau$ [s]	GHSV $\left[ \frac{\text{Nml}}{\text{h} \cdot \text{g}_{cat}} \right]$
1	1.98	61193
2	1.98	61162
3	2.03	61193

The methane oxidation reaction is assumed to be first order first respect to methane, and the reaction rate can therefore be calculated from Equation (F.4) for conversion below 20%. At such conversions, the reaction can be approximated as differential.

$$r_{CH_4} = \frac{GHSV}{V_m} * X_{CH_4} * x_{CH_4} \quad (F.4)$$

In Equation (F.4),  $X_{CH_4}$  is the conversion of methane,  $x_{CH_4}$  is the amount of  $CH_4$  in the feed and  $V_m$  is the molar volume of 22 400 cm<sup>3</sup>/mol.

Furthermore, the turnover frequency (TOF) can be calculated according to Equation (F.5), where  $r$  is the reaction rate,  $M_w$  is the molar weight of the active metal,  $x_m$  is the weight fraction of the metal in the catalyst and  $D$  is the dispersion.

$$TOF = \frac{r_{CH_4} * M_w}{x_m * D} \quad (F.5)$$

For the TOF calculations done in this report, the average value of the dispersion found from the difference results were used (58% for the 2 wt.% catalyst).



## Appendix G. Matlab script

```
% Program to plot the temperature (Y) as a function of conversion (x),
% and calculate the temperature at a given conversion.
% 11.05.2016

%Clear memory
clear all
close all
clc

format long g

%% Import data
%Taken from Excelsheet
T_exp = [253.71 %Temperature (Here: run 1)
301.45
351.81
401.49
452.18
508.65
574.57
624.90];

c_exp = [0.40 %Conversion (Here: run 1)
0.46
0.88
2.49
8.68
34.15
89.33
100.00];

%% Finding parameters for a polynom (order 6)

p = polyfit(T_exp,c_exp, 6); %CHANGE HERE IF CHANGE OF ORDER

%% Plotting the experimental values and the obtained equation

T_plot = 253:0.1:625;
c_plot = polyval(p,T_plot);

figure(1)
set(gcf, 'color', 'w');
plot(T_exp,c_exp, 'ro', T_plot,c_plot,'k-')
grid
legend('Experimental values from this work ',...
'Fitted curve',...
'Location', 'Northwest');
title('Conversion at different temperatures')
xlabel('Temperature, \it T \rm [[40]C]')
ylabel('Conversion, \rm [%]')

% Find the temperature at a given conversion C
```

```
% This happens when the difference between the function and C is a
% minimum.
T_C = zeros(1,5);
C = 10;
for i=1:5
[difference, index] = min(abs(c_plot-C));
T_C(i) = T_plot(index);
C = C + 20;
End

% Find the conversion at a given temperature
T_450 = 450;
C_450=polyval(p,T_450)
```

## Appendix H. Arrhenius plots

The Arrhenius plots were constructed to calculate the activation energy. The plots were made using the temperatures at which 10%, 20%, 30%, 40% and 50% conversion of methane was reached, estimated by small modifications of the Matlab script given in Appendix G.

Arrhenius plots for the reactions performed over the 2 wt.% catalyst and the 0.2 wt.% catalyst are shown in Figure H.1 and Figure H.2, respectively.

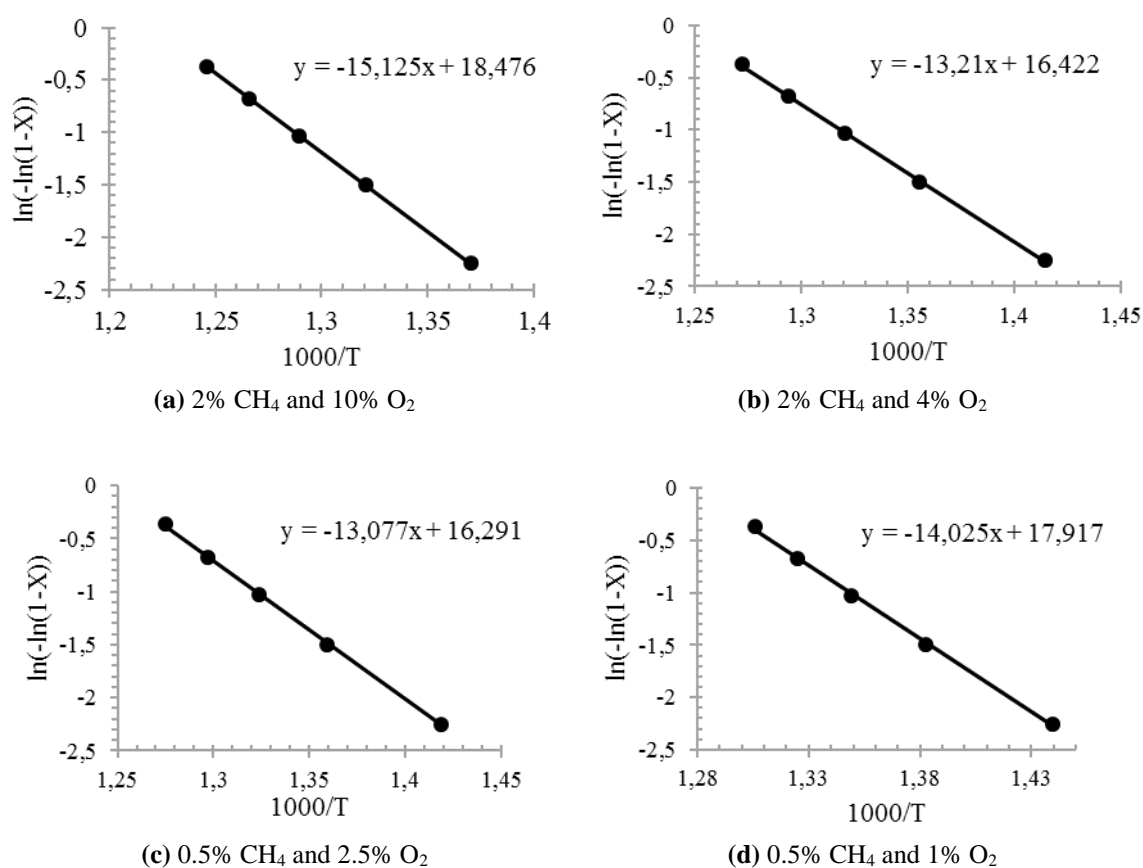
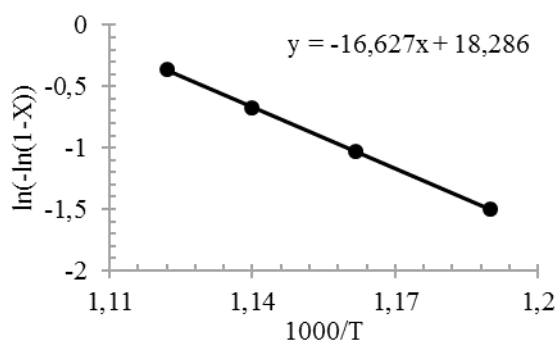
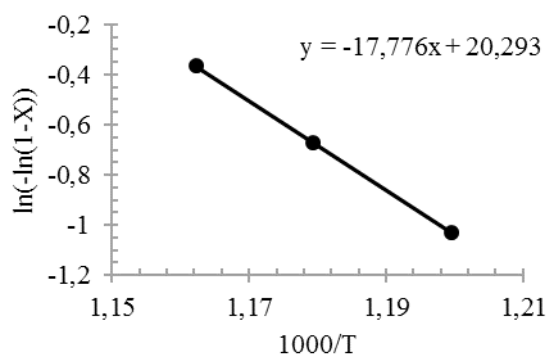


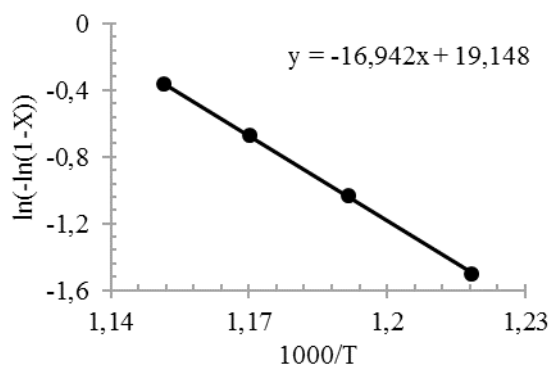
**Figure H.1.** Arrhenius plots to calculate activation energy in methane oxidation reactions performed over the 2 wt.% catalyst.



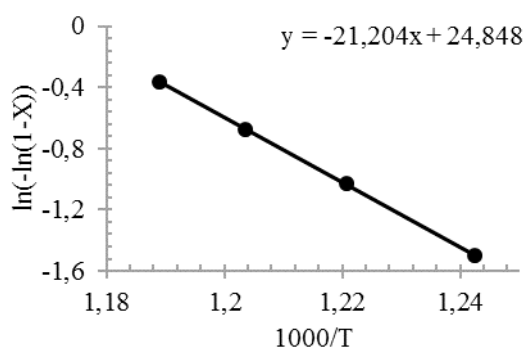
(a) 2%  $\text{CH}_4$  and 10%  $\text{O}_2$



(b) 2%  $\text{CH}_4$  and 4%  $\text{O}_2$



(c) 0.5%  $\text{CH}_4$  and 2.5%  $\text{O}_2$



(d) 0.5%  $\text{CH}_4$  and 1%  $\text{O}_2$

**Figure H.2.** Arrhenius plots to calculate activation energy in methane oxidation reactions performed over the 0.2 wt.% catalyst